

INFORMATION TO USERS

This manuscript has been reproduced from the microfilm master. UMI films the text directly from the original or copy submitted. Thus, some thesis and dissertation copies are in typewriter face, while others may be from any type of computer printer.

The quality of this reproduction is dependent upon the quality of the copy submitted. Broken or indistinct print, colored or poor quality illustrations and photographs, print bleedthrough, substandard margins, and improper alignment can adversely affect reproduction.

In the unlikely event that the author did not send UMI a complete manuscript and there are missing pages, these will be noted. Also, if unauthorized copyright material had to be removed, a note will indicate the deletion.

Oversize materials (e.g., maps, drawings, charts) are reproduced by sectioning the original, beginning at the upper left-hand corner and continuing from left to right in equal sections with small overlaps.

Photographs included in the original manuscript have been reproduced xerographically in this copy. Higher quality 6" x 9" black and white photographic prints are available for any photographs or illustrations appearing in this copy for an additional charge. Contact UMI directly to order.

**ProQuest Information and Learning
300 North Zeeb Road, Ann Arbor, MI 48106-1346 USA
800-521-0600**

UMI[®]

The Production of Toxic Emissions from Reacting Diffusion Jet Flames in a Crossflow

by

Robert Prybysh



A thesis for submission to the Faculty of Graduate Studies and Research

Department of Mechanical Engineering

University of Alberta

Edmonton, Alberta

Spring 2002



**National Library
of Canada**

**Acquisitions and
Bibliographic Services**

**395 Wellington Street
Ottawa ON K1A 0N4
Canada**

**Bibliothèque nationale
du Canada**

**Acquisitions et
services bibliographiques**

**395, rue Wellington
Ottawa ON K1A 0N4
Canada**

Your file Votre référence

Our file Notre référence

The author has granted a non-exclusive licence allowing the National Library of Canada to reproduce, loan, distribute or sell copies of this thesis in microform, paper or electronic formats.

L'auteur a accordé une licence non exclusive permettant à la Bibliothèque nationale du Canada de reproduire, prêter, distribuer ou vendre des copies de cette thèse sous la forme de microfiche/film, de reproduction sur papier ou sur format électronique.

The author retains ownership of the copyright in this thesis. Neither the thesis nor substantial extracts from it may be printed or otherwise reproduced without the author's permission.

L'auteur conserve la propriété du droit d'auteur qui protège cette thèse. Ni la thèse ni des extraits substantiels de celle-ci ne doivent être imprimés ou autrement reproduits sans son autorisation.

0-612-69577-8

Canada


University of Alberta

Library Release Form

Name of Author: Robert Prybysh
Title of Thesis: The Production of Toxic Emission from Reacting
Diffusion Jet Flames in a Crossflow
Degree: Master of Science
Year this Degree Granted: 2001

Permission is hereby granted to the University of Alberta Library to reproduce single copies of this thesis and to lend or sell such copies for private, scholarly or scientific research purposes only.

The author reserves all other publication and other rights in association with the copyright in the thesis, and except as herein before provided, neither the thesis nor any substantial portion thereof may be printed or otherwise reproduced in any material form whatever without the author's prior written permission.



Robert Prybysh
12141 Jasper Ave. #203
Edmonton, Alberta
T5N 3X8

Oct. 5, 2001

University of Alberta

Faculty of Graduate Studies and Research

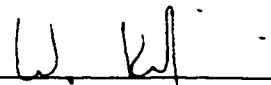
The undersigned certify that they have read, and recommend to the Faculty of Graduate Studies and Research for acceptance, a thesis entitled **The Production of Toxic Emissions from Reacting Diffusion Jet Flames in a Cross Flow** submitted by Robert Prybysh in partial fulfillment of the requirements for the degree of Master of Science .



Dr. M. David Checkel



Dr. David J. Wilson



Dr. Warren B. Kindzierski



Dr. Brian A. Fleck

Date: Oct 5, 2001

Abstract

This thesis documents an investigation into the production of toxic compounds by reacting jets in a cross flow. These reacting jets are being used as scale model flares to investigate the emissions of flare stacks used by industry to dispose of waste hydrocarbon gas. The initial investigation included the search for the production of Volatile Organic Compounds (VOC), Benzene based compounds (BTEX), and Polyaromatic Compounds (PAH). No contaminants were found in detectable quantities in the gaseous form. The particulate matter produced by reacting propane jets was collected and found to contain detectable quantities of PAH compounds. The particulate plume of the flame was located, mapped, collected, and sampled in an attempt to understand how the crossflow affected the production of particulate material. Samples were collected and chemically analyzed to determine the production rate of toxic compounds by the flame.

Table of Contents

CHAPTER 1 INTRODUCTION	1
1.1 Potential Emissions and Effects	3
1.1.1 Stripped Fuel	4
1.1.2 Gaseous Components of Partial Combustion	5
1.1.3 The Toxicity of Particulate Material	5
1.2 Prior Investigations Relevant to Flare Emissions	9
1.2.1 Jets in a Cross Flow	10
1.2.2 Simple Diffusion Flames	11
1.2.3 Jet Diffusion Flame Studies	13
1.2.4 Diffusion Flames in a Cross flow	17
1.2.5 Industrial Flare Studies	22
1.3 Emissions from Model Flares	23
1.4 Research Approach	23
1.4.1 Facility	24
1.4.2 Model Flare Stacks	26
1.4.3 Additional Equipment	27
1.5 Thesis Outline	28
CHAPTER 2 PRELIMINARY INVESTIGATION	29
2.1 Measuring Emitted VOC, Gaseous Aromatic Compounds, Aldehydes, and BTEX	31
2.1.1 Absorbent Tubes	32
2.1.2 Experimental Setup for the Measuring of Gas Phase Toxic Compounds	35
2.1.3 Tests Conducted	39
2.1.4 Production Rates Required to Reach Detectable Limits	40
2.1.5 Results of Preliminary Tests	41
2.2 Particulate Phase Polyaromatic Hydrocarbon Investigation	45
2.3 Preliminary Conclusions	49
CHAPTER 3 Particle Plume Mapping of Scale Model Flares	51
3.1 Potential Sampling Techniques	52

3.2 Fast Flame Ionization Detection	53
3.2.1 System Modifications to the FFID	55
3.2.2 Particulate Material and Gas Phase Hydrocarbons	58
3.3 Matching Time Response	59
3.4 Processing of Dual Channel FFID Signals	60
3.5 Mean Peak Frequency	62
3.6 Plume Expansion	66
3.7 Plume Mapping Conclusions	68
CHAPTER 4 PARTICULATE EMISSIONS MEASUREMENT	69
4.1 Particulate Material Measurement Overview	69
4.2 Plume Collection and Mixing	70
4.2.1 Entry Section	72
4.2.2 Mixing Section	74
4.2.2.1 Mixing Baffle	74
4.2.2.2 Mixing Tests	75
4.2.3 Measurement Section	79
4.2.3.1 Variable Speed Fan System	79
4.2.3.2 Velocity Profiles	79
4.2.3.3 Volumetric Flow Rate	81
4.2.3.4 Velocity at Sampling Location	84
4.3 Particle Filtration	85
4.3.1 Filter Flow Rate Calibration	88
4.3.2 Sampling Assembly	91
4.4 Mass Measurement	92
4.5 Particulate Material Production by Commercial Propane Flames in Cross Flow	95
4.5.1 Filter Handling	96
4.5.2 Raw Data	97
4.5.3 The Mixing Ratio	101
4.5.4 Statistical Analysis	102
4.5.5 Model Flare Stack Results –24.7 mm Diameter	104
4.5.6 Model Flare Stack Results-29.9 mm Diameter	105
4.5.7 Small Diameter Model Flare Stack Results	107
4.6 Particulate Material Emission Models	110

4.7 Conclusions	111
CHAPTER 5 PARTICLE IMAGING AND CHEMICAL COMPOSITION	113
5.1 Particle Imaging	114
5.1.1 Clean Filter Images	115
5.1.2 Particle Images	116
5.1.3 Particulate Material Formation	123
5.2 Chemical Composition	127
5.3 Conclusions	129
CHAPTER 6 CONCLUSIONS	131
6.1 Preliminary Investigation	131
6.2 Plume Location	132
6.3 Particulate Mass Measurement	133
6.4 Particulate Production Rates	133
6.5 Particle Imaging	135
6.6 Chemical Composition	136
6.7 Future Work	136
APPENDIX 1 FACILITY DETAILS	144
A1.1 Combustion Wind Tunnel	144
A1.2 Fuel Supply	146
A1.3 Model Flare Stacks	148
A1.4 Traversing Mechanism	149

APPENDIX 2 DEPOSITION	151
A2.1 Required Terms	151
A2.2 Sample Efficiency	152
A2.3 Inlet Efficiency	153
A2.4 Transport Efficiency	154
A2.5 Calculated Deposition	155
 APPENDIX 3 ERROR ANALYSIS	 157
A3.1 Facility Errors	157
A3.2 Mixing Tunnel Errors	158
A3.3 Sampling System	159
A3.4 Filter Measurement	159
A3.5 Mass Conversion	160
A3.6 The Error Equation	162
A3.7 Sample Error	166
 APPENDIX 4 SETTLING TIME	 162
A4.1 Force Balancing	168

List of Tables

Table 1.1	The dimensions of the quartz flare stacks used in these experiments.	26
Table 2.1	Descriptions of the five tests conducted to identify the presence of VOCs, including the estimated efficiencies of each test.	39
Table 2.2	Minimal production rates required to produce detectable quantities of listed compounds.	41
Table 2.3	Mole fractions of hydrocarbons found in carbon screen after tests were conducted.	42
Table 2.4	The compounds measured in the Aldehyde analysis.	43
Table 2.5	Compounds found in the charcoal absorbent tube that is designed to absorb gaseous aromatic compounds.	44
Table 2.6	Masses of PAH found by MS/GC analysis on each paper filter.	49
Table 5.1	The quantity of PAH's found in particulate material sample.	129
Table A1.1	The dimensions of the quartz flare stacks used in these experiments.	148

List of Figures

Figure 1.1	The human respiratory system.	7
Figure 1.2	The basic chemical structure of reactant in the vicinity of a hydrocarbon : air diffusion flame.	12
Figure 1.3	A laminar diffusion flame and a turbulent diffusion flame.	15
Figure 1.4	Sketches of a turbulent diffusion flame and a lifted diffusion flame.	16
Figure 1.5	Diffusion flame in a cross flow.	18
Figure 1.6	The combustion wind tunnel at the University of Alberta.	25
Figure 2.1	Manual sampling system for extracting 1 Liter samples.	30
Figure 2.2	Progression of concentration along an absorbent tube.	33
Figure 2.3	Absorbent tube fitted with both primary and secondary absorbent material.	33
Figure 2.4	Low flow measurement device.	35
Figure 2.5	Gas sampling assembly.	38
Figure 2.6	The original system used to sample for the presence of PAH and soot produced by a propane flame.	47
Figure 3.1	Combustion Tee-Top FFID tube.	56
Figure 3.2	Modified straight flow FFID tube.	56
Figure 3.3	The initial and final configuration of the combustion chamber on the FFID modules.	57
Figure 3.4	Both FFIDs were mounted in parallel.	58
Figure 3.5	A sample of the signals produced by the FFID.	61
Figure 3.6	The processed signal, on material that was stopped by the filter appears in the data.	62

Figure 3.7	Peak Frequency contour (in Hz) generated using Dual FFID Detector. Propane flame, 0.5m/s jet velocity in a 4m/s cross flow.	65
Figure 3.8	Peak frequency contour (in Hz) for a 0.5 m/s Propane jet in a 6 m/s cross flow.	65
Figure 3.9	The peak frequency contour and the thermal contour at a distance of 230cm from the base of the flare stack.	67
Figure 3.10	The peak frequency contour and the thermal contour at a distance of 250 cm from the base of the flare stack.	67
Figure 3.11	The peak frequency contour and the thermal contour at a distance of 350 cm from the base of the flare stack.	67
Figure 4.1	The particle plume collection system installed on the combustion wind tunnel at the University of Alberta.	70
Figure 4.2	The mixing baffle designed for the entrance of the mixing section.	75
Figure 4.3	The mixing profiles generated by the mixing tests using the Carbon Monoxide.	76
Figure 4.4	The mixing profile of Natural Gas for 2 m/s centerline velocity in the mixing tunnel.	77
Figure 4.5	Mixing profile for a 35 liter/min Natural Gas jet injected into the entry section with a 4 m/s centerline velocity.	78
Figure 4.6	Mixing Profile for an 18 liter/min Natural Gas jet injected into the entry section with an 8 m/s centerline velocity.	78
Figure 4.7	The velocity contours for four different motor rpm settings.	81
Figure 4.8	Pressure tap locations on a 6 arm area averaging pitot tube.	82
Figure 4.9	The mean air velocity in the plume collection system with respect to the blower RPM.	83
Figure 4.10	The velocity to RPM correlation used to determine the gas velocity at the tip of the sampling probe.	84

Figure 4.11	The assembly constructed for calibrating the flow through the alumina filters based on pressure drop.	89
Figure 4.12	The pressure to flow rate calibration for the 47 mm alumina filters with a 20 nm pore size.	91
Figure 4.13	The assembly used to draw a sample through the filter.	92
Figure 4.14	The assembly used for storage and measurement of filters.	95
Figure 4.15	Data for 1 m/s exit velocity propane flame with the 24.7 mm diameter jet in a varied cross wind.	98
Figure 4.16	Data collected for a 24.7 mm diameter jet in a constant cross wind of 2 m/s with a varied jet exit velocity.	99
Figure 4.17	All data collected for the 24.7 mm diameter stack prior to the statistical analysis.	100
Figure 4.18	The data collected for particulate mass production using the 24.7 mm model flare stack.	105
Figure 4.19	Particulate Material collection results for the 29.9 mm diameter stack.	106
Figure 4.20	The soot production correlation for the 24.7 mm and 29.9 mm stack.	107
Figure 4.21	The resulting data for the 12.3 mm diameter model flare stack.	108
Figure 4.22	Particulate Material yield curves for all the stack diameters tested and published model for 2.16 mm diameter stacks.	110
Figure 5.1	Magnification of the collection facing of the 20 nm alumina filter.	116
Figure 5.2	Image of the reverse side of the 20 nm alumina filter.	117
Figure 5.3	A side image of the filtration surface.	117
Figure 5.4	A large number of aggregates on a 20 nm filter.	119
Figure 5.5	Individual spherules are identifiable in the structure of the aggregates.	120

Figure 5.6	Particulate material collected on a 200 nm filter.	121
Figure 5.7	A soot particle produced by the combustion of a synthetic rubber.	122
Figure 5.8	A close up image of a single soot particle.	123
Figure 5.9	The acetylene model for soot formation.	124
Figure 5.10	The formation of PAH's promotes that formation of platelets.	126
Figure 5.11	Soot spherules expanded using nitric acid.	126
Figure A1.1	The combustion wind tunnel.	145
Figure A1.2	The natural gas supply system.	147
Figure A1.3	The propane supply system.	147
Figure A1.4	The orifice placement for the model flare stacks.	149
Figure A1.5	The traverse mechanism used in the test section of the combustion wind tunnel.	150

Chapter 1: Introduction

When crude oil and bitumen exists in a formation or reservoir, extreme pressure can force light hydrocarbons, which are normally vapors at ambient conditions, to exist either as a compressed liquid or as a gas dissolved with the liquid phase. Solution gas is a term used to identify light hydrocarbons that become a vapor when crude oil is extracted from the high-pressure environment in the formation [Petroleum Communication Foundation, 2000]. While solution gas can contain useful energy, the location of the production process can sometimes limit the ability to use these gases in a productive manner. As a result, these hydrocarbons become a waste product requiring disposal. The easiest way to dispose of these waste gasses is to vent them directly into the atmosphere. While this is the most economical method, many hydrocarbon gases are environmental pollutants or are strong contributors to global climate change by being a greenhouse gas. For example, methane has a climate change potential 7 times greater than CO₂ per unit volume and should not be released into the environment untreated. In addition, solution gas can contain other compounds (e.g. H₂S, Benzene) that could accumulate in the surrounding environment if released directly into the atmosphere. Since such compounds can have toxic effects when absorbed by living things, they will be called toxic compounds in this thesis.

The treatment methods usually applied to solution gas occur at gas plants where undesirable components of the solution gas are stripped and the balance is sold as sale grade natural gas. Processing solution gas in this manner is often referred to as

“conserving” the gas. Unfortunately transporting the waste gas to a treatment facility is not always economically viable due to the remote locations that the oil and gas industry operates. Additionally, on site treatment of low gas volumes is not feasible because it can reduce the economic output of the process to unreasonably low levels.

In Alberta in 1999, $23.7 \times 10^9 \text{ m}^3$ of solution gas was produced. Of this production, 94% was conserved, the remainder was vented or flared at 4499 sites [Johnson,2001]. Flaring is the practice of burning excess flammable gas produced at industrial sites with an atmospheric burner and the combustion products released directly into the environment. Flaring is considered to be an economical method of disposing of waste hydrocarbons produced by the petroleum industry by hopefully converting all the hydrocarbons to CO_2 and water vapor and significantly reducing the toxicity of H_2S by converting it to SO_2 . Unfortunately, the emissions and subsequent environmental effects of flares are not well understood since only limited research has been conducted into their ability to fully oxidize the flare stream rather than form products of incomplete combustion. Despite this lack of understanding, it is undeniable that the use of flares is an economically viable means of disposing of waste gas regardless of location, so flaring is considered to be a practical disposal technique.

Flares are currently the focus of considerable controversy regarding the emissions that are released. Flares are often used to dispose of gases with toxic components, and there is concern that flares produce numerous toxic compounds through the combustion process [Globe and Mail, 2000]. The focus of this investigation had to identify the kind and

amount of toxic or undesirable compounds flares generate. At the beginning of this study, the prominent form of toxic emissions from flares was not known, but believed to fall into three basic categories:

- Fuel from the flare that avoids the combustion process and is released directly into the environment.
- Gaseous compounds that are generated by incomplete combustion of hydrocarbon fuels.
- Particulate matter that is comprised of non-gaseous compounds produced by incomplete combustion.

Each form of emission needed to be investigated to identify its contribution to the production of toxins by flares.

1.1: Potential Emissions and Effects

The potential emission from flares can fall into three categories, stripped fuel, gaseous products of partial combustion, and particulate material. Each of these forms has a different effect and need to be considered.

1.1.1: Stripped Fuel

Fuel stripping occurs when fuel avoids the combustion process and is released into the atmosphere. While most of flare gas is composed of simple hydrocarbons (methane, ethane, and propane), it is possible for this fuel to contain toxic components. For example, H_2S is a relatively common component of solution that is flared. Flaring converts H_2S into SO_2 and water vapor. While H_2S has a LCLo (Lowest Published Lethal Concentration) of 800 ppm for a 5 minute exposure, SO_2 has a LCLo of 1000 ppm for a 10 minute exposure. By converting H_2S into SO_2 , the toxicity is notably reduced [HTPCR(#7783-06-4), Howard Hughes Medical Institute]. However, if H_2S is present in the solution gas and fuel stripping occurs, then H_2S would be released into the atmosphere untreated.

The main reason for flaring is to convert the hydrocarbons in the fuel into water and carbon dioxide. Methane, which is the simplest paraffin hydrocarbon, by volume, has 7 times the greenhouse effect of CO_2 . The effect is measured by volume and not by mass because 1 mole of CH_4 will burn to form 1 mole of CO_2 , which will have the same volume, but not the same mass. By flaring, a unit volume of methane can have its contribution to the greenhouse effect reduced by over 86%.

1.1.2: Gaseous Components of Partial Combustion

When combustion occurs but the fuel is not completely converted into CO₂ and water, other carbon based compounds can be produced. Some of these compounds include aldehydes and polyaromatic compounds (PAHs). An example of an aldehyde that could be present is formaldehyde (CH₂O) which is classified as a carcinogen (a substance that produces cancer), and a teratogen (a substance that interferes with normal embryonic development). At the beginning of this project, it was considered possible for polyaromatic compounds to be present in the vapor form even though most PAH compounds have a very low vapor pressure. Experimentation indicated that the levels of vapor form PAH compounds produced by the flame were below detectable limits by the methods used here.

1.1.3: The Toxicity of Particulate Material

Smoke is a cloud of fine carbonaceous particles suspended in air, and these particles are often made of particulate material. Interest in smoke is derived from its varied toxic effects. Particles of any composition are known to have toxic effects upon the respiratory system [Williamson,1973]. The nasal cavity and the upper respiratory system, shown in Figure 1.1, generally filter particles larger than 3 micrometers before they can enter the lungs. Cilia in these areas can capture particles greater than about 1 μm in size, expelling them with mucus flow, but smaller particles can escape these defense mechanisms and enter the lungs. While particles that are between 0.05 μm and 0.25 μm are usually

transported out of the lung by airflow before they can be deposited within the tissue, very small particles (<50 nm) have a more rapid and erratic motion, allowing for a greater tendency to impact a respiratory surface. As a result, particles with a mean diameter of less than 50 nm will have the greatest tendency to be retained within the lungs if inhaled. It should be noted that there is a lot of interest in particles that have a mean diameter of 10 micrometers (PM10) and 2.5 micrometers (PM2.5). These are mean diameter measurements, and can include a diverse range of particles, including particles with nanometer scale dimensions.

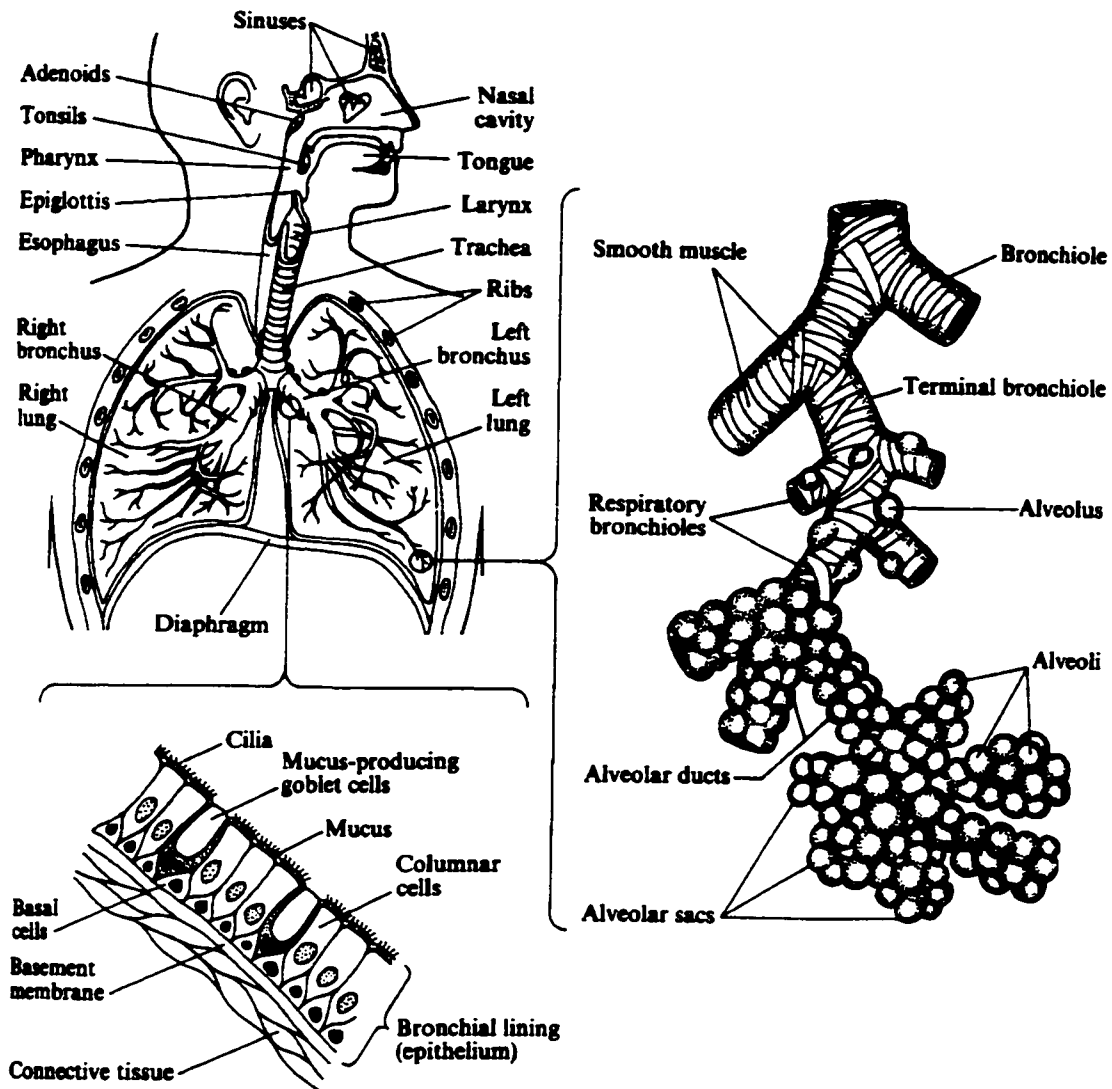


Figure 1.1: The human respiratory system [Williamson, 1973].

Particles retained in the lungs can produce numerous effects. Bronchitis is the general term used to describe a condition when the lungs become irritated and the body attempts to forcefully remove foreign material from them. Generally considered a temporary condition, it can become permanent if enough particles are deposited within the respiratory system, or continued exposure is experienced. Due to the delicate nature of

the respiratory system, the presence of carbon particles can cause physical damage to the tissues within the lungs. This can lead to Emphysema, which occurs when the Alveoli (small spherical chambers within the lungs that extract O₂ from the air) rupture, reducing the overall efficiency of the respiratory system. In rare occurrences, activated carbon can cause physical changes to the cells themselves, possibly leading to lung cancer.

While there is concern about the effects of particles as a pollutant, particulate material is rarely composed of only carbon. Within the flame, particulate material provides a surface for the collection of intermediate products of combustion [Broome, 1971]. As the particulate material grow, more volatile substances can become entrapped or condense on the surface, surviving the combustion process if smoke is emitted from the flame. Once outside the flame, the particulate material provides a method of transportation for the compounds (which normally decompose in the environment), allowing the substances to remain airborne as long as the particulate material survives. Many of the intermediate products of combustion, such as formaldehyde and many PAH compounds, are known to have carcinogenic effects, and their presence increases the toxicity of the particulate material that encapsulates them.

Not all of the health effects of smoke are well known. While the physical effects within the respiratory system have been investigated, there are theories that smoke can have a toxic effect on the entire body. Laboratory studies on animals have shown short term toxic effects throughout the entire body as a result of smoke exposure. Even short term exposure to low levels of smoke can result in reduced responses and incapacitation of the

subject [Kaplan, 1983]. This total body effect is considered to be a major contributor to many fire related fatalities. The long term effects of smoke exposure are not well understood, but it is theorized that chronic health effects (even non-respiratory effects) can develop from even short term exposure. One theory even presents the possibility that Gulf War Sickness, a term that describes the proliferation of chronic illness in soldiers after the gulf war, is a result of exposure to smoke produced by oil fires [Spector, 1998].

1.2: Prior Investigations Relevant to Flare Emissions

A flare operating in the atmosphere could be described as a jet diffusion flame that exists within a crossflow. While diffusion flames, either in a quiescent environment or in a crossflow of air, have been investigated, only limited study has been conducted directly on industrial flares. The study of diffusion flames in a crossflow can be broken into several topics:

- Jets in a crossflow, including non-reacting jets, and how they interact when introduced into a crossflow. The fluid dynamics involved and the formation of various flow structures have been well researched and are important to understanding how reacting jets will interact with the crossflow.
- The simplest form of laminar diffusion flames would be flames formed by a laminar jet, where there is no premixing of the fuel with air, and no cross flow.

- Turbulent jet diffusion flames with a higher flow rate. The turbulent nature of the flames increases the mixing and produces a much different flame appearance than from a laminar diffusion flame.
- Diffusion flames in crossflow of air that can be either laminar or turbulent. These flames can also be separated into high and low momentum flames by comparing the momentum of the fuel jet to the cross flowing air.

1.2.1: Jets in a Cross Flow

The literature on non-reacting jets in a crossflow is extensive and will not be reviewed here other than to highlight the basic features and structure of these flows. In a review paper, Margason examined publications from over 50 years of research into jet shapes, deflection, and vorticity [Margason, 1993]. Most of the reviewed research into cross flowing jets was focused on applications involving aircraft. For example, VTOL (Vertical Take Off and Landing) aircraft require thrust to be generated in directions other than the direction of motion, and there was great interest on how cross flowing jets would affect aerodynamics and lift. Some of the basic features of cross flowing jets involved the formation of the counter rotation vortex pair and the wake vorticity downstream of the jet.

Smith et al. [1998] studied jets in crossflow with less focus on aviation applications. Investigation into the concentration profiles and mixing of the jet with the crossflow was

conducted, along with the trajectory and the structure of the jet. Many of the shapes and structures that appear are a result of the interaction of the vorticity generated by the jet with the crossflow. Smith observed that eventually the jet forms into a counter rotating vortex pair, which dominates the fluid dynamics away from the jet exit.

1.2.2: Simple Diffusion Flames

A basic diffusion flame occurs when a pure fuel jet is combusted using oxygen in the surrounding environment. Figure 1.2 shows the basic structure of the environment around a diffusion flame where the oxidant is air. The flame front consumes fuel and oxygen creating a concentration gradient around the surface of the flame. This concentration gradient drives a diffusion of fuel and oxygen towards the flame, which allows the flame to continue burning. Products of combustion, including thermal energy, diffuse away from the flame, further reducing the concentration of fuel and oxygen, and also reducing the concentration of nitrogen around the flame. Heat diffuses away from the flame through various means of heat transfer and will heat the fuel and air in the proximity of the flame front [Hottel, 1949]. Buoyancy plays an important role in generating large scale fluid motions that carry the products of combustion away from the jet.

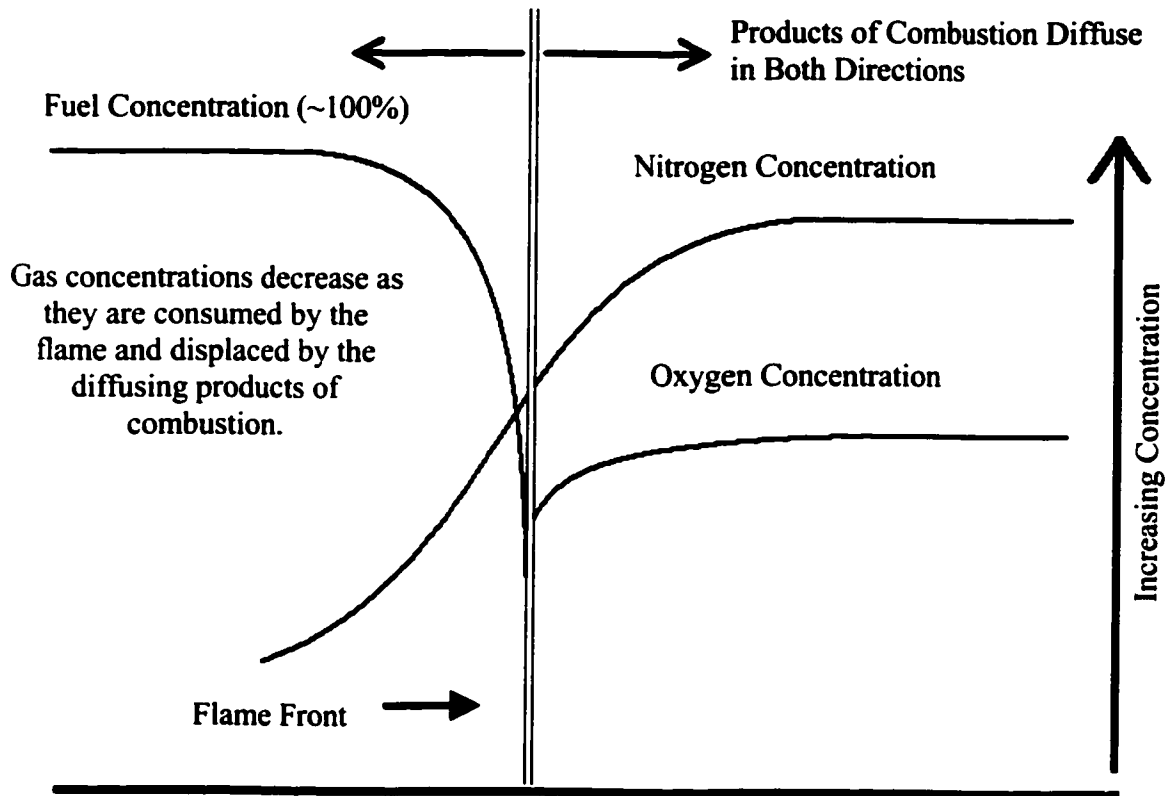


Figure 1.2: The basic chemical structure of reactant in the vicinity of a hydrocarbon : air diffusion flame.

The heating of the fuel and air in the proximity of the flame can result in dissociation. Dissociation is a process that occurs when extreme temperature causes complex molecules to decompose into simpler radicals, which are not stable at ambient conditions, and very reactive, molecules. Usually radicals react with oxygen to form H_2O and CO_2 , but these radicals could react with each other or stable molecules to form more complex chemicals. Only the number of radicals available and the residence time within the flame limits the complexity of the molecules. If the molecules are large enough, they may condense into solids and liquids, forming particles that can survive the

flame. This is the basic principal behind the formation of particulate material [Glassman, 1988].

1.2.3: Jet Diffusion Flame Studies

A jet diffusion flame is a diffusion flame that occurs when the fuel enters the oxygen environment as a jet. Jet diffusion flames in quiescent environments, shown in Figure 1.3, have been extensively investigated, both as laminar and turbulent jets. A laminar jet diffusion flame has a well defined flame front, as shown in Figure 1.3 [Hottel, 1949]. The interior of the flame is nearly pure fuel. Globally, the fuel momentum and buoyancy of the hot combustion products cause fresh air to be entrained into the flame, which sustained the combustion process. Near the flame, the transport of fuel and oxygen is dominated by molecular diffusion. A turbulent diffusion flame is also shown in Figure 1.3. The turbulence from the gas jet increases mixing and produces a wider flame. In the turbulent flame the flame front is more uneven as it is distorted by vortices and eddies that are generated by the interactions of the turbulent jet with the surrounding air. The turbulence augments the entrainment of air into the flame, but very near the flame the transport of fuel and air is still dominated by molecular diffusion.

Studies have shown that as the exit velocity of the gas jet is increased, the flame becomes longer until the flame begins the transition to turbulence. The turbulent diffusion flame is much shorter in length than the laminar diffusion flame of the same mass flow rate since the flame surface is wrinkled and has a larger surface area for molecular diffusion to

occur. Increasing the fuel flow to a turbulent diffusion flame does not increase the length because the increased flow proportionally increases the turbulence and wrinkling of the flame.

Jet diffusion flames are understood well enough that models are used to make predictions about them. For example, Roper presented a theoretical model that estimated the size and composition of laminar jet diffusion flames under many different conditions [Roper, 1977]. There are also models for predicting the length of turbulent diffusion flames. Pitts described a model that stated the length of a turbulent diffusion flame remains mostly consistent until the flame begins to blow off [Pitts, 1988].

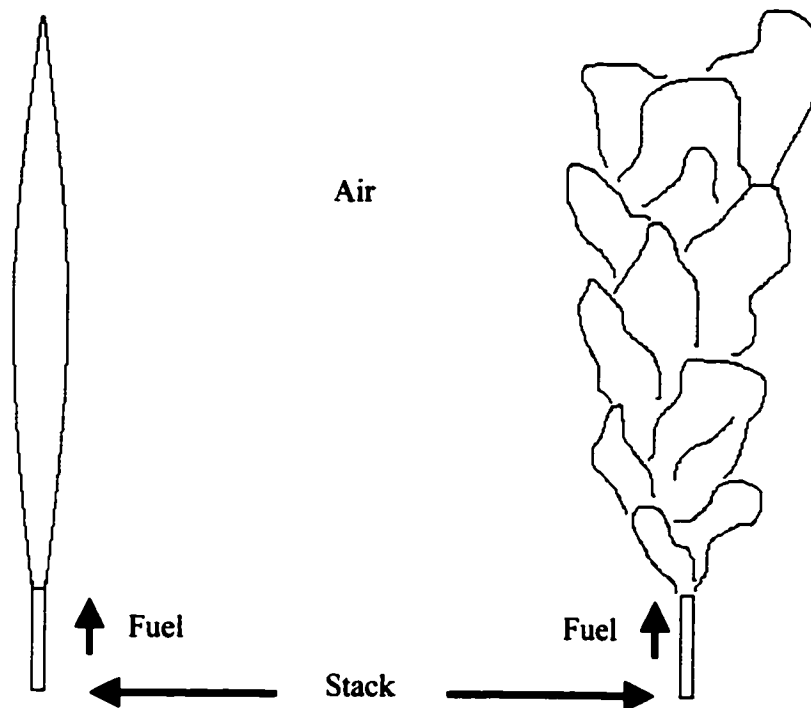


Figure 1.3: A laminar diffusion flame (left sketch) and a turbulent diffusion flame (right sketch).

Blowout occurs when the fuel flow rate is so high that the flame can not burn rapidly enough and is extinguished. Before blowing off, the flame becomes lifted, which occurs if the flame is burning, but is no longer attached to the stack [Pitts, 1988]. Lifted flames, shown in Figure 1.4, can be stable, but are susceptible to blowout. Additional work into lifted jets was also conducted by Mungal et al. [Muniz (1977), Hasselbrink (1998)], but the required fuel jet velocity for lifted flames is higher than used in continuous flaring.

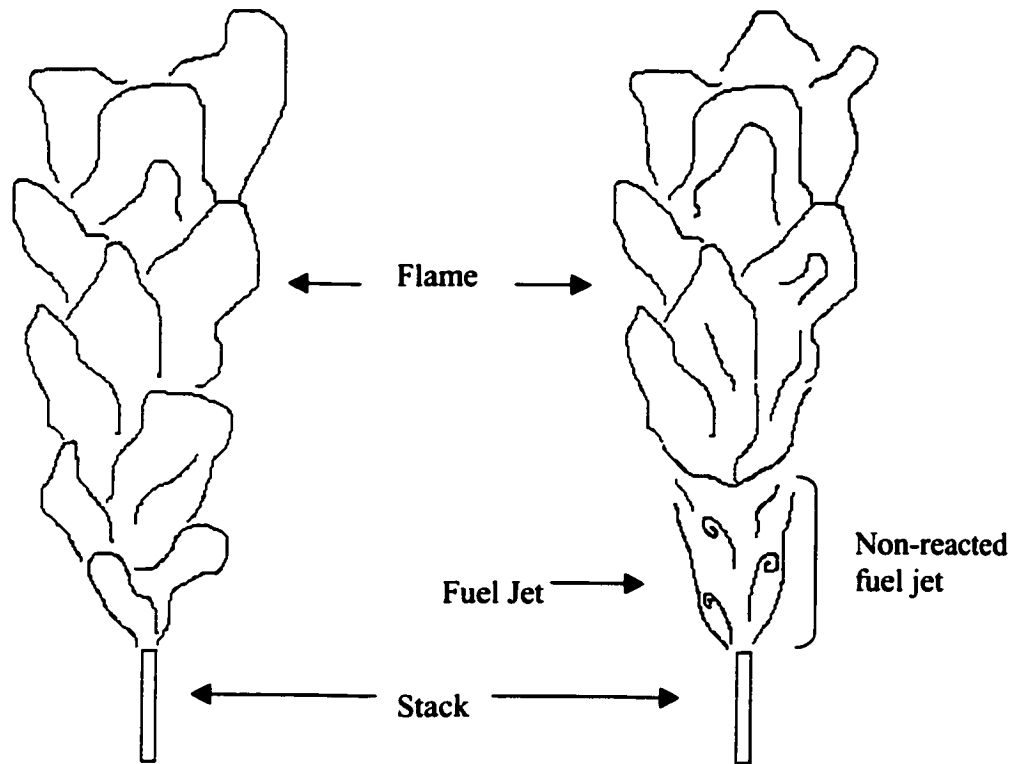


Figure 1.4: Sketches of an attached turbulent diffusion flame (left) and a lifted diffusion flame (right).

Testing of stable diffusion flames on a large scale (38 – 300 mm diameter pipes) without a crossflow was conducted by Pohl et al. [1986]. Pohl determined that as long as the flame was stable the efficiency of combustion (the conversion of the carbon in the fuel into CO_2) was in excess of 98%. Diluting the fuel gas with a non-combustible gas to reduce the energy content could generate lower efficiencies. While dilution did reduce the efficiency, the required dilution had to reduce the energy content of the fuel to about 10% over the minimal heating value required by Pohl for combustion for any effect to occur. The data collected by Pohl confirmed previous studies that stated that diffusion

flames had efficiencies in excess of 95% [Palmer (1972), Lee (1981), Siegel (1980), Howes (1981)].

1.2.4: Diffusion Flames in a Crossflow

Jet diffusion flames in a crossflow have been studied under laboratory conditions in a relatively limited number of studies. Most of these studies have chosen to describe the overall flow characteristics by the momentum flux ratio of the jet to the crossflow. The momentum flux ratio is defined as:

$$R = \frac{\rho_j U_j^2}{\rho_\infty U_\infty^2}$$

R - Momentum flux ratio.

ρ_j, ρ_∞ - Density of the gas jet and the crossflow, respectively.

U_j, U_∞ - Velocity of the gas jet and the crossflow, respectively.

The stack and the flow around the stack do not affect flames with a large momentum flux ratio. The dominant feature in a flame with a large momentum flux ratio is the counter rotating vortex pair [Smith, 1998]. In a flame with a low momentum flux ratio, the flame is described as being “wake stabilized”, where a portion of the flame is trapped in the recirculation zone [Huang, 1994] behind the stack. Figure 1.5 shows a diffusion flame in a crossflow that is typical of the flames that were studied in this thesis. U_∞ is the velocity of the crossflow, while U_j is the mean velocity of the gas jet, d_o is the diameter of the stack, and x is the distance downwind from the center of the stack.

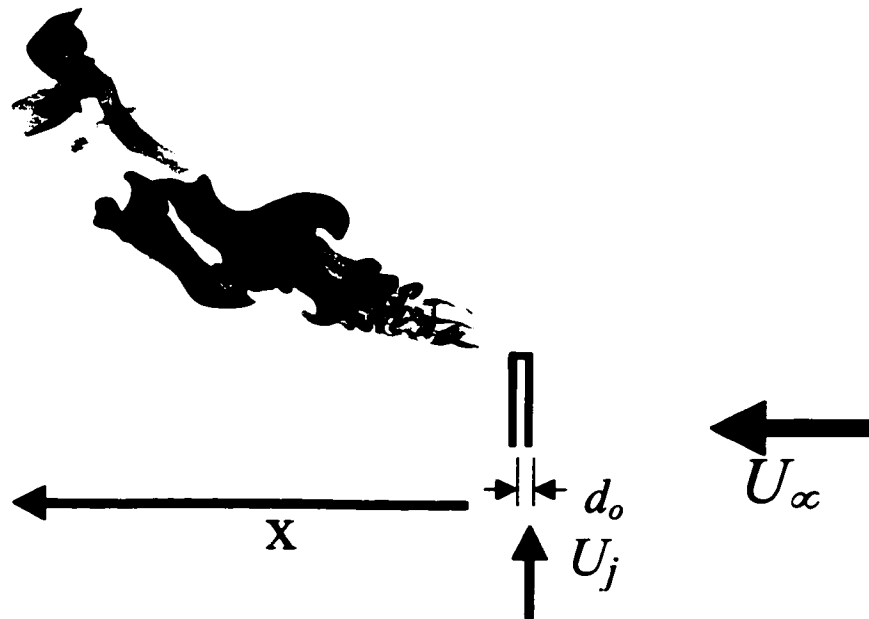


Figure 1.5: Diffusion flame in a crossflow.

Huang et al. studied jet diffusion flames at the National Taiwan Institute of Technology (NTIT) in Taiwan. Huang's work examined the structures and stability of small diameter (about 6 mm) cross flowing jet flames. Originally the focus of the research at the NTIT involved stability, and how the crossflow affected the length and trajectory of the flame [1994]. Linear traverses with numerous probes were conducted on the flames to determine the temperature contours and the concentrations of CO, CO₂, and O₂ within 6 different flame modes, as identified by Huang [1996]. Eventually, LDV was used to determine the mean velocity fields for different locations within 2 different flame modes [Huang, 1999].

In 1975, Brzustowski, Gollahalli, and Sullivan published their research into predicting the shape and length of hydrogen flames for jets from a 5 mm diameter stack in a crossflow [1975]. They attempted to scale the data up to industrial sized flare stacks with exit velocities of 80 m/s to 270 m/s. The goal was to simulate emergency releases of hydrogen from industrial processes. Later that year, they published results for propane diffusion flames in crossflow for stacks ranging from 1.3 mm diameter to 7 mm diameter [1975]. Brzustowski et. al. concluded that while cross flowing combustion jets shared many similarities with cold flowing jets, the differences were significant enough that models for cold jets could not be used to predict the size and trajectories of reacting jets.

Gollahalli and Nanjundappa investigated low velocity jets in a crossflow ($R < 1$) [1995]. Gollahalli attempted to map the thermal and concentration profiles for low momentum flames using a 4.7 mm diameter jet. Concentrations of CO₂, O₂, CO, and NO were all

mapped, although post-combustion production rates were not provided. Additionally, no attempts were made to measure the production of minor or toxic emissions.

The use of larger diameter jets to research cross flowing flames has been limited. Kalghatgi mapped the size and shape of cross flowing flames for stacks varying in size from 6 to 22 mm in diameter [1983]. Kalghatgi concluded that there were identifiable patterns in the size and shapes of cross flowing flames, and that it should be possible to predict these features for larger flames.

Limited research has been conducted into the emission of combustion products from cross flowing flames. Recently, Poudenx et. al. mapped the local efficiency within the plume of a flame in crossflow by measuring the production of CO₂, O₂, gas phase hydrocarbons, and CO within the plume, but did not explore the production of toxic emissions [2000].

More recent research into cross flowing flames has been conducted Johnson, who investigated the efficiency of combustion from jets varying in diameter from 12.3 mm to 49.8 mm [2001]. Most research was conducted with 24.7 mm diameter jets. These results showed that the crossflow speed can significantly affect the efficiency of combustion, and that the resulting inefficiencies were in the form of fuel that was being stripped from the gas stream before passing through the flame. Increasing the crossflow velocity increased the amount of fuel that was stripped, and diluting the fuel would

significantly affect efficiency. In addition, Majeski et. al. measured and modeled the length and trajectory of flares of a similar size range in a crossflow [2000].

Pohl conducted limited tests on large scale flares and determined that the particulate material production would represent an inefficiency of less than 0.5%. This study also reported that a small amount of steam would suppress the formation of particulate material by the flame [1986]. Pohl determined that the production of particulate material does not correlate with the efficiency of combustion, so any work that investigated particulate material production would have to be conducted separately from flame efficiency.

Ellzey conducted a study into the mass production rate of particulate matter from 4 mm diameter stacks burning propane for fuel [1990]. Ellzey found that the jet velocity (U_j) of the fuel and the velocity of the crossflow (U_∞) were equally influential on the particulate material production rate. These two terms (U_j and U_∞) were combined into a single term that was defined as the mixing ratio. The mass production rate of particulate matter mass for the 4 mm diameter propane diffusion flame was correlated to:

$$m_{soot} = \alpha (U_\infty U_j)^\beta$$

where α and β are constants.

Unlike many other properties of flames in a crossflow, particulate material production does not correlate well with the momentum flux ratio.

1.2.5: Industrial Flare Studies

Early research into industrial flares indicated that the combustion efficiency is very high, often >98 %. Pohl summarized work by Palmer [1972], Howes [1981], and Lee [1981] that all stated that industrial flares had measured efficiencies of approximately 95 % and greater [1986]. Other studies that attempted to include varying factors, such as wind speed and flow rate, concurred with these results [Johnson, 2001].

In 1996, the Alberta Research Council (ARC) released the results of a multi-year study on solution gas flares that concluded they were far less efficient than previously thought (as low as 62 %) and were emitting numerous toxic compounds produced through incomplete combustion [Stroscher, 1996]. Many of the reported toxins were complex polyaromatic compounds that have serious toxic effects. In addition, these compounds were reported to be present in high enough concentrations that over the period of operation of the flare, significant quantities could be deposited into the surrounding environment. In the ARC study, the tests were conducted on existing flare sites where it was not possible to rigorously control experimental variables. Further complications included mixed phase fuels and difficult sampling conditions. The conclusions derived from the ARC study contrasted with previous research into industrial flaring [Pohl (1986), Palmer (1972), Lee (1981), Siegel (1980), Howes (1981)] but could not comprehensively explain which operating conditions created these poor efficiencies and toxic emissions.

1.3: Emissions from Model Flares

As mentioned before, diffusion flames in crossflow have been investigated for a long time. Stability, length, and flame shapes for small (<10 mm) jets have been observed and modeled in many situations. With reference to jets larger than 10 mm or to the emission from jets in crossflow, very limited research has been conducted. While efficiency measurements have been conducted on industrial scale flares, these investigations were not conducted under controlled conditions. Tests that have been conducted for jets larger than 10 mm under controlled conditions have not investigated the overall emissions of these flame.

Since flaring is a very common in the petroleum industry, there is a lot of interest in how effective flaring is at disposing of waste gas. There is also a lot of interest in what compounds are produced as a result of incomplete combustion. The focus of the research described here has been to identify the main contributors of emissions from diffusion flames in a cross flow for jets with diameters between 10 and 30 mm.

1.4: Research Approach

The study by the ARC [Stroscher, 1996] prompted interest into the possible causes of the inefficiencies that were reported. Parameters that could affect the emissions from a flare include the exit velocity of the fuel gas and the effects of crossflow on the flare. The Flare Research Project at the University of Alberta was initiated to investigate the

efficiencies of scaled down model pipe flares under varied, but controlled, conditions in a controlled environment. The approach that was taken to investigate the toxic emissions was experimental, using scale model flare stacks in a controlled environment. The facility used is a 350 m³ wind tunnel, which was used to generate a laminar crossflow. The wind speed and gas jet exit velocity were both controlled, while temperature, atmospheric pressure, and gas composition were all monitored and recorded. Quartz tubes were used as scaled down model flare stacks. The fuels used were simple hydrocarbons, primarily methane (natural gas is often used) and propane, which could be blended with inert compounds, including N₂ and CO₂.

1.4.1: Facility

A 350 m³ wind tunnel with a test section of 1.2 m high and 2.4 m wide and is shown in Figure 1.6, was modified to house model scale flares and provide a controlled, adjustable, crossflow. The wind tunnel is capable of producing steady winds from 1 m/s to 35 m/s [Bourguignon, 1999]. The main drive is a 3.05 m diameter axial blower powered by a 150 kW DC electric motor capable of operating up to 850 rpm. The flame is located in the test section of the wind tunnel, which has been equipped with an alumina tile ceiling and a shielded floor to protect the structure from the flames. The walls are made of Plexiglas to allow visualization but are far enough from the flame that they are not damaged by heat.

Figure 1.6 shows the wind tunnel as it was originally designed to measure the efficiency of the flame burning in the test section. Standard operating procedures have the products of combustion thoroughly mixed with the air within the wind tunnel by 6 mixing fans placed in two separate mixing sections. After the flow was mixed, the flow was laminarized and accelerated in the plenum before it re-entered the test section where the burner tube was located. Prior to the flow reaching the burner tube, samples of gas from the wind tunnel could be withdrawn to analyze the composition of the gasses in the tunnel.

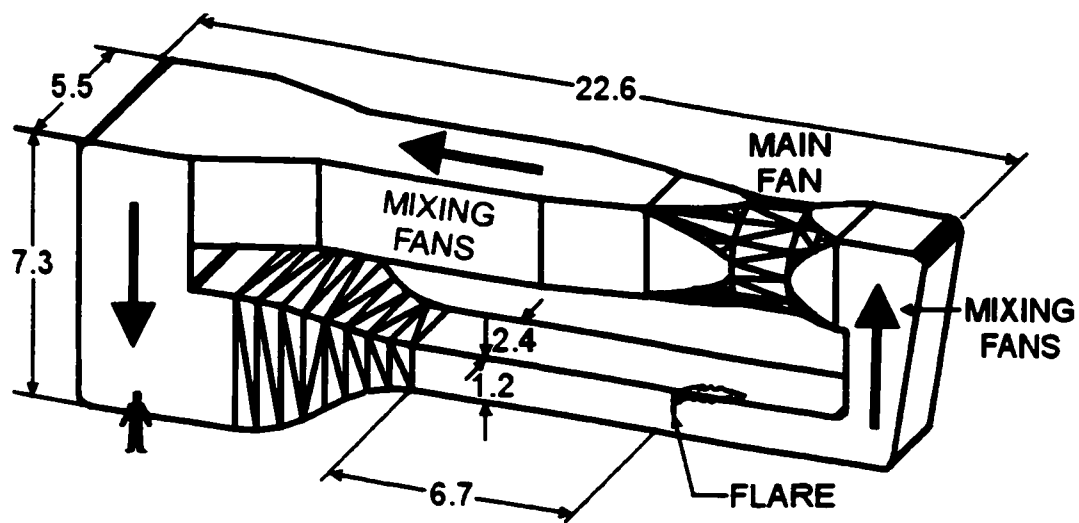


Figure 1.6: The combustion wind tunnel at the University of Alberta.

A more complete description of the facility is available in Appendix 1.

1.4.2: Model Flare Stacks

The model scale flare stacks used in these experiments were made from quartz tubes that extended approximately 0.85 m into the wind tunnel. Details of the four stacks are listed in Table 1.1. The model flare stacks were fitted with turbulence generators that produced the turbulent flow profile that would be expected with full scale flare stacks [Johnson, 2001].

Table 1.1: The dimensions of the quartz flare stacks used in these experiments

Outer Diameter (mm)	Inner Diameter (mm)
12.3	10.8
19.0	16.6
24.7	22.1
29.9	26.8

The fuels available for the test included propane, ethane, and natural gas. Various dilution gasses could be added to the fuel stream to alter the heating value, including CO₂, N₂, and air. Computer controlled mass flow controllers set and monitor the flow rate of each gas being supplied to the flare stack. A retractable hydrogen pilot flame was used to ignite the flare stream. For safety reasons, the fuel lines, dilution gas lines, and ignition lines are all fitted with shut off solenoids and the area around the wind tunnel was monitored by both ceiling and floor level gas detectors.

1.4.3: Additional Equipment

A series of gas analyzers continuously monitored the concentration of major gas components within the wind tunnel. CO₂, O₂, CO, and hydrocarbons were all monitored to both prevent any dangerous gas buildup from occurring and to monitor the depletion of O₂ within the tunnel. The analyzers were calibrated prior to use with Primary Master calibration gas ($\pm 1\%$ of the quoted bottle concentration) to ensure accuracy.

For experiments that required manipulation of equipment within the wind tunnel, a traversing mechanism was used in the tunnel. The mechanism could reach almost any place in the test section, but only operated automatically in a 2-D plane perpendicular to the tunnel flow. The position along the length of the test section was manually set prior to experimentation. The traverse was powered by a set of stepper motors and control could be done either manually with an indexer or by preprogrammed computer control.

The wind tunnel could be operated either as a closed loop facility or in a partially open loop configuration. After operating as a closed loop and collecting all of the products of combustion, a set of dampers could be opened between tests to replace the contaminated air within the wind tunnel with fresh air. When the wind tunnel was run in an open loop configuration, the dampers were opened allowing outdoor fresh to continuously replenish the air within the tunnel. This open loop configuration was used in experiments where the accumulation of combustion products was not desired.

1.5: Thesis Outline

The first step in measuring the emissions from a jet diffusion flame in crossflow was to identify the primary sources of emissions. Chapter 2 of this thesis provides a review of how various forms of emissions were investigated, and shows that particulate emissions were determined to be the primary contributor. Once the particulate emissions were determined to be a substantial contributor to emissions, a method was required to quantitatively measure the amount of particulate produced.

The means to measure the production rate of particulate was to collect the particulate plume generated by the flame and collect by filtration a portion of the particulate matter. Chapter 3 focuses on how the location of what is an essentially invisible particle plume was identified in order to collect it all.

The collection of the plume and measurement of the particulate emission rate is detailed in Chapter 4. Included in this chapter are the details of how the plume was collected, the construction of the apparatus, and the mass production results.

Chapter 5 describes the characteristics of the flare-generated particles. A Scanning Electron Microscope (SEM) was used to determine the size and shape of the particles. Additionally, the chemical composition of the particulate material was determined through chemical analysis.

Chapter 2: Preliminary Investigation

At the outset of this research three hypotheses were proposed to account for release of toxic emissions from scale model flares that were exposed to a crossflow. The first proposed mechanism was the release of toxic compounds that exist in the fuel stream and manage to avoid the combustion process altogether (fuel stripping). The second mechanism was the production and emission of vapor phase compounds, not present in the fuel stream, by the combustion process in the form of either volatile organic compounds (VOCs) or aromatic compounds. The third mechanism was the emission of solid particulate compounds as a result of incomplete combustion.

The fuel used in these model flare studies was either sales grade natural gas or commercial propane. The composition of the hydrocarbons accumulated in the wind tunnel during tests was determined by providing samples of gas from the wind tunnel in a 1 liter Tedlar bags to an independent lab for analysis with a gas chromatograph / flame ionization detector. Figure 2.1 indicates how the samples were extracted from the wind tunnel. A sample of the fuel gas used in the test was also provided to determine the exact composition of the fuel. The results indicated that nearly all of the vapor phase hydrocarbons that escaped the flame were those originally present in the fuel; only a small portion was changed by the combustion. It is important to remember that solution gas flared in the field may contain some toxic compounds such as H₂S and chlorine compounds. For fuel containing toxic compounds, the stripping of fuel would be important. However, within this study, the release of unmodified fuel stream compounds

was not a significant source of toxic emissions because the fuel streams were simple hydrocarbon mixtures that are not inherently toxic [NTP, #74-82-8].

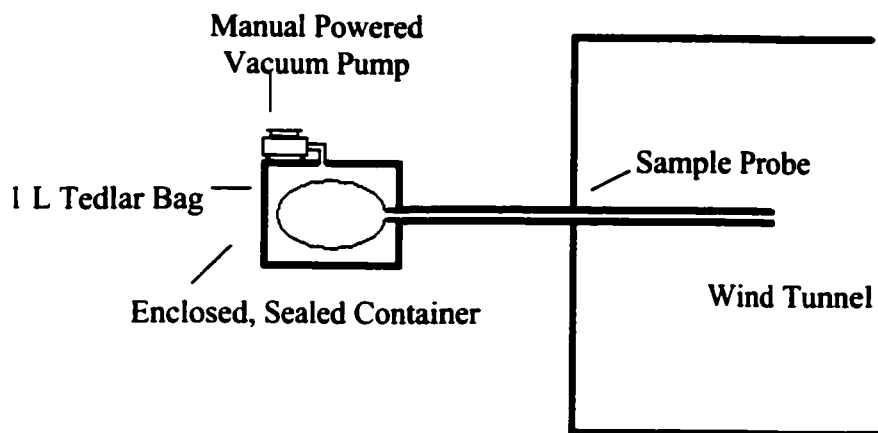


Figure 2.1: Manual sampling system for extracting 1 Liter samples.

The focus of this chapter is to describe preliminary experiments into the investigation of VOC, gaseous aromatic compounds, aldehydes, BTEX (Benzene, Toluene, Ethyl Benzene, and Xylene) and particulate emitted from model flares in crossflow. For the vapor phase, a prescribed mass of fuel was burned in the tunnel and then a well mixed sample of gas was extracted from the wind tunnel and slowly drawn through the appropriate absorbent tube to capture the gas phase compounds of interest. The contents of these absorbent tubes or filters were then analyzed using methods appropriate for each compound. The hydrocarbon flames produced negligible quantities of these volatile compounds. Only the low efficiency flames appeared to produce trace quantities of Benzene. It was concluded that volatile compounds produced by the flare were not significant contributors of toxic emissions from flames fueled with simple hydrocarbons.

To measure the particulate emissions, a portion of the plume was collected and drawn through a filter. Particulate material produced by combustion is considered to be toxic, mainly due to its small particle size. Chemical analysis of the filter indicated that the particulate material also contained polyaromatic compounds, which would cause additional toxic effects.

2.1: Measuring Emitted VOC, Vapor Phase Aromatic Compounds, Aldehydes, and BTEX

One of the possible paths for the emission of toxic compounds by flaring involves the production and emission of vapor phase compounds by the flame. These compounds are in the form of partially oxidized fuel, as with many of the aldehydes, or basic aromatic compounds produced in an oxygen deficient region of the flame. As the fuel approaches the flame zone, it is heated until it begins to pyrolyze (the process of compounds breaking down into radicals as a result of high temperature) [Glassman, 1988]. These radicals can react with oxygen or with each other to form new compounds. Time is also an important factor. When the fuel is exposed to an elevated temperature for a longer period of time, more pyrolysis will occur. Larger flames will expose the fuel to an increased temperature for a longer period of time, resulting in more fuel being pyrolyzed, which will result in more non-fuel compounds being produced. Diffusion flames produce more non-fuel compounds as the temperature is increased since the extra thermal energy will cause more fuel to pyrolyze into radicals, but the oxidation of the radicals is still limited by the rate at which oxygen can diffuse into the flame.

The most accurate method of measuring trace vapor phase components is to concentrate these compounds in an absorbent tube and analyze the contents of the tube. For these experiments a specified amount of fuel was burned in the closed loop wind tunnel, allowing the components to accumulate. After the fuel was burned, a sample of the gas from the wind tunnel was removed and a known volume of the sample was passed through the absorbent tubes. The absorbent tubes were then delivered to an independent lab for gas chromatograph analysis followed by either a mass spectrometer analysis or flame ionization detection analysis. The quantities of each compound in the absorbent tubes could then be used to estimate the emission rate of each compound by the flame.

2.1.1: Absorbent tubes

Measuring the flow through the absorbent tubes proved to be difficult as small and steady flow rates were needed to prevent breakthrough for the absorbent tubes (breakthrough occurs when the buildup of concentration over the course of the test allows some of the target material to escape from the tube). Figure 2.2 indicates the concentration of the collected material at progressive times during the sampling. T_1 represents the beginning of the sampling, T_2 would be sufficient time to conclude the experiment, and T_3 occurs if the sampling was conducted for too long a time period. To detect when breakthrough has occurred, most absorbent tubes are fitted with both primary and secondary absorbent material as seen in Figure 2.3. If any of the material that was being tested for appears in the secondary absorbent, then this indicates that breakthrough has occurred and the test

must be discarded. Reducing the sample flow rate through the tube so the primary absorbent has more time to absorb the selected material can prevent breakthrough.

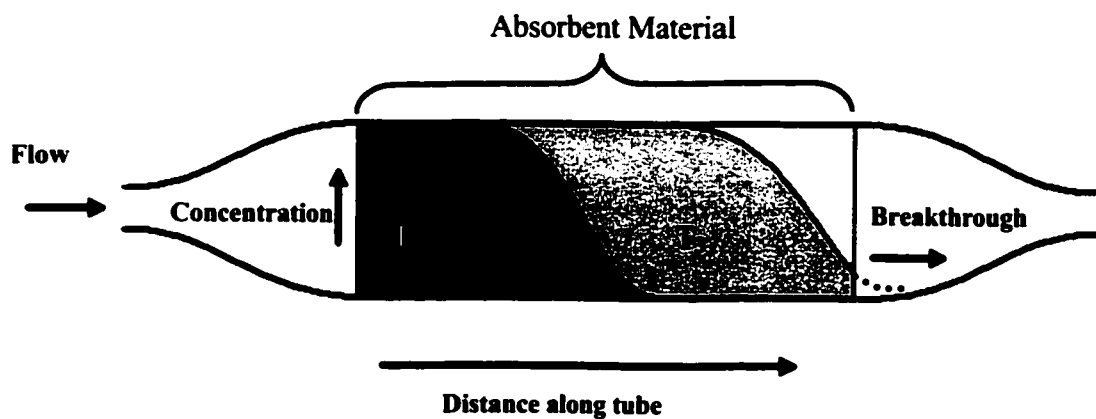


Figure 2.2: Progression of concentration along an absorbent tube.

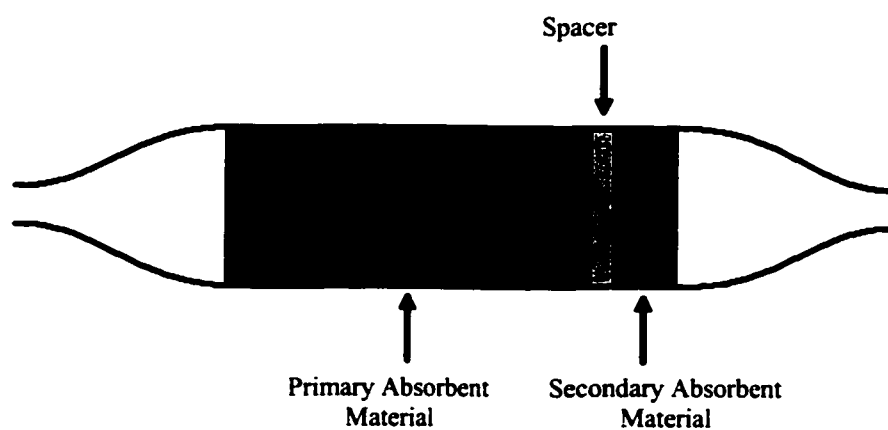


Figure 2.3: To detect breakthrough, absorbent tubes are fitted with both primary and secondary absorbent material.

To measure the low flow needed to prevent breakthrough in the tubes, a soap film flow meter was constructed. A 1.4 m, clear acrylic tube was filled with measured volumes of

water and the height of each volume was etched onto the side of the tube. The volume of the acrylic tube was calibrated with a pipette and etchings were placed every 10 ml. The device (as shown in Figure 2.4) was operated by passing the gas discharged from the sample tubes through a reservoir of fluid that would maintain a surface when gas was passed through it (a soap solution was used for this device). As the gas produced a bubble (or a soap film that separated the gas flow from the local environment) the volume of gas trapped by the interface was measured with the series of etchings on the side of the tube.

By measuring the volume of gas flow and recording the time, the flow rate of sample being drawn through the absorbent tubes could be measured. Measurements were made periodically throughout the test to ensure that the flow did not change. The total volume of fluid that passed through the absorbent tube was determined by multiplying the volume flow rate by the total time that sample gas was passed through the absorbent tube.

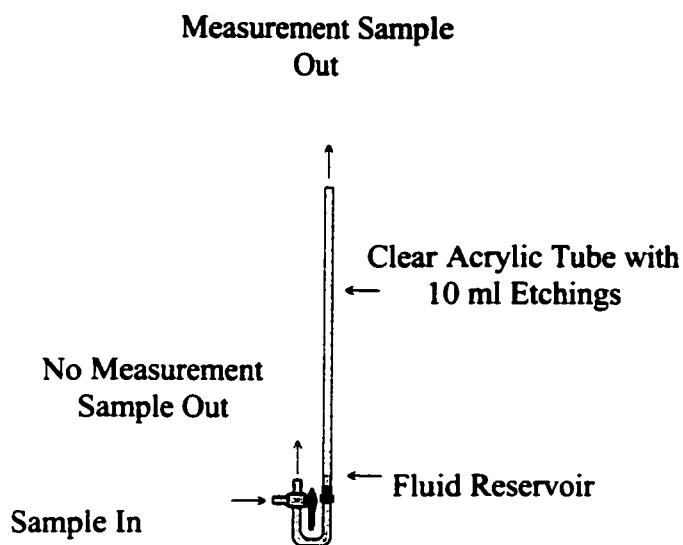


Figure 2.4: Low flow measurement device constructed to measure the flow through the absorbent tubes. Flow could be diverted through either the clear tube for measurement, or diverted away for normal operation.

2.1.2: Experimental Setup for Measuring Gas Phase Toxic Compounds

To measure production of gaseous compounds, a model scale flare was operated within the closed circuit wind tunnel facility. The wind tunnel had a volume of 350 m³ with a 1.2 m by 2.4 m test section. A 150 kW DC electric motor that used computerized control to maintain the cross wind speed generated the cross flow within the wind tunnel. For these experiments, fuel gas was introduced to the flame by the 22.4 mm diameter model flare stack made of fused quartz. The flare was active for a set amount of time to allow a buildup of gas phase compounds in the wind tunnel environment. Additional details of the tunnel, flow and fuel supply system are given in Appendix 1.

The large volume of the wind tunnel became a hindrance since it took a long time to pass a sample through the absorbent tubes and it was known that a facility of this size has a finite leak rate. This meant the time required to conduct the tests became a limiting factor. An 8 hour sampling (such as required by the BTEX, the absorbent used to absorb aromatic ring based compounds was very slow acting) would have significant errors introduced if the sample could not be protected from contamination from the surrounding for the duration of the sampling time. To prevent contamination, the collection and measurement of the VOCs was conducted by grabbing a 0.8 m³ sample in a series of Tedlar bags as shown in Figure 2.5 soon after the flare burning finished and the tunnel gases were fully mixed. The 0.8 m³ sample was collected by sealing the Tedlar bags in an enclosed box with a sample line connecting the deflated bags to the wind tunnel, then the box was evacuated with a vacuum pump, causing the Tedlar bags to rapidly inflate until they were filled with the 0.8 m³ sample. This sample was then drawn in parallel through a set of absorbent tubes using multiple vacuum pumps. A commercial analytical company chemically analyzed each sample in accordance with the NMAM (NIOSH Manual for Analytic Methods) standards and procedures listed below. For the trace hydrocarbon scan no specific standard was used so the method of analysis has been listed. The tests conducted were:

1. Aldehyde scan: The absorbent tube contained a silica gel, which absorbed and concentrated chemicals from the aldehyde group. A flow rate of 500 ml/min for 1 hour was required to prevent breakthrough. A minimum

concentration of $3.3 \mu\text{g}/\text{m}^3$ was required to reach the detectable limit. The full analytical procedure is described in NMAM 2016.

2. **BTEX (Benzene, Toluene, Ethyl Benzene, and Xylene):** The absorbent tube contained a charcoal within a glass shell, which absorbed single aromatic ring compounds. A flow rate of 50 to 100 ml/min for up to 8 hours was required to prevent breakthrough. A minimum concentration of $10 \mu\text{g}/\text{m}^3$ was required to reach the detectable limit. Each absorbent tube was fitted with a fibrous filter to prevent contamination by particulate matter that may contain aromatic compounds. The test was conducted in accordance with NMAM 1501.
3. **Trace hydrocarbons scan:** This measured the concentration of simple polymer compounds and reported the concentration of each (from C_1 to C_{12}) using Mass Spectrometry / Gas Chromatography. This test required a 1 liter sample of the gas to be analyzed, contained in a Tedlar bag. The sample was analyzed using gas chromatograph / flame ionization detection.
4. **Gaseous Polyaromatic Hydrocarbon Analysis:** Measured in accordance with NMAM 5515. The flow rate through the absorbent tube was 2 Liters/min for 100 minutes. A minimum concentration of $1.5 \mu\text{g}/\text{m}^3$ was required to reach the detectable limit. Identified the presence of PAH compounds in the gaseous medium within the wind tunnel.

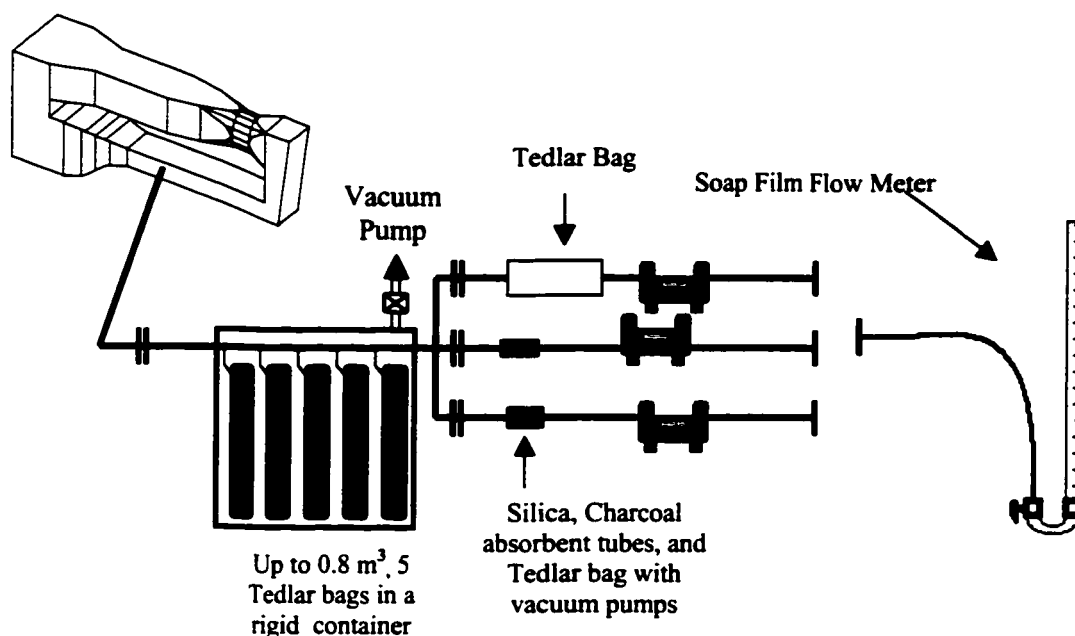


Figure 2.5: Gas sampling assembly including Tedlar collection bags, absorbent tubes, sample pumps and flow measuring device.

Once each absorbent tube was analyzed and the amount of each compound determined it was simple to determine the mass production rates of the compounds. The fuel to CO₂ conversion efficiency of each flare could be accurately estimated from the work done by Johnson (2001), and the initial and final concentration of CO₂ was known from the gas analyzers. Since the volume of sample that was passed through each tube was known, and the volume of the tunnel was known, the accumulation of CO₂ within the wind tunnel and the mass of the compounds in the tubes could be used to determine the total amount of each compound produced. The total amount of each compound was then compared to the amount of fuel that was burned and the time duration of the experiment, this would indicate the production rate of each compound that was investigated.

2.1.3: Tests Conducted

This preliminary investigation was designed to identify if certain compounds were emitted from the flame at detectable levels. A set of five tests using relatively extreme and varying conditions was run in the wind tunnel. Each test condition is listed and described in Table 2.1.

Table 2.1: Descriptions of the five tests conducted to identify the presence of gaseous and vaporous compounds, including the estimated efficiency of each test.

Test Number	Name	Description	Estimated Efficiency (Johnson, 2001)
1	Background Sample	This sample drew air from a recently purged wind tunnel and passed the air through the absorbent tubes to determine the background concentration of chemicals of interest.	-
2	High efficiency natural gas flare	2 m/s exit velocity jet (40 Liters/min) of natural gas in a 2 m/s crossflow.	97.7%
3	Low efficiency natural gas flare	2 m/s exit velocity jet (40 Liters/min) of natural gas in a 12 m/s crossflow.	87.4%
4	High efficiency propane flare	2 m/s exit velocity jet (40 Liters/min) of propane in a 4 m/s crossflow.	99.9%
5	Low efficiency propane flare	2 m/s exit velocity jet (40 Liters/min) of propane in an 18 m/s crossflow.	91.9%

The test series was designed to span natural gas and propane at both high and low efficiencies to determine if the combustion efficiency affected the production rate of non-fuel pollutants. All tests were conducted for 10 minutes using a 24.7 mm diameter stack fitted with a turbulence generator to produce a turbulent velocity profile.

2.1.4: Production Rates Required to Reach Detectable Limits

For each compound there is a detectable mass and this leads to a minimum required production rate to reach the detectable limit of each experiment. The minimum production rate was determined by calculating the concentration of each compound in the sample required to accumulate the detectable limit in the absorbent tube, assuming no leaks in the sample retention system and that breakthrough did not occur. The calculation for determining the minimal production rate is:

$$MPR = \frac{DL * V_{Tunnel}}{V_{Sample} * m_{fuel}}$$

MPR - The Minimal Production Rate (Mass Compound / Mass Fuel)

DL - Detectable Limit (Mass)

V_{Tunnel} - Volume of the wind tunnel (~350 m³)

V_{Sample} - Volume of the sample (i.e. ~48 L for the BTEX)

Table 2.2 lists the detectable limits and the corresponding specific production rates for each compound of interest.

Table 2.2: Minimal production rates required to produce detectable quantities of listed compounds.

Compounds	Detectable Limit	Minimum Production Rate (Methane)	Minimum Production Rate (Propane)
Benzene	0.5 µg	13 µg/g fuel	4.5 µg/g fuel
Toluene, Ethyl Benzene, Xylene	5.0 µg	130 µg/g fuel	45 µg/g fuel
Aldehyde Group	0.1 µg	4.12 µg/g fuel	1.4 µg/g fuel
PAH Compounds	0.3 µg	0.46 µg/g fuel	0.16 µg/g fuel

2.1.5: Results of Preliminary Tests

This preliminary series of tests produced results for trace hydrocarbon, aldehyde, BTEX, and PAH compounds.

The results of the trace hydrocarbon scans are listed in Table 2.3. They show that after the flare was run in the tunnel, the composition of the hydrocarbons corresponded to the fuel that was being combusted. The two tests with high efficiency flames each showed only a trace of methane. This could be attributed to the background gasses in the tunnel. About 2 to 4 ppm of methane naturally exists in the atmosphere and this was the dominant hydrocarbon found in the samples after a high efficiency test.

The tests with low efficiency flames indicated that a small amount of ethane was present in each test. The low efficiency natural gas test contained 127 ppm of methane in the sample and 4 ppm of ethane that was not present in the background but was present in the

fuel. The low efficiency propane test had 143 ppm of propane as well as 10 ppm of ethane, which was approximately the same ratio that was in the fuel [Johnson, 2001]. Based on this data set, it has been concluded that most of the hydrocarbons that were emitted from the flame were the basic hydrocarbons in the fuel, rather than being formed by the fuel pyrolysis. Johnson has proposed a mechanism for gaseous fuel being stripped and dispersed from a diffusion flame in crossflow [Johnson, 2001].

Table 2.3: Mole fractions of hydrocarbons found in carbon screen after tests were conducted.

Carbon Number	Test1: Background (PPM/Mole Fraction)	Test 2: High Efficiency Natural Gas (PPM/Mole Fraction)	Test 3: Low Efficiency Natural Gas (PPM/Mole Fraction)	Test 4: High Efficiency Propane (PPM/Mole Fraction)	Test 5: Low Efficiency Propane (PPM/Mole Fraction)
C ₁	4/1.00	4/1.00	127/0.97	4/1.00	12/0.07
C ₂	0.00	0.00	4/0.03	0.00	10/0.06
C ₃	0.00	0.00	0.00	0.00	143/0.87

The aldehyde screen results are listed in Table 2.4 and showed no significant increase in aldehyde composition. Each test showed the presence of aldehyde compounds, but the quantities showed no significant difference from the background sample. From this data it was concluded that while it was likely that the combustion process was forming aldehydes, they exist only in trace quantities.

Table 2.4: The compounds measured in the Aldehyde analysis
($\mu\text{g}/\text{absorbent tube}$).

Compound	Chemical Symbol	Background	Test 1: High Efficiency Methane	Test 2: Low Efficiency Methane	Test 3: High Efficiency Propane	Test 4: Low Efficiency Propane	Detectable Limit ($\mu\text{g}/\text{tube}$)
Formaldehyde	CH_2O	53	65	50	45	69	0.1
Acetaldehyde	$\text{C}_2\text{H}_4\text{O}$	4.1	3.8	5.5	6.6	16	0.1
Acetone	$\text{C}_3\text{H}_6\text{O}$	0.4	0.3	0.8	0.9	2.7	0.1
Propionaldehyde	$\text{C}_3\text{H}_6\text{O}$	22	19	26	29	17	0.1
Crotonaldehyde	$\text{C}_4\text{H}_6\text{O}$	<0.1	<0.1	<0.1	<0.1	<0.1	0.1
Butyraldehyde	$\text{C}_4\text{H}_8\text{O}$	<0.1	<0.1	<0.1	<0.1	0.8	0.1
Benzaldehyde	$\text{C}_7\text{H}_6\text{O}$	1.8	1.9	2.5	3.4	0.7	0.1
Isovaleraldehyde	$\text{C}_5\text{H}_{10}\text{O}$	<0.1	<0.1	<0.1	<0.1	<0.1	0.1
Valeraldehyde	$\text{C}_5\text{H}_{10}\text{O}$	<0.1	<0.1	<0.1	1.1	0.2	0.1
o-Tolualdehyde	$\text{C}_8\text{H}_8\text{O}$	<0.1	<0.1	<0.1	<0.1	0.5	0.1
m&p-Tolualdehyde	$\text{C}_8\text{H}_8\text{O}$	<0.1	<0.1	<0.1	<0.1	<0.1	0.1
Hexaldehyde	$\text{C}_6\text{H}_{12}\text{O}$	0.3	0.8	0.6	2.9	0.9	0.1
2,5-Dimethylbenzaldehyde	$\text{C}_9\text{H}_{10}\text{O}$	<0.1	<0.1	<0.1	<0.1	<0.1	0.1

The concentrations of gaseous aromatic compounds in samples of background air drawn from the wind tunnel were all below the detectable limit. This was expected since very low levels of these compounds are found in the atmosphere. Likewise, no aromatic compounds were detected in either of the high efficiency tests, as shown in Table 2.5. However, both of the low efficiency tests indicated trace quantities of benzene in the samples (1 μg per sample or twice the detectable limit). The BTEX tube required 100 ml/ min for 8 hours, so 48 liters of wind tunnel air contained 3.5×10^{-7} liters Benzene. Based on the calculated concentration this represented approximately 0.0009% mass conversion of the fuel into benzene for each of the low efficiency cases. The formation of benzene is a significant component in the proposed mechanism for the formation more complex aromatic compounds, since it represents the basic aromatic ring (C_6 in a ring structure) that polyaromatic compounds are constructed [Glassman, 1988].

When the bag samples were tested for certain PAH (polyaromatic hydrocarbons), analysis did not detect any of these compounds within the vapor phase of the wind tunnel gasses. The low vapor pressure of PAH compounds makes it very difficult for these compounds to exist in the vapor phase. For example Naphthalene has a vapor pressure of 50 Pa at 25°C [NTP #91-20-3] and most other PAH compounds do not have a quoted vapor pressure. At equilibrium for the temperatures and pressures that occurred in the wind tunnel, PAH compounds would condense to a non-gaseous form. Hence, if the combustion process produced PAH compounds, they would rapidly disappear from the vapor phase.

Table 2.5: Compounds found in the charcoal absorbent tube that is designed to absorb gaseous aromatic compounds.

Test Conducted	Background	Test 1: High Efficiency Methane	Test 2: Low Efficiency Methane	Test 3: High Efficiency Propane	Test 4: Low Efficiency Propane
Benzene	< Detectable Limit	< Detectable Limit	1.0µg Collected (D.L.=0.5µg)	< Detectable Limit	1.0µg Collected (D.L.=0.5µg)
Toluene	< Detectable Limit	< Detectable Limit	< Detectable Limit	< Detectable Limit	< Detectable Limit
Ethyl Benzene	< Detectable Limit	< Detectable Limit	< Detectable Limit	< Detectable Limit	< Detectable Limit
Xylenes	< Detectable Limit	< Detectable Limit	< Detectable Limit	< Detectable Limit	< Detectable Limit

In conclusion, the only significant hydrocarbons in the vapor phase were the fuel that was stripped from the flare stream. The quantity of compounds produced by the flare and detected by the BETX, aldehyde screen, and PAH screens were all below the detectable limits of the tests, except for a few of the aldehydes that were detected in trace quantities.

2.2: Particulate Phase Polyaromatic Hydrocarbon Investigation

PAH compounds are complex compounds containing multiple aromatic rings. These compounds tend to be very rare in the vapor form and when produced by a combustion process rapidly condense into a non-gaseous phase. As a result, PAH compounds are a component of the particulate material that was produced by the flame. Extensive research has been conducted into the composition of smoke produced by internal combustion engines [Kittelson, 1979], but investigation into smoke produced by flaring has been mostly limited to flares that are not in crossflow [Pohl, 1986] or to very small jets [Huang (1994, 1996, 1999), Brzustowski (1975), Gollahalli (1975)].

A recent report by the Alberta Research Council indicated that PAH compounds were a common pollutant produced by flames, but there were concerns about the experimental techniques [Stroscher, 1996]. Most of these concerns were a result the experiments being conducted in uncontrolled conditions, which generated questions about the reliability of the data produced.

For the work presented in this thesis, the model scale flares did not produce a visible particulate material plume, but this does not mean that particulate material were not present. It is possible for a very disperse particulate material plume comprised of fine particles to be present without creating a visible plume. As a result, the plume needed to be sampled to determine if particulate material or PAH compounds were present.

The experiment conducted to examine the presence of PAH compounds involved sampling a portion of the plume and filtering the particulate matter from the gas phase. The sample was extracted from the tunnel through a 152 mm diameter sample tube into a filter chamber as shown in Figure 2.6. The 152 mm sample tube was positioned to collect what was believed to be the center of the particle plume, ensuring that some of the particles would be collected. Beyond the sampling tube, the gas flow was expanded into a 500 mm diameter filter chamber and a 600 mm diameter Whatman paper filter rated to remove particulate with a mean diameter of 11 μm . While a majority of the particles produced by the plume were expected to be much smaller than this, only the presence of PAH compounds was being investigated at this time so not all the particles were needed. The expansion and drop in gas velocity was necessary due to the differential pressure generated by the filter.

A 5 hp centrifugal blower generated the suction. This blower did not generate significant volume but it was sufficient to draw a plume sample through the filter. With the filter in place, the blower would pull 4.5 m^3/min with a differential pressure of 6.3 kPa, which

allowed each test to be conducted in a 4 m/s cross flow and still closely match the crossflow velocity.

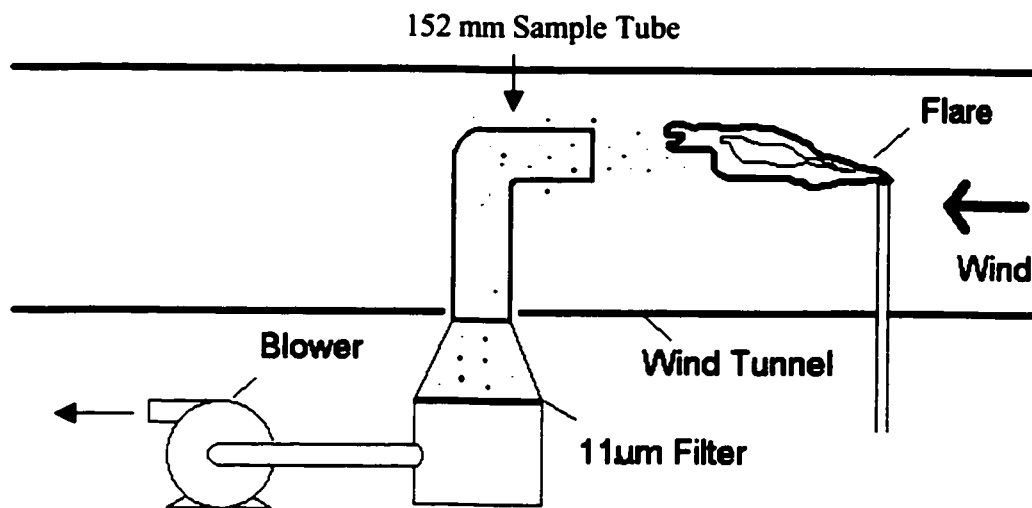


Figure 2.6: The original system used to sample for the presence of PAH and particulate material produced by a propane flame.

Tests were conducted with natural gas and propane fuel. Tests with methane showed negligible particulate material production. Two tests were conducted with propane flares:

1. A high efficiency test comprised of a 20 liters/min propane flame from a 24.7 mm model flare stack, which corresponds to a 1 m/s exit velocity. This test was conducted for 7 min (140 liters of propane).
2. A low efficiency test comprised of a 10 liters/min propane flame from a 24.7 mm model flare stack, which corresponds to a 0.5 m/s exit velocity. This test was conducted for 10 min due to the lower exit velocity. The different fuel flow rate was selected due to the limit of 4 m/s cross flow. It has been

shown that efficiency is related to the momentum ratio [Johnson, 2000], so reducing the exit velocity would reduce the efficiency even if the cross flow remains the same.

The filters were analyzed and the results listed in Table 2.6 indicate the mass of PAH found on each filter. While the listed masses are very small, it must be noted that only a portion of the plume was collected and even less of the mass was filtered. The presence of detectable quantities of these compounds in the sample indicates that the particulate material and the embedded PAH compounds within the particulate material represent a significant component of the toxic emissions from the model scale flares.

Table 2.6: Masses of PAH found by MS/GC analysis on each paper filter.

Chemical Compound	Mass in High Efficiency Test (µg)	Mass Low Efficiency Test (µg)	Detectable Limits (µg)
Naphthalene	0.39	0.33	0.05
Acenaphthene	0.05	0.05	0.05
Acenaphthylene	0.05	0.05	0.05
Fluorene	0.33	0.23	0.05
Phenanthrene	0.52	0.67	0.05
Anthracene	0.05	0.05	0.05
Fluoranthene	0.30	0.44	0.05
Pyrene	0.36	0.59	0.05
Benz(a)anthracene	0.05	0.05	0.05
Chrysene	0.05	0.05	0.05
Benzo(b&j)fluoranthene	0.05	0.15	0.05
Benzo(k)fluoranthene	0.05	0.05	0.05
Indeno(1,2,3-cd)pyrene	0.05	0.11	0.05
Benzo(a)Pyrene	0.05	0.09	0.05
Dibenz(a,h)anthracene	0.05	0.05	0.05
Benzo(g,h,i)perylene	0.05	0.31	0.05

2.3: Preliminary Conclusions

Based on tests described here, the production of toxic compounds by sub-scale model flares was a result of the emission of particulate material and particulate phase compounds. From the tests conducted a number of other conclusions were derived:

- Fuel stripping is a significant contributor to inefficiency, but the simple hydrocarbons used to fuel the model scale flares have a very low toxicity, so they do not contribute to the toxic emissions of the flares.

- Volatile organic compounds could not be detected in quantities that warranted further investigation.
- The emission of vapor phase polyaromatic compounds could not be detected.
- The particulate produced by the flares contained measurable quantities of polyaromatic compounds. These compounds are very toxic and the presence of these chemicals increases the toxicity of the smoke emitted by the flame.

Based on the results from the preliminary experiments, it was concluded that future experiments would focus on the collection and analysis of the particulate and smoke emission from the flame.

Chapter 3: Particle Plume Mapping of Scale Model Flares

After it was determined that the particulate material emitted from the flame was responsible for a majority of the toxic emissions released by the model scale flare, quantitative measurements needed to be made to determine the mass emission of these toxic compounds. The most reliable method to do this measurement was to separate the particulate material from the gas flow onto a very fine filter and gravimetrically measure the change in filter mass. To produce global measurements of particulate production, a means of locating the whole plume was required. Measuring the plume at a single point was not acceptable since the plume of a flare is not homogenous so a single point measurement would not provide accurate global estimations of particulate material production. It is important to remember that the plumes that were being observed did not show visible signs of particulate emission, which increased the difficulty of locating the plume. Once the plume was located, the whole plume and all the particulate material could be collected as part of determining the total particulate material mass emitted.

To detect the particle plume, an experimental technique used to measure particulate emissions from diesel IC engines was adapted to the problem of locating the particulate plume [Fukushima, 2000]. This method involved converting a Fast Flame Ionization Detector (FFID) to measure particle number density. This approach was used to systematically sample across the wind tunnel downstream of the flame to identify the spatial structure and boundaries of the particle plume emitted from the flame.

This chapter describes a number of potential techniques for locating particle plumes that were competing with the FFID technique. The modifications required to convert the FFID from a gaseous hydrocarbon detector into a particle detector are then described and the results are presented. Based on the results presented in this chapter, it was determined that the particle plume coincided with the thermal plume in all of the cases tested.

3.1: Potential Sampling Techniques

A number of techniques were considered for locating the particle plume of a scale model flare:

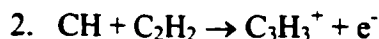
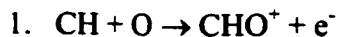
1. Sample multiple points within the tunnel and filter each to determine the amount of particulate matter passing through that point. If done in a systematic process, a particle map could be generated based on the amount of particulate material collected at every location. In addition to finding the location of the particle plume, the mass of particulate matter produced at each location would be determined allowing for the possibility of estimating of the total particulate production. However, a filter requires a minimal amount of material for reliable mass measurement (minimum of a few hundred micrograms) and, due to the disperse nature of the particle plume, there would be a lengthy sampling time. Such a technique was judged to be too time consuming to be effective for use in this study.

2. A laser extinction technique could be used to measure the density of non-gaseous material in the path of the beam [Mullholland, 2000]. By firing a laser of a known intensity through the plume of the flame and measuring the strength of the beam with a detector, the particle density along the path could be determined. To incorporate this system in the wind tunnel where the experiments were taking place without causing a significant disturbance to the flow would require replacing a section of the walls and frame of the wind tunnel with the equipment required to allow an unobstructed path for the laser beam to follow. The beam would also need to enter and exit the wind tunnel at different positions and angles to accurately map the boundaries of the particle plume. It was determined that this technique would not be used due to the availability of alternatives.
3. Fast Flame Ionization (FFID) techniques were being developed to determine the amount of particulate material in diesel engine exhaust during transient operating conditions [Fukushima, 2000]. A dual channel FFID that could be modified to detect particulate matter was available. While the conversion process required extensive modification to the sampling system, it was deemed the best method available.

3.2: Fast Flame Ionization Detection

A flame ionization detector is typically used to determine the concentration of hydrocarbons in gas samples. When carbon is combusted a complex series of reactions occurs. Some of these reactions produce free electrons that can be detected with an

ionization detector [HFR400 Fast FID User Manual V2.1]. The two reactions most commonly associated with free electron production are:



A fixed flow of the gas sample being measured is passed through a hydrogen flame that has a small ion detector surrounding it. When the hydrocarbon is oxidized, the ion detector detects the ions that escape the flame and attach to its surface. The ion current can be used to indicate the concentration of hydrocarbons in the gas sample. By altering the calibration or using various conversion factors, different hydrocarbons, alcohol, or carbon containing acids could be detected [HFR400 Fast FID User Manual V2.1].

In a fast flame ionization detector, the sampling lines are shortened and the combustion chamber is located close to the point being sampled. The diameters of the lines and the sizes of the chambers are scaled down to reduce mixing and increase frequency response. The result is a device that can respond to very rapid changes in hydrocarbon concentration while exposing the sample to a minimal amount of transport through sampling lines.

If a particle containing solid carbon passes through the flame, the increase in carbon combustion rate produces a spike in the signal. Normally the sample capillaries of FFID devices are designed separate particles and thus prevent particle noise. By redesigning

the sample capillaries and sample transport mechanism it is possible to use the system as a carbon particle detector.

3.2.1: System Modifications to the FFID

The base instrument on which these modifications were made was a Cambustion HFR400 FFID. The only modification of the FFID was to change the sampling tube to allow the system to detect particles. Originally the combustion chambers on the HFR400 were equipped with tee-style sampling tubes, as shown in Figure 3.1. The tee-style sampling tube prevented particles from entering the flame by extracting a small portion of the sample through a sharp turn. The momentum of the particles would carry them past the turn and away from the flame. These particles would then be deposited themselves in the constant pressure chamber.

The sample tube was contained within a constant pressure chamber at the base of the combustion chamber. The constant pressure chamber is designed to maintain the stability of the flame when pressure fluctuations occur at the sampling location. Such fluctuations are very common when sampling from the combustion cylinders of IC engines, but rarely occur when sampling from the plume of the flame. Unfortunately, removing the constant pressure chambers reduced the flame stability when a sample was passed through the detector. To maintain the hydrogen flame the constant pressure chamber needed to be retained when the modifications were made to the sample tube, as a result, the flame remained very stable.

Sun and Chan [1996] developed a straight through sampling tube, as shown in Figure 3.2. The straight tube design did not have any bends to separate particles from the flow [Brockmann Contract, # DE-AC04-76DP00789] (the pressure stabilization openings into the constant pressure chamber maintain the stability of the flame under varying sampling conditions). The internal diameters for the sample capillary and the expansion tube were 0.25 mm and 1.27 mm respectively. This study used tubes with similar, although the modules used with the available dual channel FFID were able to accommodate a larger expansion diameter.

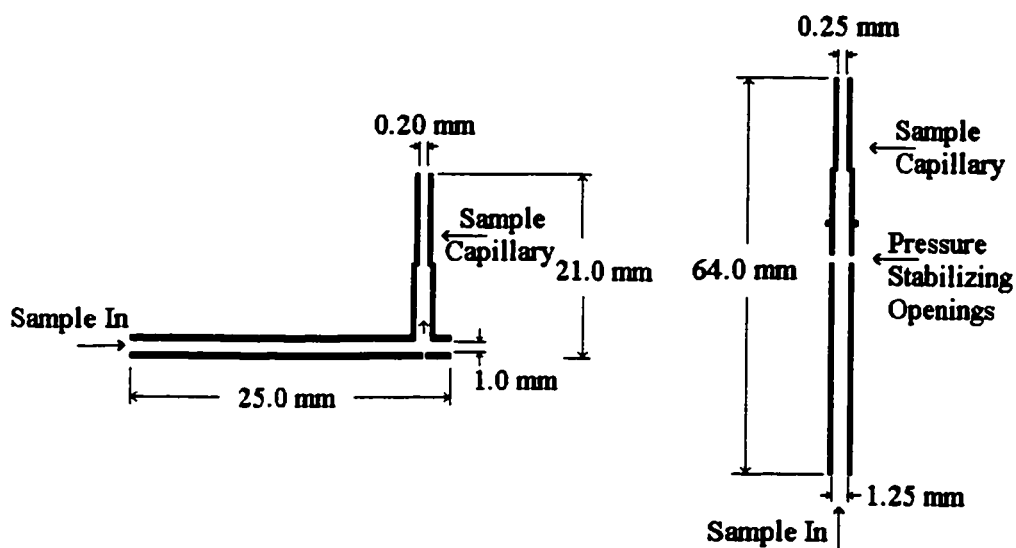


Figure 3.1: Combustion Tee-Top FFID tube

Figure 3.2: Modified straight flow FFID tube

The original constant pressure chambers were developed to accommodate the tee style FFID sampling tubes that were included in the original design. When the tee-style tubes were replaced with the straight tube configuration, the sample capillary was inserted through an opening in the original constant pressure chambers. This opening was used for maintenance access to the FFID sampling tubes if the sample capillary were to become blocked and was normally sealed with a brass plug. The original and final configurations of the module are shown in Figure 3.3. The final configuration directed the sample flow through this opening into the straight flow sample tube through the bottom of the constant pressure chamber, avoiding any additional redirections of flow that would result in the loss of particles [Brockmann, Contract # DE-AC04-76DP00789].

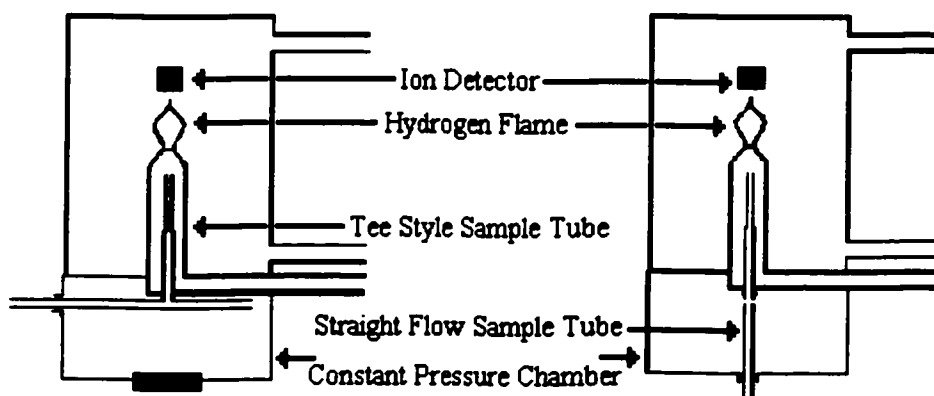


Figure 3.3: The initial and final configuration of the combustion chamber on the FFID modules.

3.2.2: Particulate Material and Gas Phase Hydrocarbons

The modified FFID was capable of detecting both particulate material and gas phase hydrocarbons. The intent of the design was to determine the number of carbon containing particles in the sample, not the gaseous hydrocarbon content. To eliminate the signal generated by the gaseous hydrocarbons within the sample, Sun and Chan proposed using a FFID module to analyze a filtered (particulate-free) portion of the sample [Sun, 1996]. The resulting signal corresponded to gaseous hydrocarbons. This could be subtracted from the signal generated by a second FFID module analyzing an unfiltered sample. Both modules are shown in Figure 3.4. This was the technique that was adopted for this study.

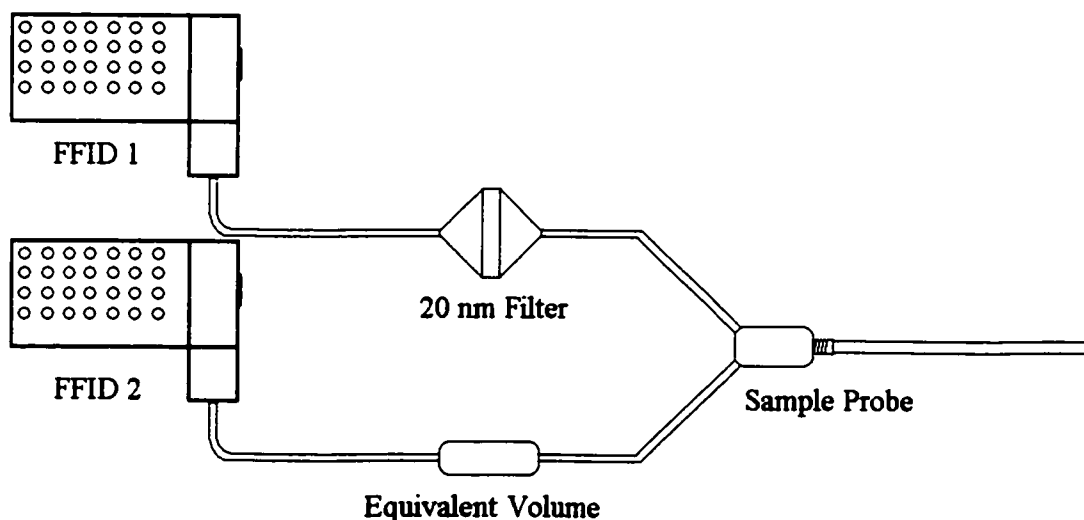


Figure 3.4: Both FFIDs were mounted in parallel with a 20 nm filter fitted to one module and a dead volume fitted to the other.

The smallest particle that was believed to occur was a single spherule, which has a diameter of 20 – 50 nm. Based on this assumption, a Whatman Anodisk™ filter with a pore size of 20 nm was selected to filter the gas stream through one of the FFIDs.

3.3: Matching Time Response

To properly process the two signals that are being generated by parallel FFID modules, the flow to each module must be the same. Since one of the modules has both a filter and filter holder there would be a large difference in pressure between the sample as well as a difference in lag time due to differing volumes the sampling system.

To reduce the variance in differential pressure between the two systems, each module was fitted with a 0.3 m long flow tube with an internal diameter of 120 μm . In comparison the pressure drop across the filter was very small compared to the pressure drop across this flow tube. This reduced the difference in pressure between the filtered and unfiltered system to a negligible amount, and produce equivalent flows through the two modules.

A static volume chamber was added to the sample tube of the unfiltered FFID to eliminate the volume difference. The chamber had the same volume as the filter holder and the internal measurements were designed to eliminate any recirculations that could develop in the flow. These two modifications allowed for the inclusion of the filter

within one sample flow without causing significant differences in the flow properties of the two sample streams.

3.4: Processing of Dual Channel FFID Signals

The FFID signals from the dual FFID system are illustrated in Figure 3.5. The signal generated by the module analyzing the filtered sample is depicted in gray and does not show any significant peaks. The small fluctuations in the signal attributed to small changes in the background concentration of gaseous hydrocarbons at the point being sampled. The unfiltered signal is depicted in black and shows many peaks that are not present in the filtered signal. To eliminate the background noise from the signals, the standard deviation of the filtered signal was determined. A threshold of 6 standard deviations was set to differentiate between the noise and the peaks.

The number of samples that were needed to complete a grid determined the number of standard deviations that the threshold was set to (most of the sample grids used over 350 sampling points, each with 60 seconds of sampling). If the sample size remained the same, setting the threshold to 6 deviations would mean that (statistically, if the distribution of the noise was normal) one peak per contour would result from random noise instead of a particle.

When processing the dual channel FFID signals, the filtered signal was subtracted from the unfiltered signal and the resultant signal was set to zero for all values less than the

noise threshold. The resulting signal is depicted in Figure 3.6. The spikes that remained were attributed to particulate matter in the sample flow. By counting the spikes, the number of particles that passed through the unfiltered FFID could be determined.

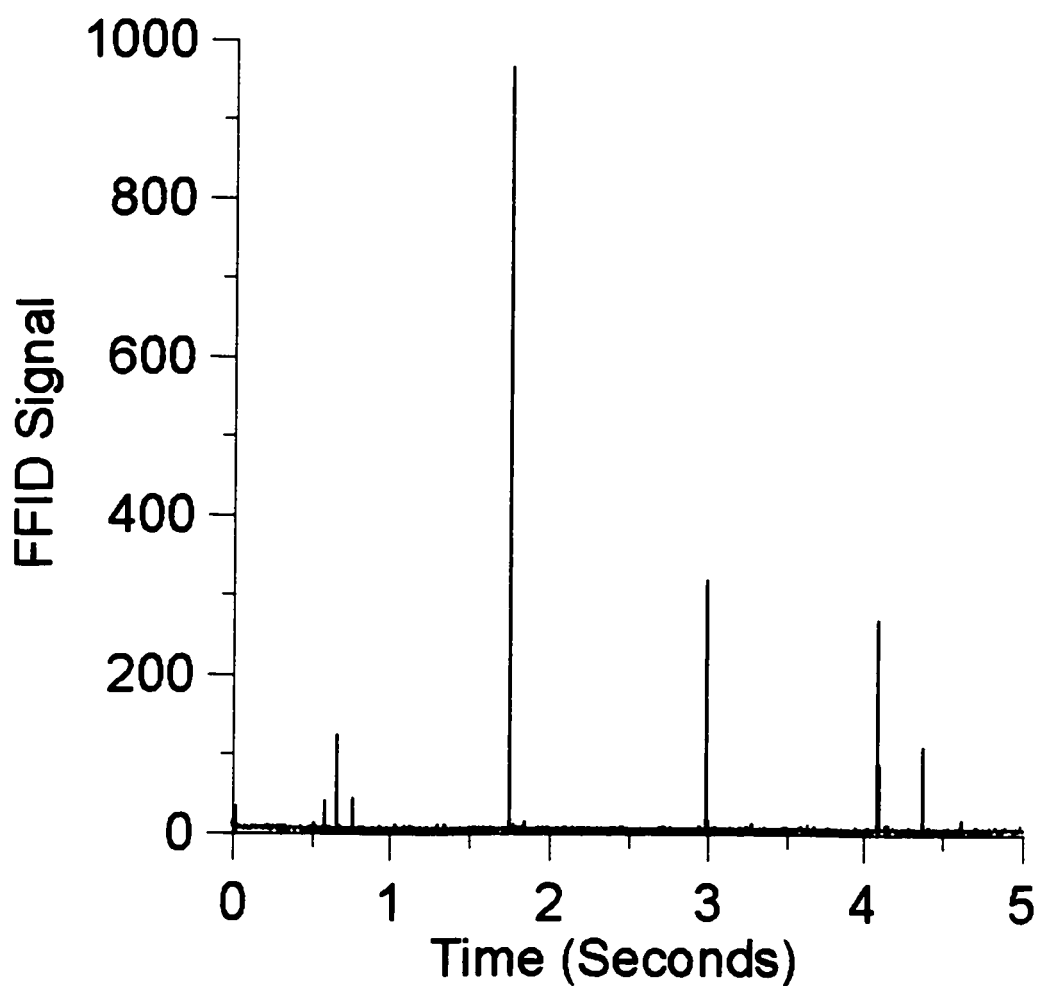


Figure 3.5: A sample of the signals produced by the FFID. The filtered sample is depicted in gray and indicates no peaks. The unfiltered sample (depicted in black) has a spike for each particle that passed through the flame.

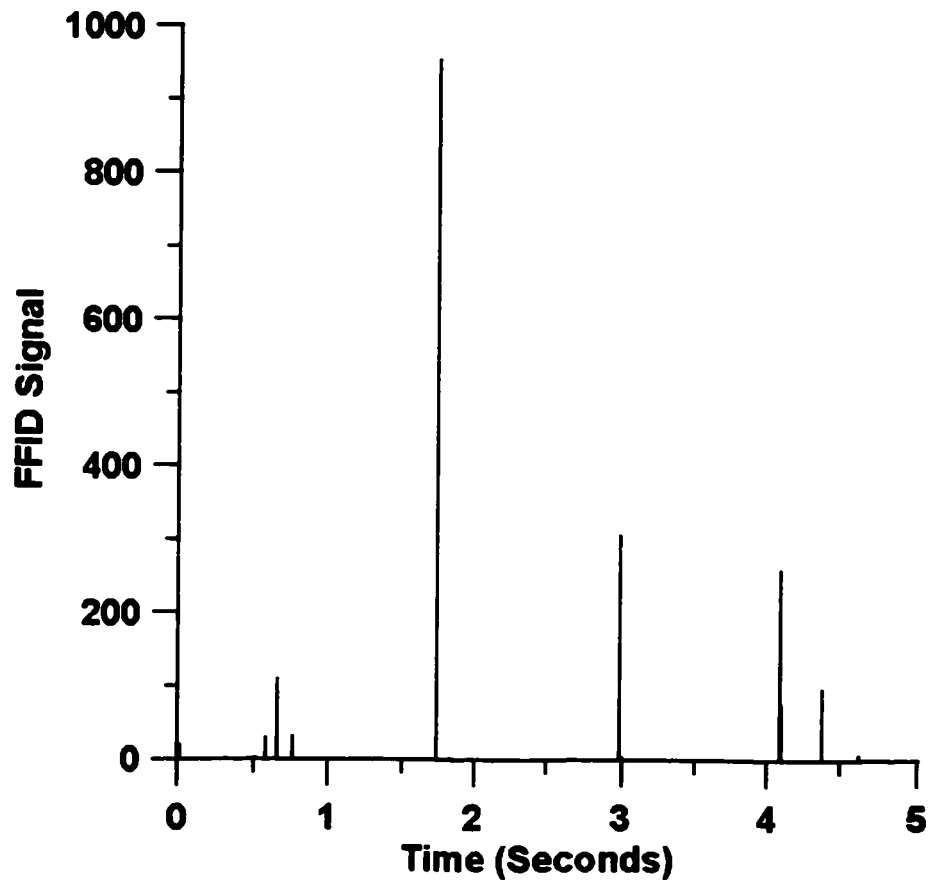


Figure 3.6: The processed signal, only data produced by material that was stopped by the filter appears in the data.

3.5: Mean Peak Frequency

Counting the number of peaks detected by the FFIDs that exceed the noise threshold produced a qualitative map of the particle plume downstream of a scale model flare. The number of peaks generated in a 60 second sample period (approximately 216000 samples when sampling at 3600Hz) is referred to as the peak number. Due to the large number of samples and relatively small number of peaks, two peaks would rarely, if realistically ever, appear in close enough proximity to each other to be counted as a single

peak. By dividing the peak number by the total sampling time the dependency is removed, resulting in the mean peak frequency.

If the mean peak frequency is measured in multiple locations, such as a grid with 2 cm spacing, then a contour could be generated. Figure 3.7 shows a particle map of a mean peak frequency contour generated by a propane jet with an exit velocity of 0.5 m/s burning in a 4 m/s crossflow. The sampling plane was located 2.3 m downstream from the stack, beyond the flame that extended approximately 2 m downstream. The model flare stack used in this experiment was 64.5 cm tall, so the point of maximum particle density is approximately 25 cm above the top of the stack.

For comparison, the thermal plume for the same flare is shown in Figure 3.7. The thermal plume was mapped using a Type K thermocouple mounted with the sampling probe. Both the particle and temperature contours correspond to a “kidney” shaped plume that is characteristic of low cross wind flows. However, the peak values of the two plumes are different in position. The maximum temperature in the thermal plume is located within the core of the counter rotating vortices [Poudenx, 2000]. In contrast, the maximum density of particles is located in the upper center of the “kidney”. This location is directly behind downstream of the tail of the flame.

It had been shown that increasing the crossflow velocity changes the shape of the thermal plume [Poudenx, 2000]. Figure 3.8 shows the particle contour and thermal contour plots for a 0.5 m/s propane jet in a 6 m/s crossflow. The probe was located 2.2 m from the

stack, or approximately 50 cm beyond the flame under these conditions. As expected, the thermal contour had changed as a result of the increased cross flow. The thermal plume reduced in width and became more pronounced in the wake region directly behind the stack. The particle plume had corresponding changes, mimicking the shape of the thermal plume. The maximum peak frequency was still located directly behind the flame tip, which implies that this region is responsible for a majority of the particulate material emission, regardless of the crossflow. The peak frequency had also been reduced to approximately 15% of the corresponding density for 4 m/s crossflow maximum, suggesting a reduction in particulate material emissions similar to the theories developed by Ellzey using smaller diameter jets [1990]. When the crossflow was increased, the amount of fuel combusted in the mean tail of the flame becomes reduced as the combustion in the recirculation behind the stack becomes more prominent, which could result in a reduction in the particulate material production. Increased mixing could also be a factor as more air is forced into the combustion region by the crossflow.

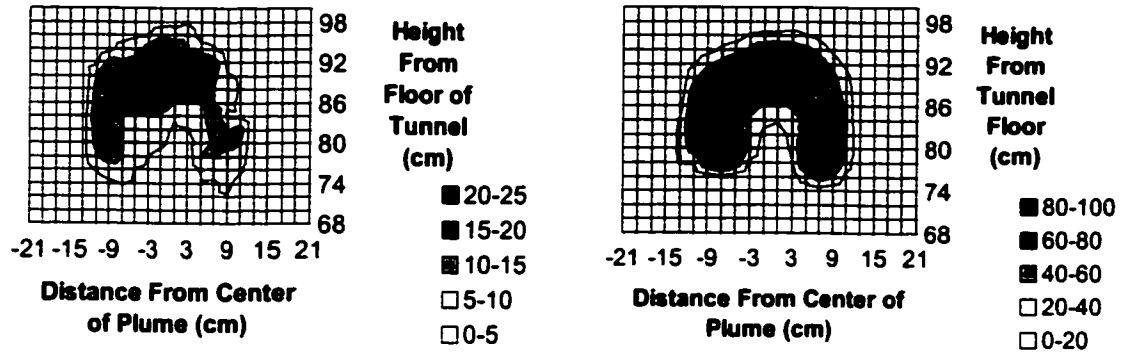


Figure 3.7: Peak Frequency contour (in Hz) generated using Dual FFID Detector. Propane flame, 0.5 m/s jet velocity in a 4 m/s crossflow. Detector positioned 2.30 m downstream from model flare stack. Temperatures measured with a Type K thermocouple mounted in conjunction with the probe. Temperatures in °C.

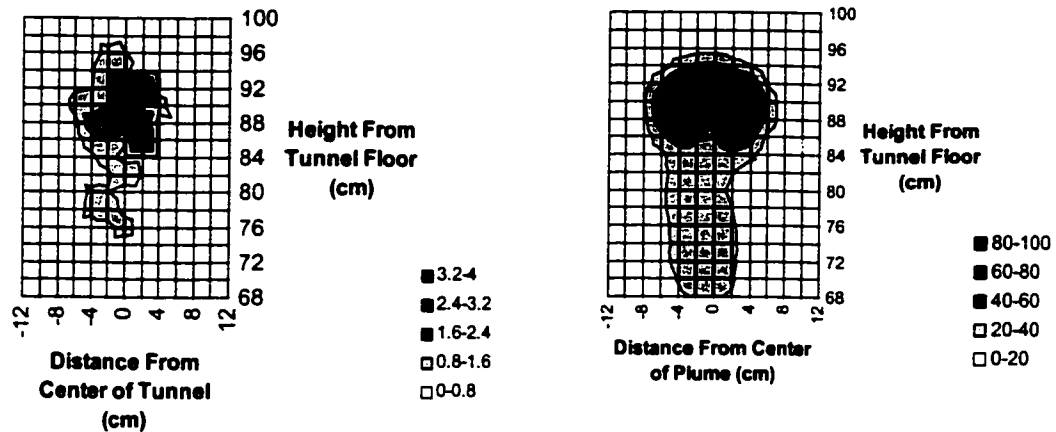


Figure 3.8: Peak frequency contour (in Hz) for a 0.5 m/s Propane jet in a 6 m/s crossflow. Stack is 0.8 m in height and the contour is 2.20 m downwind of the stack. Temperatures measured with a Type K thermocouple mounted in conjunction with the probe. Temperatures in °C.

3.6: Plume Expansion

The main goal of mapping the plume was to locate the particle plume so that it could be collected and the mass production of the particulate matter determined. There were only a few meters of space behind the flame in the tunnel to collect the plume so the rate of plume expansion was only needed in this location. It was originally determined that the location of the particle plume corresponds to the location of the thermal plume directly after the flame, but an examination of the expansion of each plume was needed to ensure that this was true for varied distances behind the flame. To visualize the rate of expansion, each plume was mapped at varying distances from the stack: directly behind the flame (230 cm from the stack), 20 cm downstream of the first measurement (250 cm), and finally at the furthest possible plane of collection (350 cm from the stack).

Figures 3.9-3.11 show both the particle plumes and the thermal plume generated by a 10 liters/min propane jet from a 24.7 mm flare stack in a 4 m/s crossflow for different distances from the stack. As the plume moves away from the flare stack, both the thermal and particle plumes expand. The primary discovery was that the boundaries of the particle plume continued to correlate with the thermal plume for all of the possible collection distances from the flare stack. This indicated that within the possible range of collection distances in this wind tunnel, collecting the thermal plume would collect the particle plume.

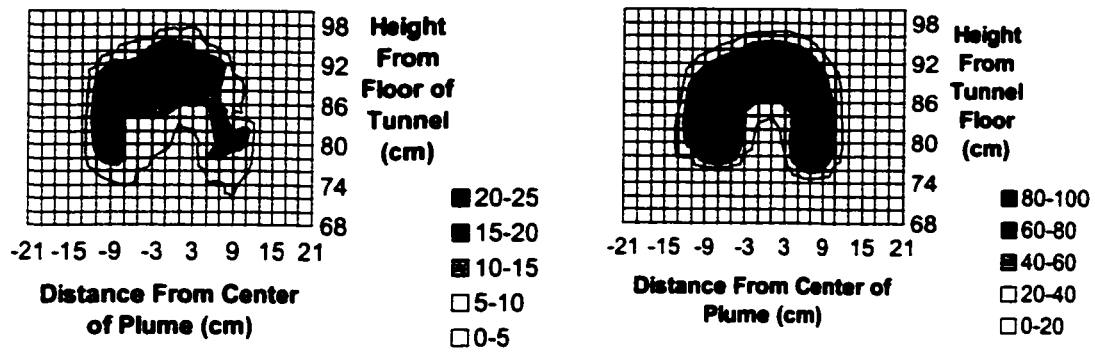


Figure 3.9: The peak frequency contour (left) and the thermal contour (right) at a distance of 230cm downstream of the flare stack.

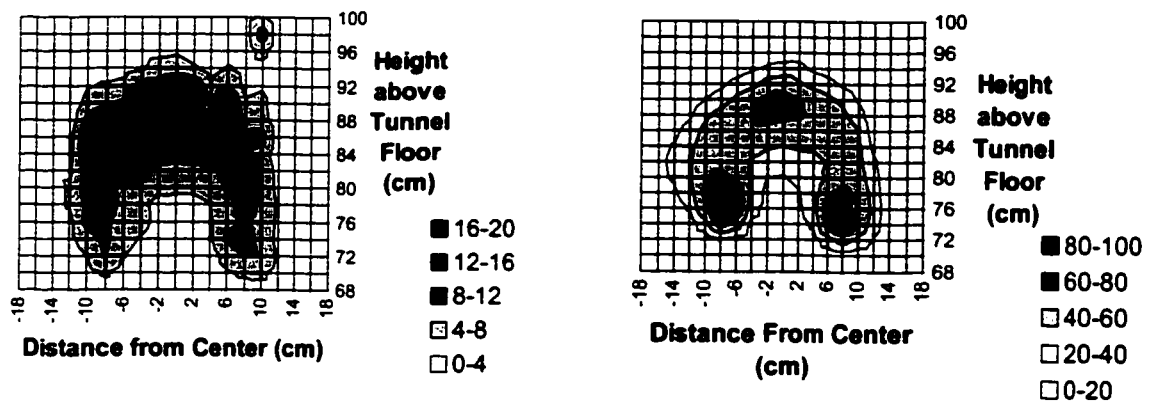


Figure 3.10: The peak frequency contour (left) and the thermal contour (right) at a distance of 250 cm downstream of the flare stack.

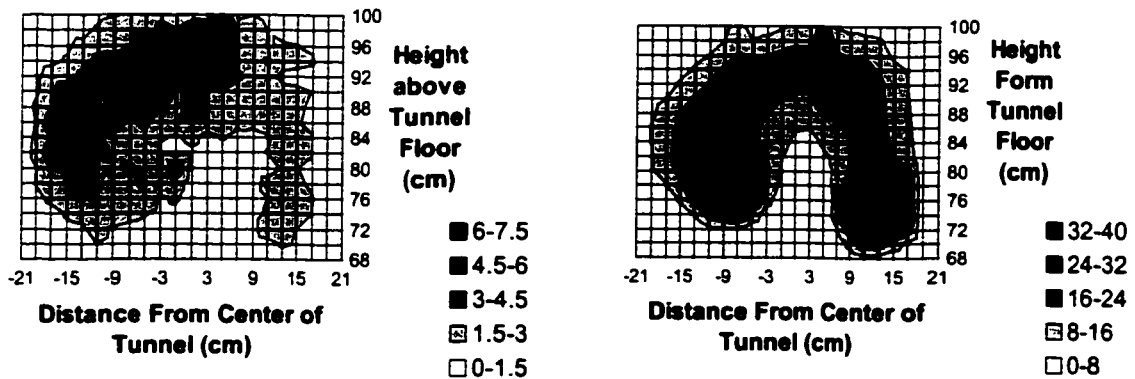


Figure 3.11: The peak frequency contour (left) and the thermal contour (right) at a distance of 350 cm downstream of the flare stack.

3.7: Plume Mapping Conclusions

The FFID was able to map the spatial distribution of the particle plume. Based on the mean peak frequency contours produced with the dual channel FFID, it has been determined that the boundaries of the particle plume are contained within the boundaries of the thermal plume for the crossflow velocities selected (2 m/s to 6 m/s). If a collection system is designed to collect the entire thermal plume, then the entire particle plume will also be collected. It was found that the peak particle concentration is always directly behind the tail of the flame for the conditions studied. The peak temperature changes location within the thermal plume as the crossflow velocity is changed, but the peak particle concentration was always found behind the tail of the flame, regardless of crossflow velocity.

As the crossflow was increased, the quantitative concentration of particles decreased more radically than could be explained by direct dilution. This would suggest that as the crossflow was increased, the number of particles emitted was reduced.

Chapter 4: Particulate Emissions Measurement

This chapter presents the measurements of the mass emission rates of particulate matter by model scale propane flares in a cross flow. It was decided that gravimetric measurements were the most reliable means of measuring particulate material production. However, the plume was too large to filter in its entirety so a system was developed to provide quantitative measurements of particulate material emission rate based on a sample of the particle plume. This chapter describes the measurement technique, and presents the results of these experiments.

4.1: Particulate Material Measurement Overview

In the process of locating the particulate material plume (Chapter 3), it was shown that the particle plume does not have a uniform spatial distribution. Single point sampling within the plume could not yield accurate mass emission rates since it would indicate a local mass emission, not a global mass emission value. The strategy adopted to measure the global particulate material emission rate of the flame was to collect the entire plume in a sampling duct, mix the flow into a homogeneous mixture, then isokinetically extract a known fraction and filter that sample.

Designing a system to measure the mass production of particulate material involved a number of challenges. With the location of the plume known, a collection system was designed to collect the entire plume. Within the collection system, the gas flow

containing the plume was mixed to create a homogenous mixture. The velocity of the gas flow was measured to establish the isokinetic sampling rate at different points along the system. A filtration technique was developed, taking into account the properties of particulate material and available filters. Accurate mass measurement required a means of filter storage and a highly accurate scale. The layout of the plume collection and filtration sampling systems is shown in Figure 4.1.

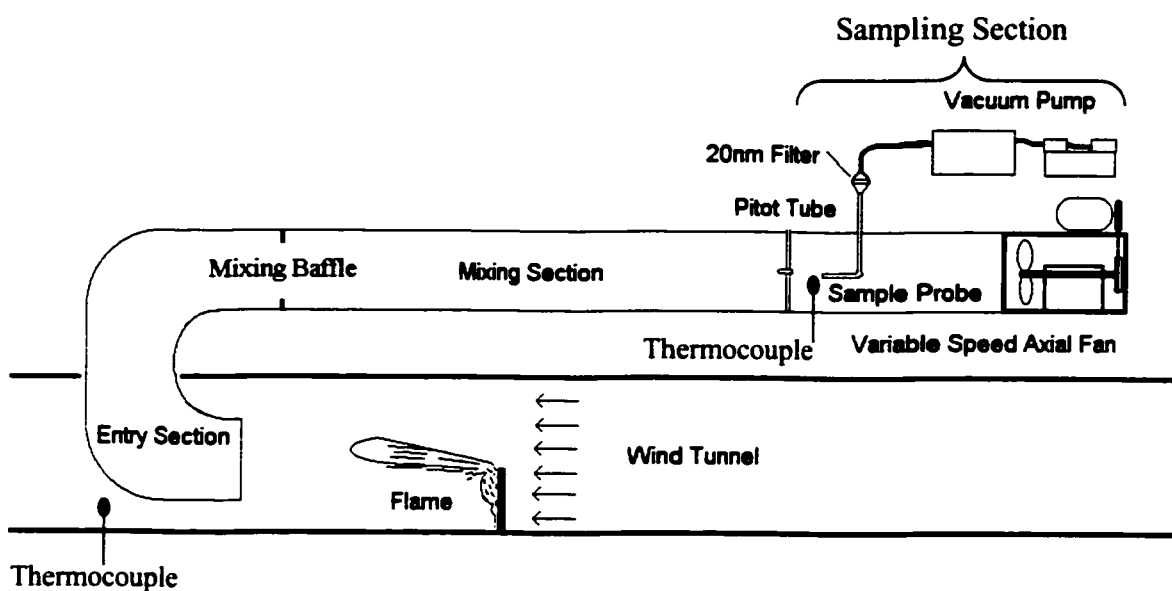


Figure 4.1: The particle plume collection system installed on the combustion wind tunnel at the University of Alberta.

4.2: Plume Collection and Mixing

With the plume location mapped using the FFID techniques discussed in Chapter 3, it was possible to collect the entire plume for sampling purposes. A 0.6 m diameter duct was installed on the roof of the combustion wind tunnel. As shown in Figure 4.1, this duct had 3 main sections: a section to collect the plume, a section for mixing the plume

into a homogeneous mixture, and a section for collecting and filtering a measured sample. Because the entire flare product plume was sampled, fresh air was continuously added to the wind tunnel, maintaining a uniform wind tunnel composition. Each section needed to be designed to handle different problems.

The goal behind the structure is to collect the entire plume, mix it, and then isokinetically extract a known volume of sample from the gas flow. Due to the size of the plume, it was not feasible to filter the entire plume flow. If the size of the sample probe and the size of the duct were both well known, then by knowing the plume flow rate and the flow rate of an isokinetically collected sample, the total particulate material yield could be calculated by measuring the particulate material yield on the sample filter.

The total particulate material yield would be:

$$Y_{soot} = \frac{\dot{M}_{PM}}{\dot{M}_{fuel}} = \left[\frac{\Delta m_{filter} / \Delta t}{\dot{M}_{fuel}} \cdot \frac{Q_{duct}}{Q_{filter}} \right]$$

- Y_{soot} - The total particulate material yield or conversion rate of fuel mass to particulate as a mass fraction.
- $\dot{M}_{PM}, \dot{M}_{fuel}$ - The mass flow of particulate material and fuel, respectively (g/s).

Δm_{filter}	-	The change in filter mass during experiment (grams).
Δt	-	The test duration (seconds).
$Q_{\text{duct}}, Q_{\text{filter}}$	-	The flow through the duct and the flow through the filter, respectively (liters).

The loss of particles due to settling and deposition was considered. The loss of particles due to the particle settling velocity was considered to be negligible after the settling velocity was analyzed (Appendix 4). Also losses due to deposition were negligible (Appendix 2).

4.2.1: Entry Section

In Chapter 3, the location and spatial distribution of the particle plume was mapped using a dual channel FFID. From those tests it was concluded that, for the range of jet velocities and wind speeds tested, the particle plume was contained within the boundaries of the thermal plume and that the highest concentration of particles was located directly behind the tail of the flame. As long as the thermal plume was collected, virtually all of the particle plume would also be collected.

From the particle plume maps, it was determined that using a 0.61 m diameter duct would be acceptable for most the cross winds that were to be measured with the 24.7 mm diameter model flare stack. Smaller flare stacks would produce smaller particle plumes,

so the 0.61 m duct would also be acceptable for these stacks. Galvanized ducting 0.61 m in diameter was used to construct the majority of the system.

The entry section was mounted into the wind tunnel so that the plane of collection was 3.5 m from the flare stack. However, at low crossflow velocities, the plume expands to sizes larger than 0.61 m diameter at a distance of 3.5 m downstream of the flare stack due to air entrainment into the plume. Some of the particles could escape collection if the plume was allowed to expand. To avoid this problem, a number of extension ducts were used to position the plane of collection at 2.90 m, 2.30 m, or 1.70 m from the flare stack. This ensured that the plane of collection could be located directly behind the flame at a point where the plume diameter was less than 0.61 m for the range of wind speeds used in the tests.

To ensure that the entire thermal plume was being collected, a series of thermocouples were installed in the entry section at the 3.5 m plane of collection. Four thermocouples were installed on the inner edge of the mixing section, the first at the highest point on the plane of collection, and the rest at 90° intervals around the edge of the plane of collection. A fifth thermocouple was installed outside the duct and could be repositioned to different locations around the outside edge of the collection plane as needed. As the plume moved down the extension duct, it would expand, so the internal thermocouples were expected to show a change in temperature from the ambient temperature within the tunnel when the thermal plume was being collected. The external thermocouple would only indicate an increased temperature if part of the thermal plume passed outside the entry section

duct. This allowed for measurements of the location of the thermal plume for different sizes of model flare stacks, and would indicate when an extension duct was required to collect the entire thermal plume. All the thermocouples used were shielded to minimize any effects from thermal radiation emitted by the flame.

4.2.2: Mixing Section

The mixing section was the largest part of the plume collection tunnel assembly. With a diameter of 0.61 m and a length of 9.2 m the mixing section had a length to diameter ratio over 15:1 to mix the plume and collected air homogeneously. Early tests with concentrated gas jets indicated that the flow rate in the tunnel did not generate enough turbulence to fully mix the gas flows, resulting in stratification of the different gases. The mixing profiles indicated that there was sufficient mixing across the horizontal axis, but there was insufficient vertical mixing. To further promote mixing, an asymmetric mixing baffle was installed at the beginning of the mixing section, and further tests confirmed good mixing.

4.2.2.1: Mixing Baffle

To maximize mixing while minimizing flow blockage, an asymmetric mixing baffle was designed to increase the vertical mixing while minimizing the blockage across the horizontal axis. As shown in Figure 4.2, the mixing baffle has a larger obstruction along the vertical axis, and smaller surfaces across the remaining axis.

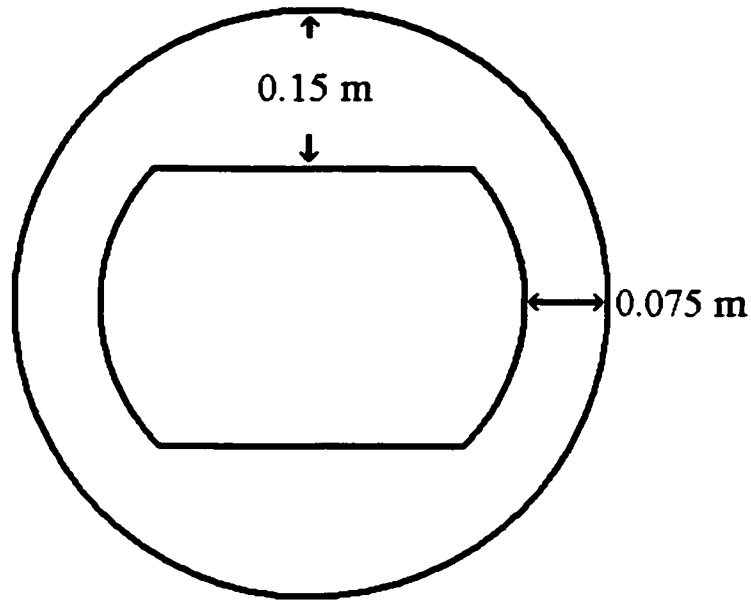


Figure 4.2: Mixing baffle designed for the mixing section.
The baffle had an outside diameter of 0.61 m and a thickness of 1.6 mm.

4.2.2.2: Mixing Tests

The ability of the mixing section to mix the flow of gas into a homogenous blend was tested by adding tracer gases to the gas flow and then traversing the sampling section with an online gas analyzer to see if the gas was homogeneously mixed across the tunnel. Two tracer gases were used: natural gas, which has a lower density than air and would tend to collect along the top of the mixing tunnel, and Carbon Monoxide which has a density similar to air. This section presents the results of the mixing tests with the mixing baffle in place.

The initial mixing tests involved a 200 ppm carbon monoxide jet. The gas was inserted at the plane of collection through a 6.4 mm outer diameter tube at a volume flow rate required to generate 4.0 ppm overall concentration (the tracer gas flow was changed when the volume flow rate in the mixing tunnel was changed). The tracer gas concentration profile was measured in the sampling section by traversing the duct with a sample probe connected to a NDIR (Non-Dispersive Infrared) carbon monoxide detector with a 200 ppm range and a resolution of 0.01 ppm. Figure 4.3 shows the results of the vertical and horizontal traverses. The centerline velocity in the mixing tunnel was set approximately to 2.0 m/s. Tests conducted at higher wind speeds did not indicate a reduction in mixing as a result of increased velocity.

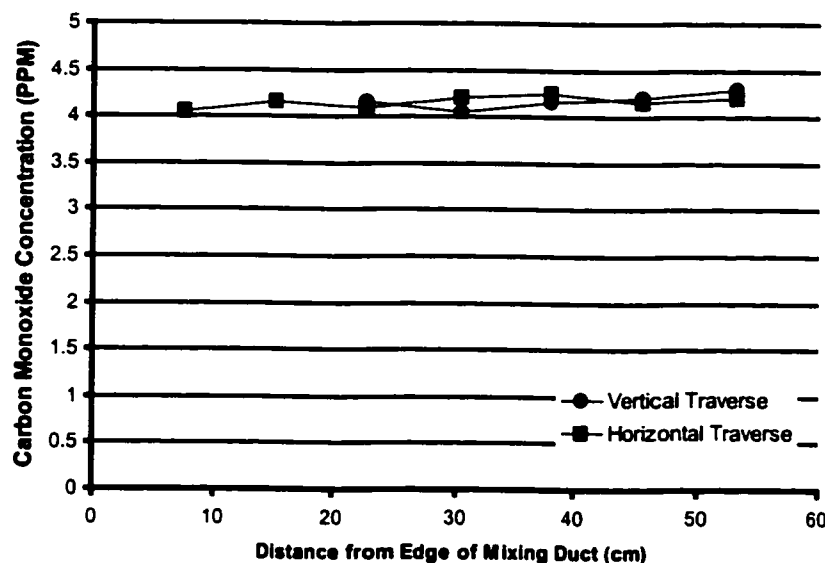


Figure 4.3: Mixing profiles generated using Carbon Monoxide. The gas flow was set to approximately generate a mean concentration of 4.0 PPM. The velocity in the mixing tunnel was set to a centerline velocity of 2 m/s.

To ensure that the mixing tunnel would generate a homogenous mixture with a hot gas plume, the tests were repeated with natural gas (primarily methane), which has a lower density than air. By injecting a concentrated jet of natural gas into the entry section of the tunnel, a difficult mixing situation was generated. The mixing test started with a centerline velocity of 2 m/s. Natural gas was injected into the entry section through a 6.4 mm outer diameter line at a rate of 7 liters/min, which was set using a mass flow controller. The resulting concentration profiles, measured with a FID that had a range of 250 ppm and a resolution of 0.4 ppm, are shown in Figure 4.4. The actual concentration varied from 210 PPM to 212 PPM, representing less than 1 % error due to imperfect mixing.

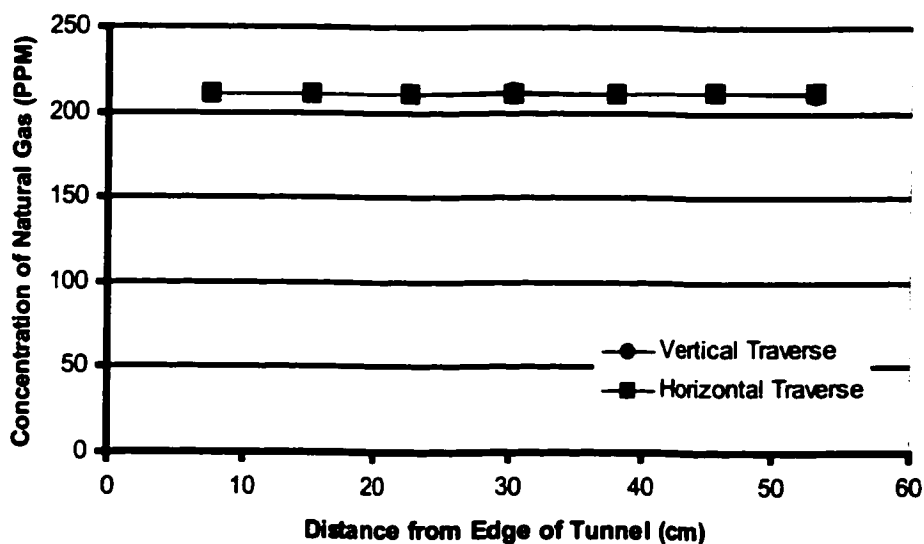


Figure 4.4: The mixing profile of Natural Gas for 2 m/s centerline velocity in the mixing tunnel.

To ensure that mixing was effective for the range of cross wind velocities used in these experiments, the mixing test was repeated with the methane jet for both 4 m/s and 8 m/s

centerline velocity. The results are shown in Figure 4.5 and Figure 4.6. In each case, all measurements were within $\pm 1\%$ of the mean value. These tests determined that the mixing tunnel was effective in blending separate, concentrated gas flows into a single homogenous mixture with a variance within 1 % of the mean concentration.

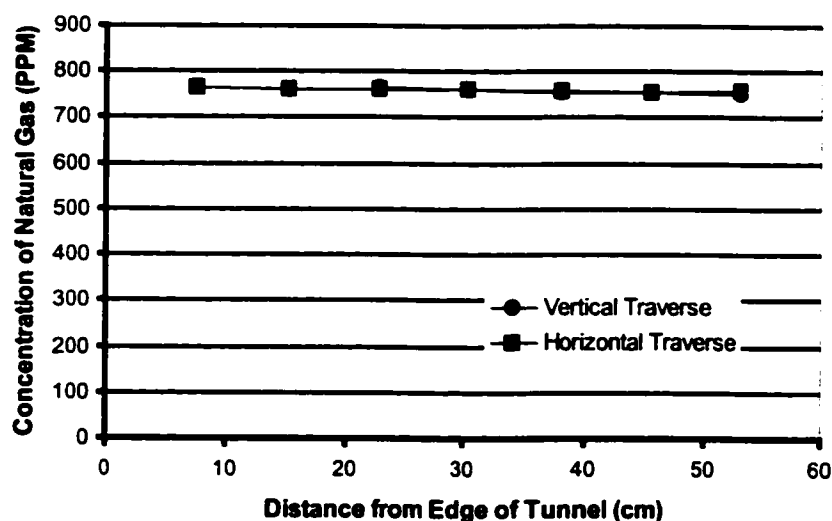


Figure 4.5: Mixing profile for a 35 liters/min Natural Gas jet injected into the entry section along at an asymmetric location. The plume collection system had a 4 m/s centerline velocity.

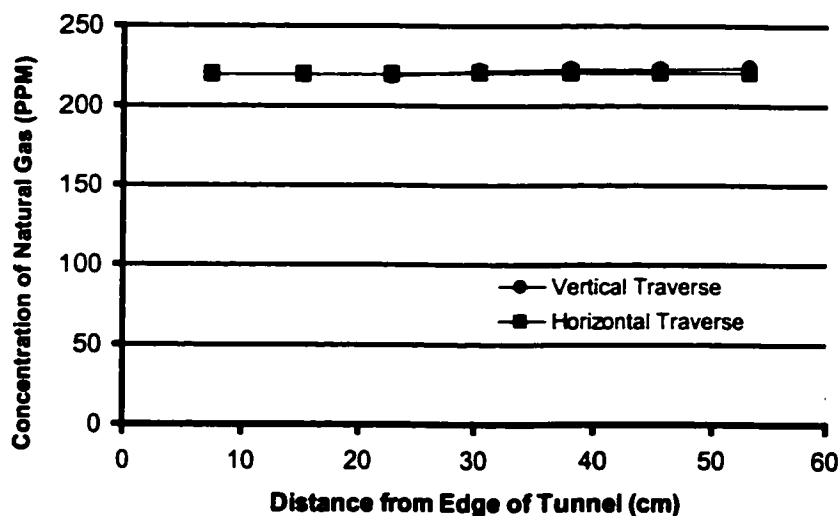


Figure 4.6: Mixing Profile for an 18 liters/min Natural Gas jet injected into the entry section. The plume collection system had an 8 m/s centerline velocity.

4.2.3: Sampling Section

The sampling section of the plume collection system contained the variable speed fan, the sampling probe, and the velocity measurement equipment necessary to monitor the operation of the mixing tunnel. The sampling section was 1.0 m long and was constructed from the same 0.61 m diameter galvanized ducting as the rest of the plume collection system. A number of fittings were attached to house the various pieces of equipment that were used in this section.

4.2.3.1: Variable Speed Fan System

An axial variable speed fan was mounted in the sampling section, and was used to drive the flow through the mixing tunnel. The 0.61 m diameter axial fan was belt driven by a 2 HP variable frequency drive (VFD). The VFD provided digital control of the motor rpm, allowing control of the volume flow through the mixing tunnel to ensure near isokinetic, or slightly greater flow velocity at the plane of collection in the main tunnel. The variable speed fan was rated to move 281 m³/min when unobstructed.

4.2.3.2: Velocity Profiles

The sample probe for the collection of particle material was not designed to sample from the exact axial center of the sampling section but from a distance of 0.15 m from the edge of the tunnel. This design was implemented for a number of reasons. Velocity/total flow

measurement equipment was going to be placed along the axial center of the sampling section. The sampling probe would need to be kept away from this equipment. The length of the sampling probe was minimized to minimize disposition of particulate material within the sampling line. The sampling velocity needed to be isokinetic with the velocity of the flow at the point of sampling. By moving the sampling point away from the axial center of the mixing section, the velocity of the sampling point would be reduced as a result of the shape of the velocity profile. This would reduce the pressure required to feed the sample through the filter.

The velocity profiles for the different flow velocities needed to be measured to extract an isokinetic sample from the gas flow with the sample probe off the axial center of the sampling section. The velocity measurement was conducted by traversing the sampling section with a pitot tube. The velocity profile was measured with reference to the rpm setting on the drive and normalized to determine the contour of the profile. The resulting data sets for the horizontal and vertical profiles for 4 different motor power settings are shown in Figure 4.7. The velocity profile remained nearly flat (not much difference between the centerline and sampling velocity) for all of the different velocities.

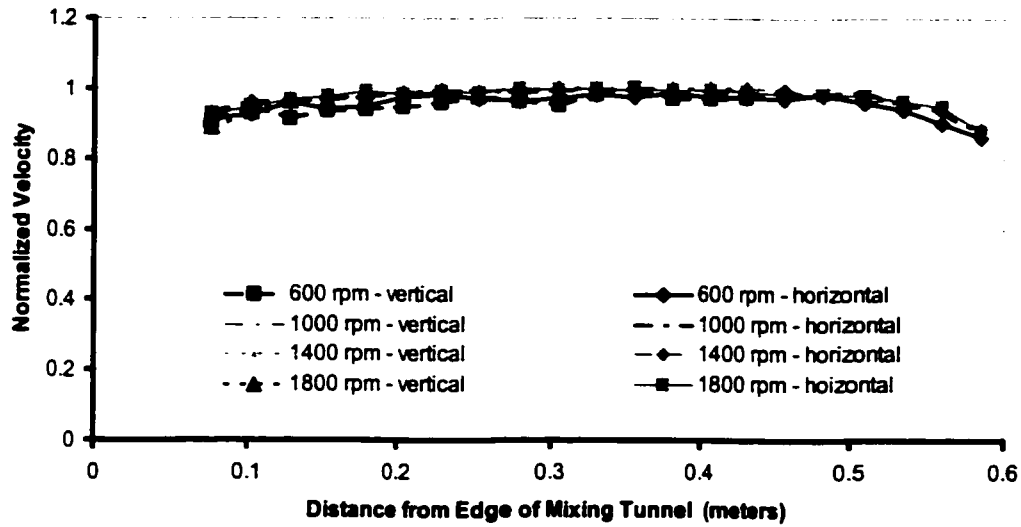


Figure 4.7: The velocity contours for four different motor rpm settings. Both the vertical and horizontal traverses are shown.

4.2.3.3: Volumetric Flow Rate

At the plane of collection, the gas flow had a non-uniform flow profile. The volume flow rate of gas flowing through the mixing tunnel needed to be determined to know the velocity of gas flow into the entry section. To measure the volumetric flow rate, an area averaging pitot tube was constructed and installed in the sampling section of the mixing tunnel. The tube was constructed to prior in a standard manner but needed to be calibrated once installed [ASHRAE Standard 51-75].

An area sampling pitot tube works by averaging the stagnation pressure at a number of different points at different radii from the center of the mixing tunnel and comparing the averaged stagnation pressure to a single static pressure measurement. Figure 4.8 shows the locations of the 24 stagnation pressure taps that are spaced to represent equivalent flow volumes. Two Ashcroft pressure transducers were used to measure the pressure difference. To calibrate the instrument, a jet of methane was introduced to the entry section of the mixing tunnel. As a result of the tunnel being well mixed, the resulting concentration of mixing gasses could be used to indicate the volume flow rate of air entering the tunnel. By calculating the volume flow rate from the concentration and comparing the results to the indicated pressure difference, the area averaging pitot tube could be used to monitor both the volume flow rate through the tunnel and the velocity of gas at the entry section of the tunnel.

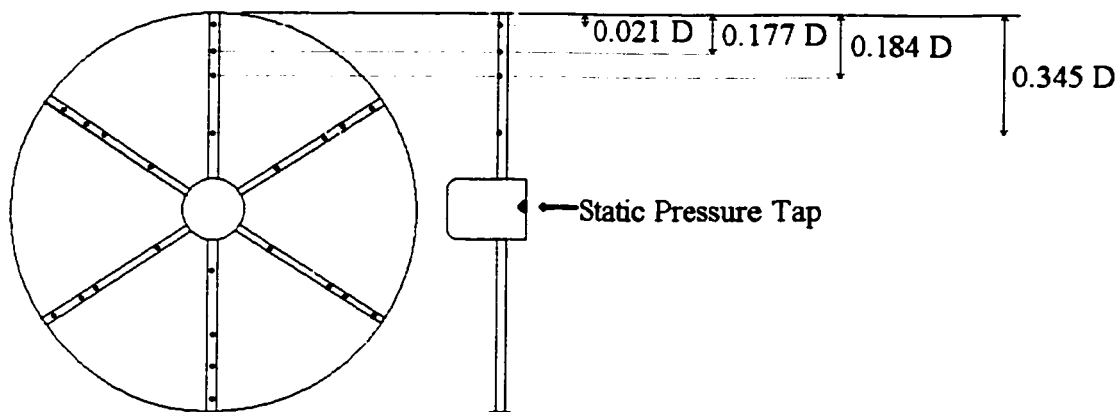


Figure 4.8: Pressure tap locations on a 6 arm area averaging pitot tube. 24 individual stagnation pressure taps are pressure averaged and compared to a single static pressure tap to measure a volume flow rate.

During operation with hot gas plumes, a thermocouple was installed near the area sampling pitot tube to monitor the temperature of the gas flow to compensate for any changes in density. The composition of the gas in the mixing duct is assumed to be similar to air due to the large quantity of entrained air within the plume and the excess air that is pulled into the mixing duct during plume collection. The correlation for ambient air is given in Figure 4.9.

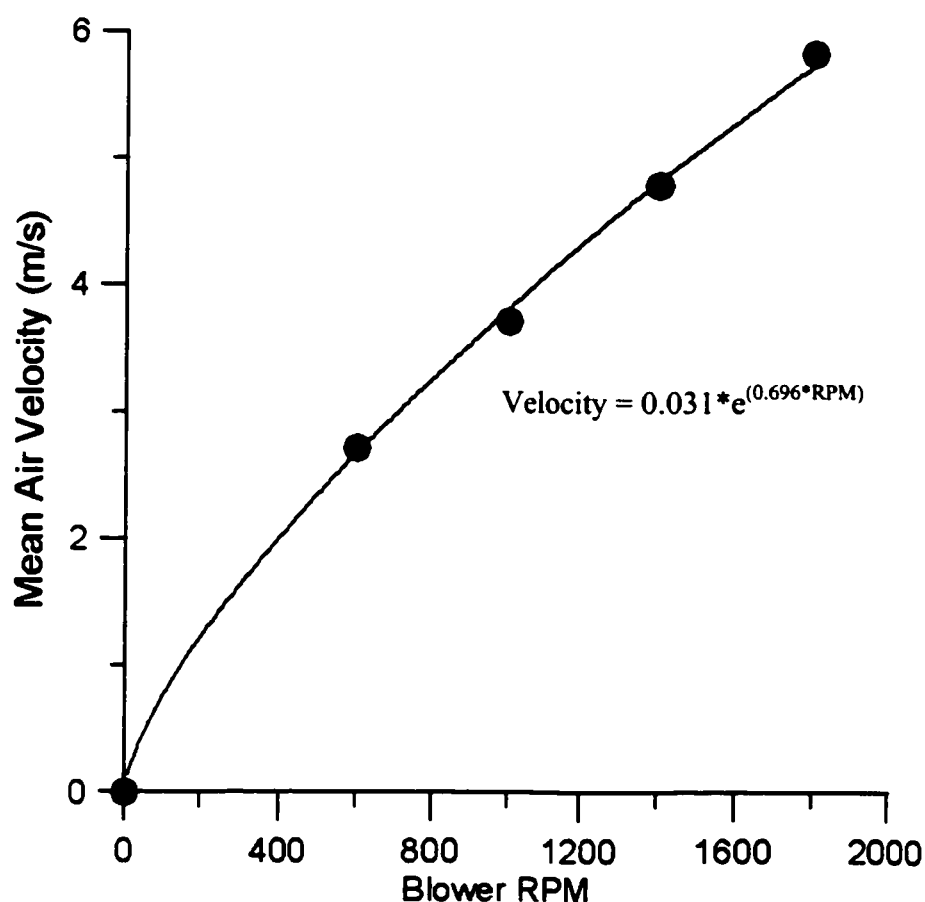


Figure 4.9: The mean air velocity in the plume collection system with respect to the blower RPM.

4.2.3.4: Velocity at Sampling Location

The sample was not extracted along the central axis of the mixing tunnel but at a location 0.15 m from the edge of the mixing tunnel. To extract an isokinetic sample, the velocity at the point of sampling must be known for all different motor settings. By using the normalized velocity profiles, it was possible to determine the actual velocity at the sampling location based on the motor speed. The motor speed was compared to the volume flow rate of the tunnel at that setting, and a relationship of volume flow to sample flow was determined. Figure 4.10 shows the correlation used for velocity at the sample probe in relation to blower motor speed. By using this correlation and the volume flow rate correlation (determined by the area sampling pitot tube), the tip velocity was related to the volume flow rate. The sample point velocity was used to determine the required sampling vacuum to generate sufficient filter sample flow for isokinetic sampling.

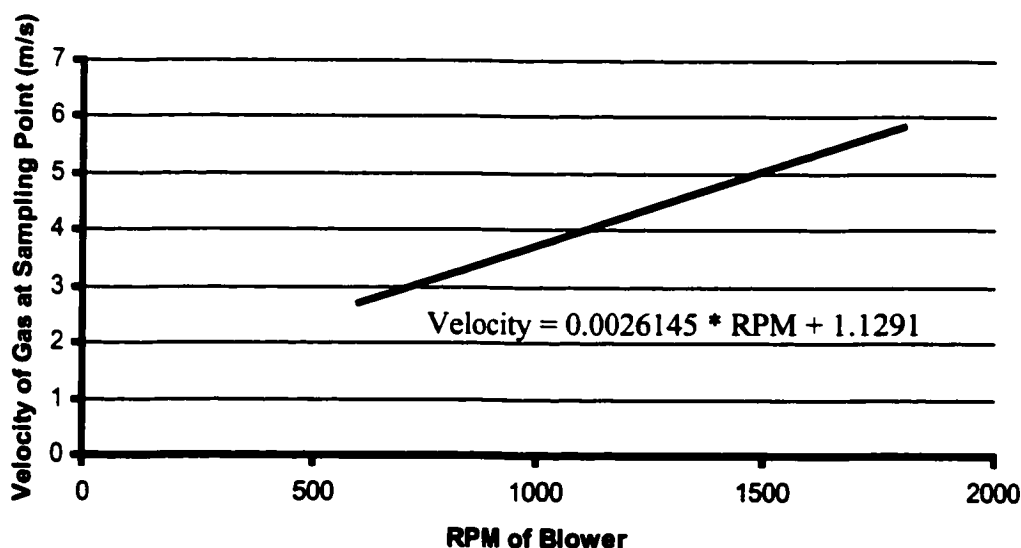


Figure 4.10: The relationship between blower motor speed and gas velocity at the tip of the sampling probe.

4.3: Particle Filtration

Combustion generated particles are comprised of many spherules clustered together into larger particles called aggregates [Calcote, 1981]. A spherule is a 20 – 50 nm diameter particle which is the elementary particle involved in particulate material emission (discussed in further detail in Chapter 5). Previous combustion particulate research (mostly with engines) has not normally seen individual spherules as particles, but the types of particles being produced by the model scale propane flare were not known. As a worst case, it was hypothesized that a filter capable of capturing individual spherules would be required to collect all of the particles produced by the flame.

Particulate material produced by IC engines has been comprised of spherules with a mean diameter of 20 to 50 nm [Kittelson, 1979]. This value was used as an estimate to begin tests and select a filter system, once the filtering system was selected and our own particle sizing was conducted on collected samples it would be possible to confirm the spherule size.

Particle detection can be accomplished by impacting methods or by filtration. Impacting methods force the particles out of the flow onto a collection surface, either by rapid momentum changes or by electrostatic means. A very high flow rate could be established through an impacting device, but a number of difficulties would be encountered.

1. The suspected particle size was too small to be sure that an impacting type of device would be able to collect the particles. Very small particles are difficult to remove from gas flows since they will follow the flow very closely [Cadle, 1975].
2. The physical impact that removes the particles from the flow could affect the structure of the particles, fragmenting the aggregates into smaller particles. This fragmentation would result in inaccurate conclusions from the imaging of the particles, possibly making the particles look smaller than they really are [Cadle, 1975].
3. Impacting devices capable of collecting nanometer scale particles tend to have a large mass, resulting from the large surface area and multiple flow directional changes required. Scales capable of measuring microgram weight changes on surfaces do not have a large operational range (typically less than 50 g). Such a device would not be usable with a high resolution measuring device.

Filters for gasses can be membrane or fiber types. A membrane filter is a surface that has been perforated or constructed with openings of a known size. It collects all particles larger than the openings on the filter surface. Fiber filters, constructed from a mat of fibers, have a very low restriction when compared to other filters but generally specify collection efficiency, and collect particles throughout the depth of the filter. Less than 100% of the particles would be collected and imaging the particles would be difficult. Fiber filters were used in the preliminary experiments to detect the presence of particulate

material, but further experiments would require more control. Due to the suspected small size of the particles, and the desire to image the particles once they were collected, it was decided that a membrane filter would be desirable.

Membrane filters were the only devices that could accurately filter particles with very small diameters and collect the particles on the surface of the filters for straightforward imaging. A specific filter (Whatman Anodisc 47 with 20 nm pore size) was selected for a number of reasons:

1. Most flame generated particles are collections of spherules and have a mean diameter larger than 20 nm. Individual spherules are found with mean diameters in the 20-50 nm range. The 20 nm pore size of the filter meant that it would collect all (or nearly all) of the particles emitted by the flame.
2. The filters had a laminar flow design that allowed for comparatively high air flow rates through the filter (the filters are similar to laminarizing elements used in pipe flow) further described in Chapter 5. In addition, the alumina design allowed for large differential pressures to be applied to the filter without damaging the filter structure.

In addition to fitting the requirement for collecting particulate material samples from the plume of the flame, these filters were also used as the filtering medium in the FFID plume mapping (Chapter 3). The alumina structure allowed the filter to survive the potentially elevated temperatures from the plume without affecting filter performance.

The filter was placed in a 47 mm filter holder made of two components held together by a threaded collar. The filters have a polymer ring around the edge of the filtration surface to help seal the filter in the holder. The filter holder was equipped with an O-ring to contact the polymer ring and enhance the sealing of the filter to the holder. This produced a compression style seal to the filter without causing any torque on the filter during sealing or unsealing of the holder.

4.3.1: Filter Flow Rate Calibration

A calibration for the airflow through the alumina filter was required to measure the flow rate during the experiments. The adjustable variable in the sampling process was the vacuum applied to the filter. By calibrating the flow through the filter based on the pressure drop across the filter, the flow could easily be manipulated by adjusting the vacuum pressure downstream of the filter. To calibrate the flow through the filter based on the pressure, the assembly detailed in Figure 4.11 was constructed.

A 140 kPa (20 psi) Validyne pressure transducer calibrated was used to measure the pressure drop across the filter. The flow rate was measured using a bellows style gas volume meter calibrated by ATCO gas (commercial natural gas supplier) and a stopwatch to provide a time for the volume transferred. The volume resolution on the meter was 0.01 liters and the stop watch resolution was 0.01 s, so long duration samples were taken to minimize any error from activating and deactivating the timer. The primary source of

error was the starting and stopping of the watch. For a calibration test that runs for several minutes this error could be considered to be negligible.

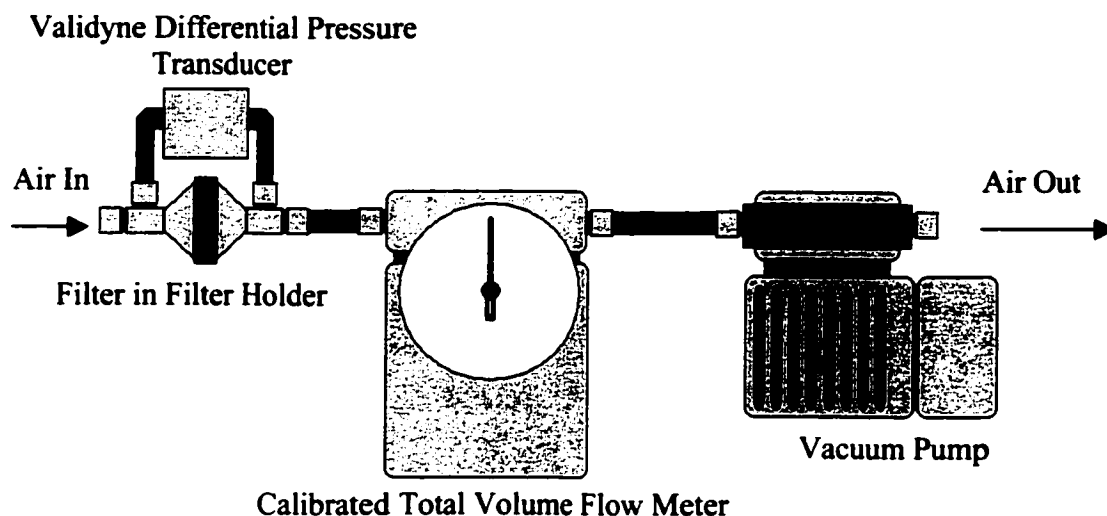


Figure 4.11: The assembly constructed for calibrating the flow through the alumina filters with respect to pressure drop.

A series of measurements conducted at ambient conditions produced the pressure to flow calibration shown in Figure 4.12. The filters produced a nearly linear flow to pressure characteristic for up to 68.9 kPa (10 psi) pressure drop where the flow through the filter was 6 liters/min. There was a slight curvature in the relationship, and this was accounted for when the filters were in operation. Using a polynomial fit, the flow calibration for the filter was determined to be:

$$Q_s = 0.013 + 0.104 * dP - 0.0002 * dP^2$$

Where Q_s is the Sample Flow Rate in liters/min and dP is the Pressure Drop in kPa.

In addition to measuring the pressure drop with relation to flow through the filter, attempts were made to alter the pressure drop by adding material to the filter. The experiment was repeated while various powdered substances were added to the inlet of the filter holder and allowed to accumulate on the filter. These compounds included chalk dust and finely ground graphite powder. After conducting numerous tests in this fashion, it was determined that the flow through the filters was not affected by the accumulation of material on the filtration surface. It is an effect similar to attempting to plug a chain link fence with basketballs. The particles are too large to fit into the holes and the pressure drop due to the particles is small compared to the pressure drop from the filter. The test was not conducted using actual particulate material, but the microphotography indicated that the actual particles were also relatively large compared to the filter pore sizes (Chapter 5).

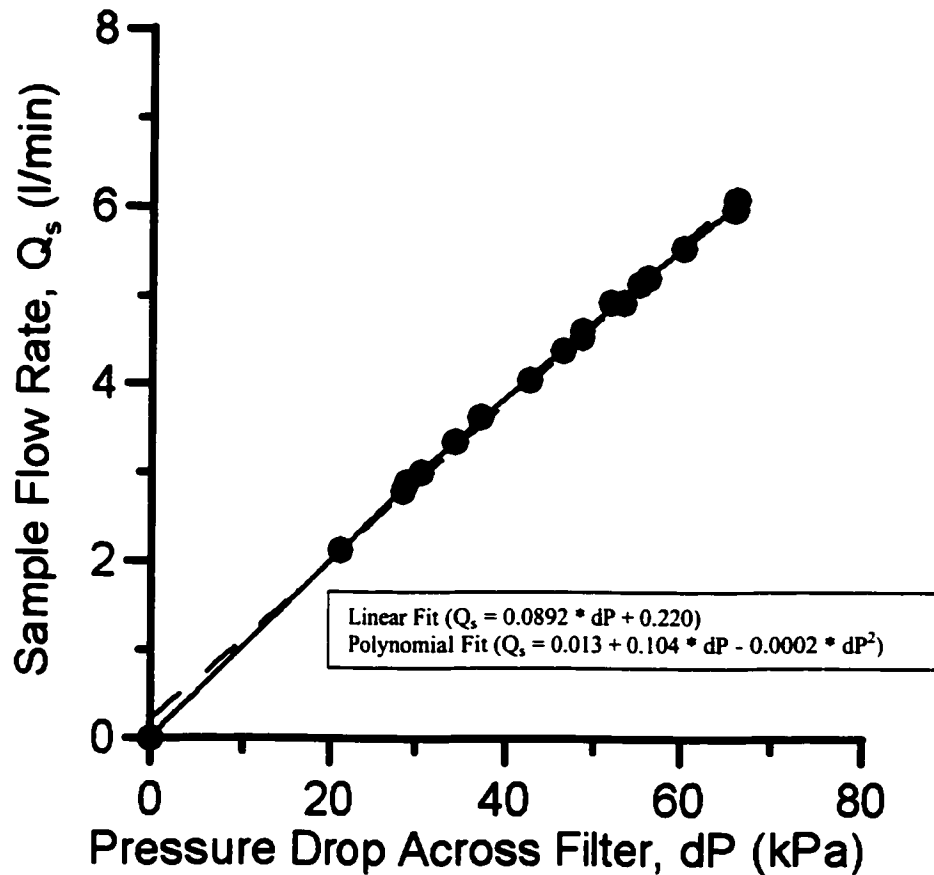


Figure 4.12: The pressure to flow rate calibration for the 47 mm alumina filters with a 20 nm pore size.

4.3.2: Sampling Assembly

The vacuum applied to the filter determined the flow through the filter and the flow through the filter was used to control the sampling velocity. To extract an adjustable sample of particle laden gases through the filter, an adjustable vacuum needed to be applied to the filter. The vacuum pump was a two-stage diaphragm pump that generated 6 liters of flow while applying 68.9 kPa of vacuum. The vacuum controller was an electronic device with a digital display that monitored the pressure in the sample line and

was used to control the flow through the filter. By allowing air to enter the sample line through a bypass valve after the sample had been filtered, the vacuum applied to the filter was manipulated without altering the operating speed of the vacuum pump. Figure 4.13 shows the final assembly used to draw a sample through the filter. This system could be used to make quantitative single point mass measurements from the plume.

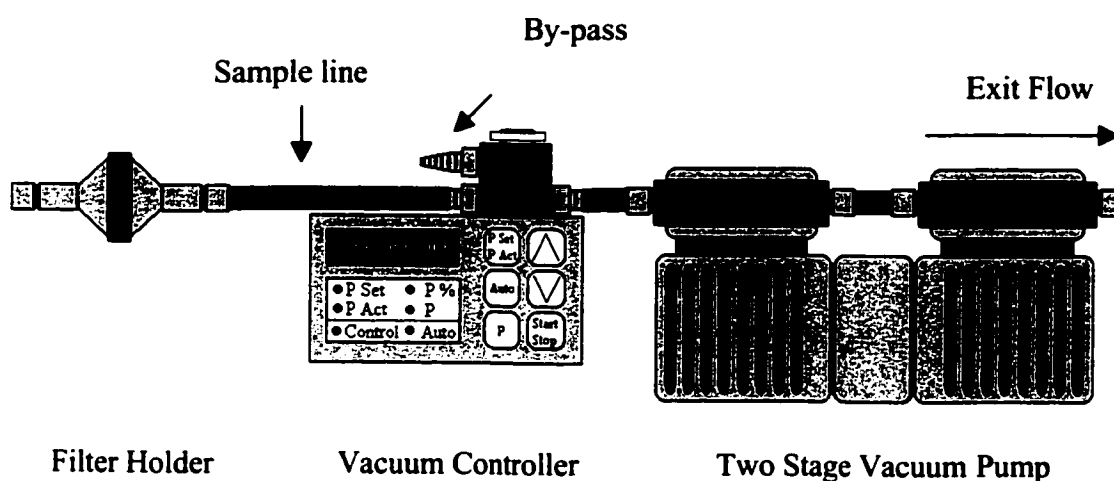


Figure 4.13: The assembly used to draw a sample through the filter. The vacuum pump generates a constant vacuum while the vacuum controller maintains a fixed vacuum in the sample lines.

4.4: Mass Measurement

The mass of each filter had to be determined both before and after particulate matter was collected to determine the mass of particulate matter that was deposited on the filter. The actual mass of particulate material produced by the flame was estimated to be very small

for commercial grade propane and nearly non-existent for natural gas, so a very sensitive scale was required. A scale with a 0.01 mg resolution was selected to measure the mass of all the filters. The scale was a ANG GR-202 with a 42 gram measurement range. The sensitivity of the scale resulted in a slow response and settling time, so the scale was connected to a computer with a RS-232 serial data line and the mass was recorded over a period of time to determine when a stable mass reading had been achieved. This required a significant amount of time to measure all the filters required for the experiments, but this was unavoidable.

When dealing with a mass resolution of 0.01 mg, the environmental conditions of the filter become important. To maintain a consistent environment for the filters, both the scale and the filters were stored in a static environment chamber, as shown in Figure 4.13. The chamber maintained a consistent temperature and humidity for the equipment. The temperature was set to 25 ± 0.1 °C, and 50 ± 0.1 % relative humidity, NMAM 5515 (NIOSH Manual for Analytical Methods) indicates that refrigeration is not required for filter samples, so the temperature was maintained at a temperate 25 °C for the benefit of the other equipment that was installed in the chamber, which may not function properly at refrigerated conditions. When measuring the mass of a filter, the chamber was temporarily deactivated to eliminate any vibrations generated by the refrigeration and dehumidification equipment that could affect the scale. The chamber was sealed, and tests indicated that it could be deactivated for more than sufficient time to measure filters without affecting the internal environment. At all other times the chamber actively maintained the set storage environment.

NMAM 5515 indicated that filters had to be protected from UV light during storage and allowed to stabilize for a minimum of 24 hour in the measuring environment prior to mass measurement. The filters were stored in the environment chamber, which maintains a constant environment at all times and has a window with an UV absorbent window to protect the samples from degradation. Filters could be manipulated through a pair of glove boxes in the door of the chamber, allowing the scale to be operated while preventing any contamination of the internal environment. Filters were only exposed to an uncontrolled environment during transportation for testing, and were immediately returned to the chamber when testing was completed. Measurement did not occur for 24 hours if the chamber was opened for any reason to allow the temperature and humidity to stabilize from the disturbance.

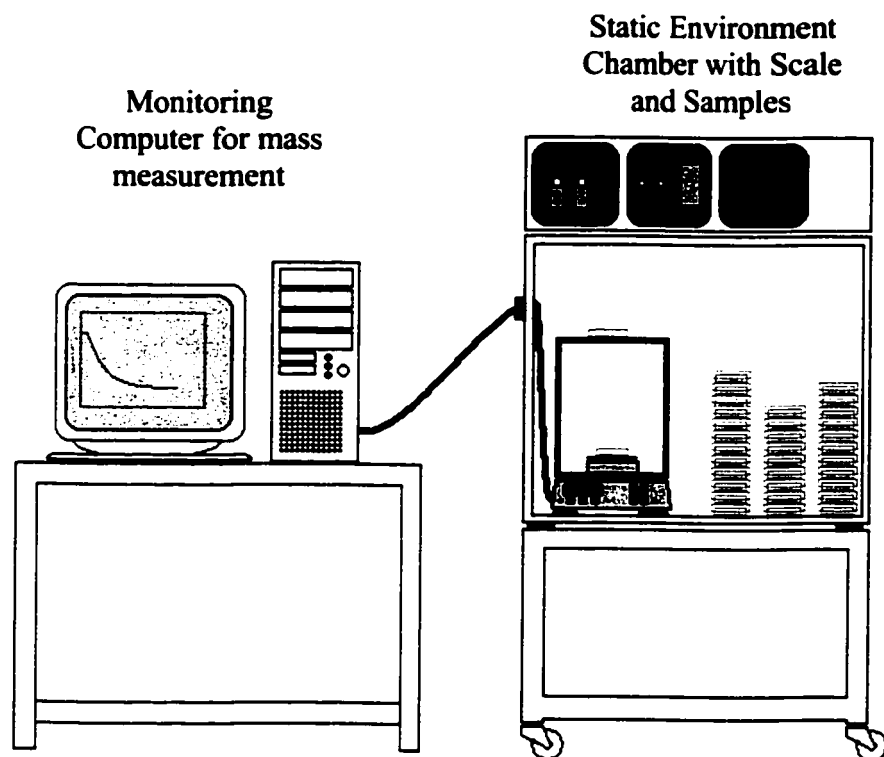


Figure 4.14: The assembly used for storage and measurement of filters. The environmental chamber maintains the environment while the computer monitors the scale readings through the RS 232 connection.

4.5: Particulate Material Production by Commercial Propane Flames in Crossflow

The primary fuel used for the particulate matter production experiment was commercial grade propane. While natural gas is the most common fuel in typical flaring, it was not a strong enough particulate generator to be useful for measuring particulate emission rates. The composition of commercial grade propane is mostly propane, but small amounts of other compounds are present (96.6 % propane, 2.6 % Ethane, remainder Butane). As described in Chapter 3, it was determined that propane emitted a small, but measurable,

amount of particulate material. Propane was the gas of choice for the experiments on how crossflow velocity affects particulate material production.

4.5.1: Filter Handling

Measuring the amount of particulate material produced by a model scale flare was a delicate process. The handling of the alumina filters required extra care and attention. Due to the small masses involved, even fingerprints on the filter holder could generate a substantial increase in the mass of the filter. As a result, special precautions were taken when handling the filters:

1. Filters were kept in individual petri dishes. Each dish was sterile and clean before the filter was placed in the dish. Each filter has its own dish and the dishes were not reused. Each dish was labeled for identification purposes. The dishes protected the filters from contamination from dust and airborne particles.
2. Cotton gloves were worn at all times when handling the filters and filter dishes. This prevented oils from the handler's skin from contaminating the filters.
3. The filters were only removed from the environmental chamber for a short period of time. Once the mass of particulate was collected on the filter, the filter was returned to the environmental chamber to stabilize.

4. Filters and dishes were transported in a closed container when not stored in the chamber. This allowed for easier handling and protected the filters from contamination.
5. Control Blanks, filters that never leave the chamber, and Test Blanks, filters that are moved, but not experimented upon, were maintained to monitor for any drift in the measurements.

Multiple samples were collected for each set of sampling conditions. This allowed for the identification of contaminated filters by processing the data collected with a statistical analysis. If an individual data point was very unlikely to appear based on the data resulting from the rest of the filters collected at that set of conditions, that individual data point could be ignored.

4.5.2: Raw Data

The initial tests were conducted with a 24.7 mm diameter flare and a 1 m/s exit velocity propane jet. The data set collected is displayed in Figure 4.15. There appears to be a decrease in fuel to particulate material conversion as the cross wind was increased, but without data for a cross wind of less than 2 m/s, it is difficult to prove that conclusion.

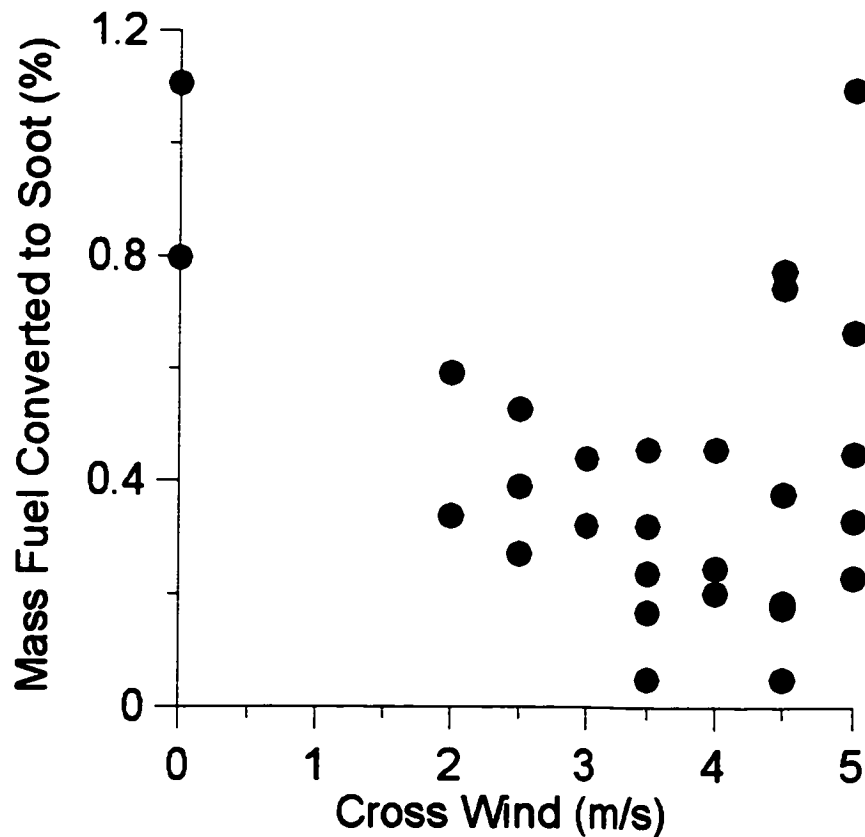


Figure 4.15: Data for 1 m/s exit velocity propane flame with the 24.7 mm diameter jet in a varied cross wind.

It was also possible to acquire data by maintaining a constant cross wind velocity and varying the jet exit velocity. By setting a constant cross wind of 2 m/s and altering the exit velocity of the propane jet a number of samples were collected. The data shown in Figure 4.16 indicated a strong decrease in particulate material emission as the cross wind velocity was increased.

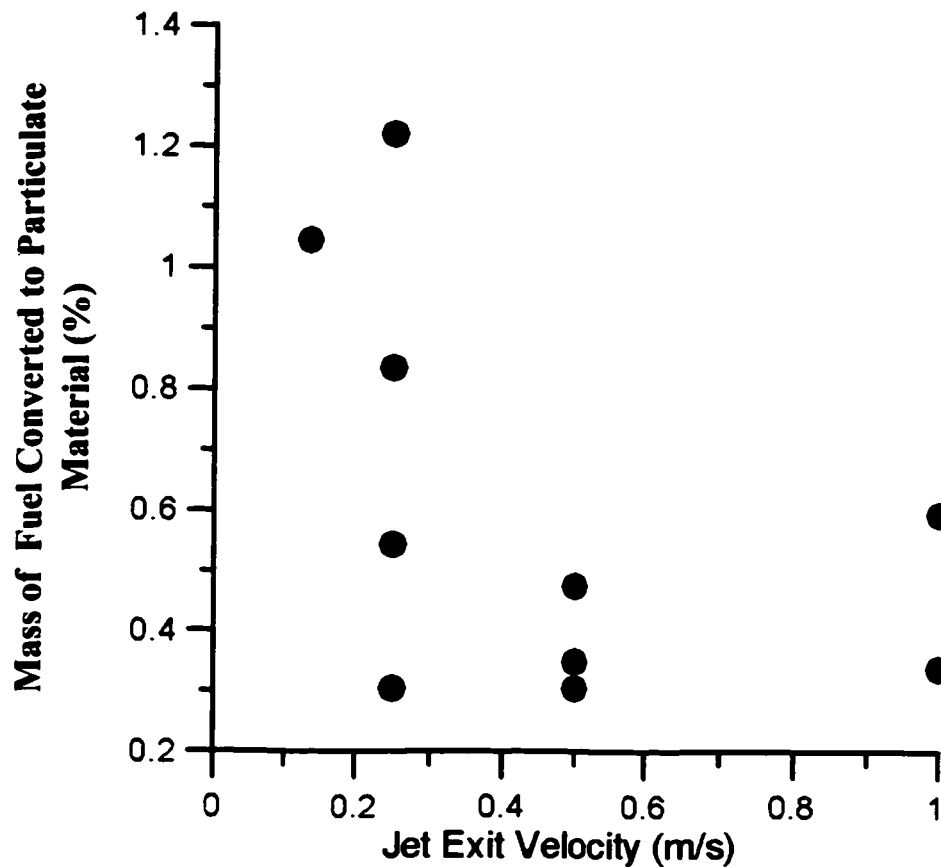


Figure 4.16: Data collected for a 24.7 mm diameter jet in a constant cross wind of 2 m/s with a varied jet exit velocity.

When both sets of data were compared, both indicated a decrease in the mass of fuel that was converted into particulate material as the crossflow was increased. What was needed was a means to relate the two data sets. Ellzey stated that for small diameter jets, increasing the mixing ratio would decrease the amount of fuel that was converted into particulate material [Ellzey, 1990]. Ellzey stated that the independent variable was the

mixing ratio ($U_{\infty} * U_j$) and that as this variable increased the amount of fuel that was converted into particulate material was decreased. This was consistent with the observed data for the 24.7 mm diameter flare stack. The data sets from the constant jet exit velocity and the constant cross wind were combined into a single data set that was dependent on the mixing ratio and additional tests were conducted to fill any gaps in the data (including additional data for zero crossflow). Figure 4.17 shows all the data values collected from the tests conducted on the 24.7 mm diameter flare stack with respect to the mixing ratio.

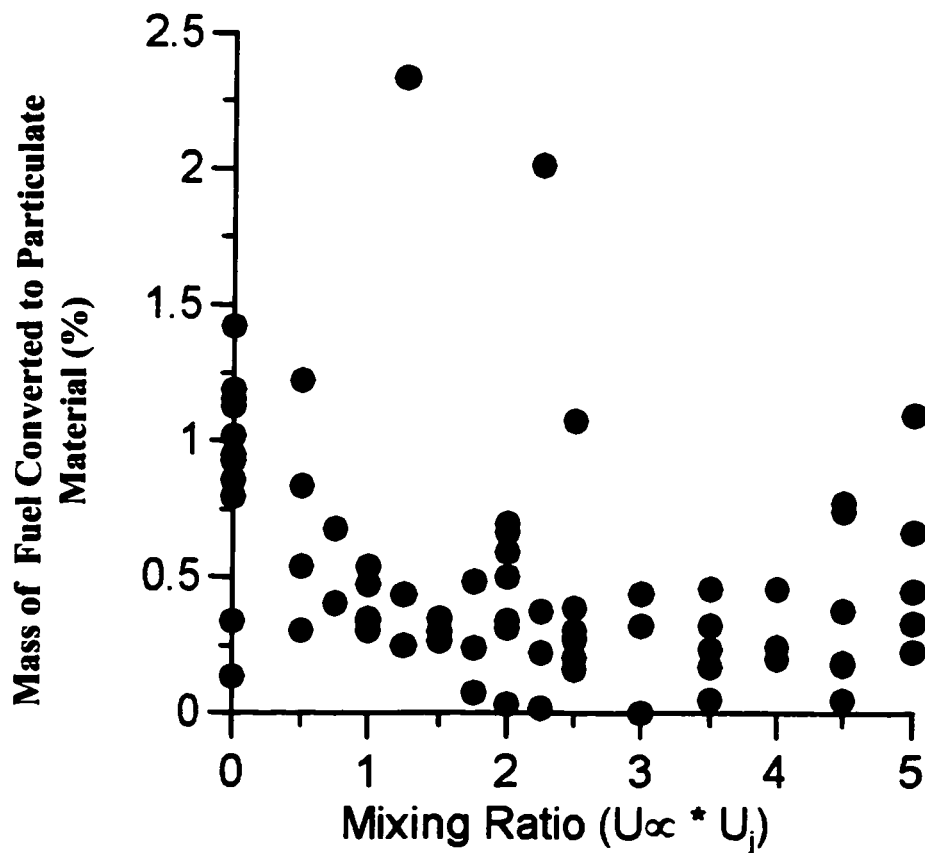


Figure 4.17: All data collected for the 24.7 mm diameter stack prior to the statistical analysis.

4.5.3: The Mixing Ratio

It was previously determined by Gollahalli et al. [1975] that both the crossflow velocity and the jet exit velocity are very important to the mixing incurred by the flame and that it is the mixing that determines the characteristics of the flame in crossflow. This information was used to define the mixing ratio, which is the product of the jet exit velocity and the crossflow velocity. It was determined by Ellzey et al. that the production of particulate material is dependent equally on each term and will correlate to this parameter [1990]. Based on this information, the particulate material production by the model scale flames investigated in this experiment was examined for relationships with each velocity (U_{∞} and U_j) and also classified by the mixing ratio ($U_{\infty} * U_j$).

After statistical analysis a function was fit to the data in the form of:

$$m_{soot} = \alpha (U_{\infty} U_j)^{\beta}$$

m_{soot} = The particulate material yield (mg particulate material / g fuel)

α, β = Constants

U_{∞} = Velocity of the crossflow (m/s).

U_j = Mean jet exit velocity (m/s).

This was the form of the function used by Ellzey et. al. [1990] to fit particulate material production data using small diameter model stacks.

The model developed by Ellzey had some limitations. When there is no cross flow, the mixing ratio is zero, and the model predicts infinite production of particulate material. To improve on this, an exponential model was developed. The new model was in the form of:

$$m_{soot} = \alpha + \beta * e^{(-U_{\infty} U_j)}$$

m_{soot} = The particulate material yield (mg particulate material / g fuel)

α, β = Constants

U_{∞} = Velocity of the crossflow (m/s).

U_j = Mean jet exit velocity (m/s).

The exponential model predicts a finite quantity of particulate material in a zero cross flow situation and a stable quantity at high cross flow. The model is not physically based, but does provide a reasonable fit to the data.

4.5.4: Statistical Analysis:

The data sets produced by measuring the amount of mass collected on the filters needed to be analyzed to eliminate points affected by contamination during handling or bad measurements. Selecting the analysis technique was not a difficult process since a number of constraints were present on the data.

1. The data values would likely have a small amount of naturally occurring variation, but contaminated samples would likely have a large variance from most of the collected data. The most common forms of contamination, such as a fingerprint, produced a significant added mass compared to the amount of particulate material that was collected. The data values were assumed to be normally distributed with most data points collected around a mean value.
2. The filters could not lose mass. This provided a lower limit of how much material could be collected. If a filter collected negative mass, or lost mass in the process of filtering particulate matter, then the filter was obviously contaminated or damaged and the data should not be used.

Based on this analysis, it was determined that a Gamma distribution would be used since it can be used to fit data sets with a bounded limit of zero and an increasing probability distribution. The data sets were fit with a gamma distribution and the mean and variance were determined. Any data point that had a probability of <5 % or >95 % was removed from the data set.

A majority of the data for the 24.7 mm diameter stack appeared to have a mean of approximately 0.4 % conversion. The data indicated that the conversion rate rapidly increases close to a mixing ratio of zero, so the gamma distribution was only applied to all the data with a mixing ratio greater than 1. For data with a mixing ratio less than one, the gamma distribution was applied to each set of mixing ratios separately. Due to the small sample sizes for each data set of mixing ratios below 1, the small sample variance

was calculated and used to determine the gamma distribution for these tests [Scheaffer, 1995].

4.5.5: Model Flare Stack Results –24.7 mm Diameter

The processed data set collected from the 24.7 mm diameter model flare stack is presented in Figure 4.18 (5 % to 95 % data determined from the gamma distribution). The values show a rapid decrease in particulate material production as the mixing ratio was increased. This was expected because it agreed with the trend of FFID particulate count taken while the plume mapping was conducted (Chapter 3).

The collected data indicate that the mass production rate of particulate material becomes stable as the mixing ratio is increased beyond 3. The model developed by Ellzey was fit to the data. However, Ellzey's model produces an infinite amount of particulate material at a mixing ratio of zero (occurring in zero crossflow experiments). To compensate for this, an exponential model was applied to the data set, producing a relationship with a finite value at a mixing ratio of zero.

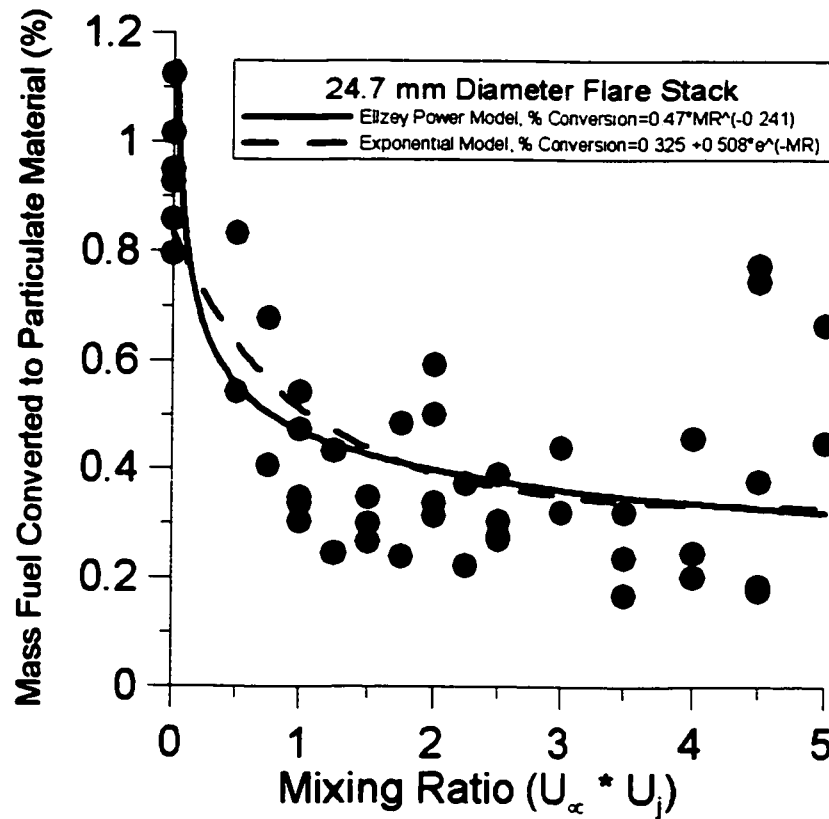


Figure 4.18: The statistically processed data set collected for particulate mass production using the 24.7 mm model flare stack.

4.5.6: Model Flare Stack Results-29.9 mm Diameter

To determine if changing the stack diameter had any effect on the production of particulate material, a series of experiments were conducted using a larger diameter stack. The 29.9 mm diameter stack was selected because it had a cross sectional area 50 % larger than the 24.7 mm diameter stack, but still generated a flame size manageable in the combustion wind tunnel facility. The statistically processed data set for the larger stack is shown in Figure 4.19.

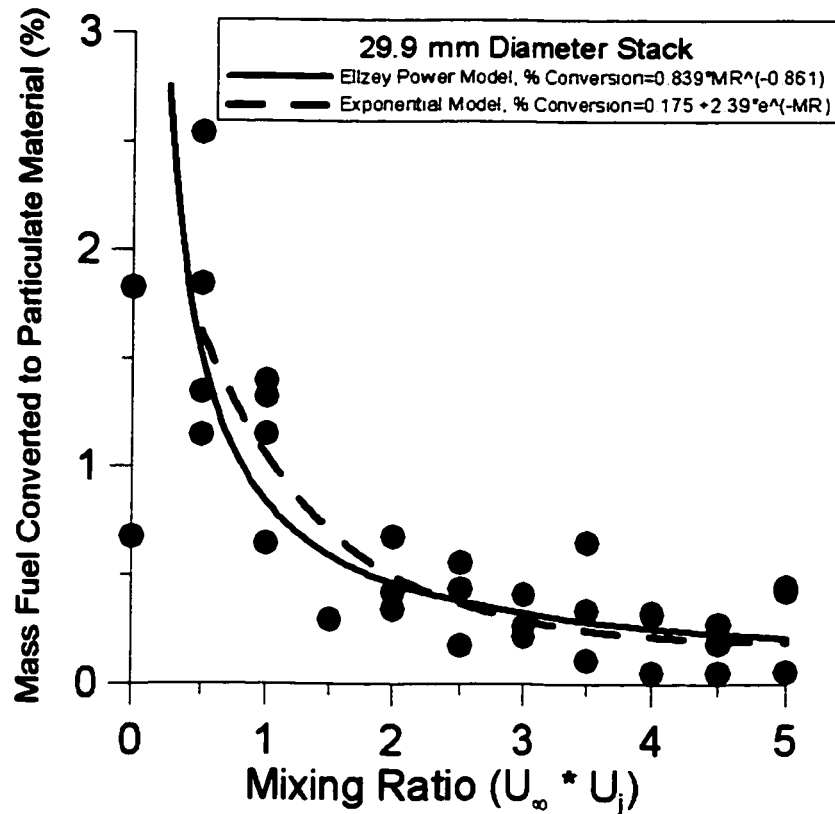


Figure 4.19: Particulate Material collection results for the 29.9 mm diameter stack.

The 29.9 mm diameter stack showed the same trend of decrease in particulate material emission with mixing ratio indicated by the 24.7 mm stack. The main difference is that particulate material production for mixing ratios less than 2 appeared to be higher for the 29.9 mm diameter stack, as indicated in Figure 4.20. At mixing ratios above 3, both stacks appear to convert between 0.2 and 0.3 % of the fuel into particulate material.

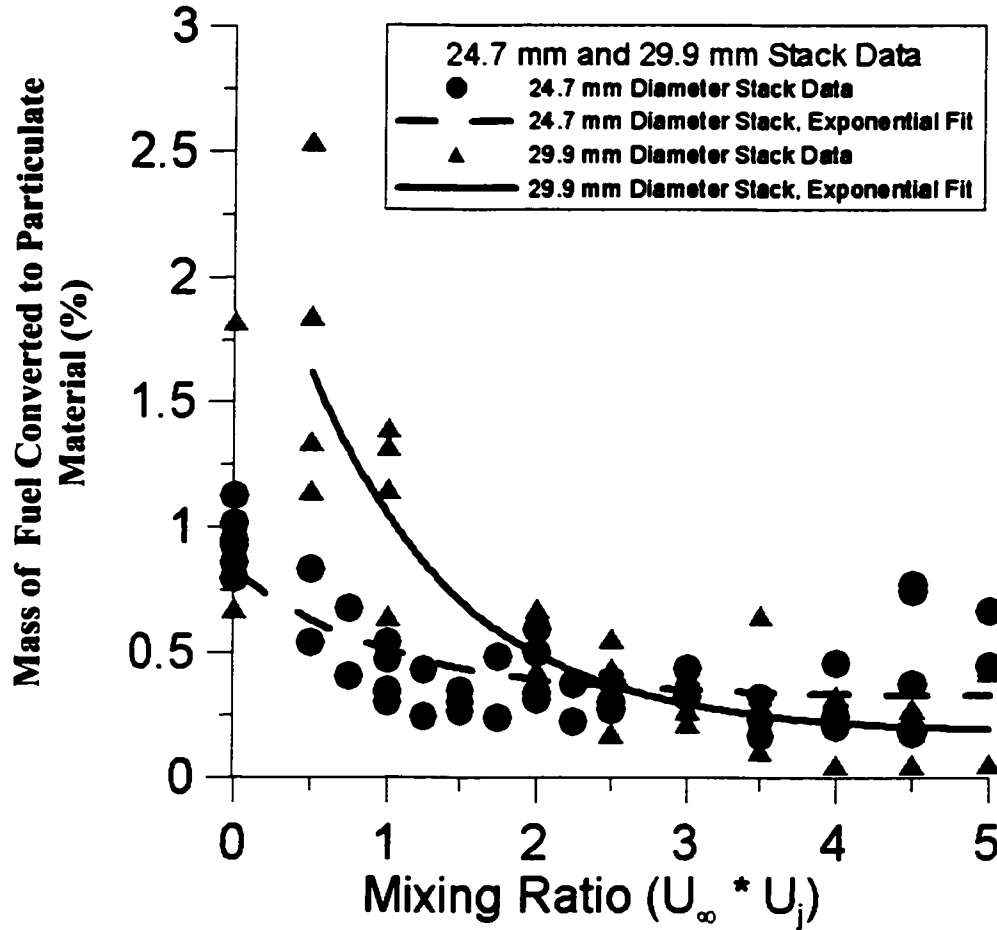


Figure 4.20: The comparison of particulate material production correlations for the 24.7 mm and 29.9 mm stack.

4.5.7: Small Diameter Model Flare Stack Results

If increasing the cross-sectional area of the model flare stack resulted in a flame that emitted more particulate material per unit of fuel, then it could be theorized that decreasing the cross-sectional area would reduce the particulate material conversion rate. A series of particulate material collection tests was conducted with the 12.3 mm model flare stack. The results, shown in Figure 4.21, did not follow the previous hypothesis.

The fractional rate of particulate material production was much higher (200 % to 300 % higher) for the 12.3 mm stack than either the 24.7 mm or 29.9 mm stacks.

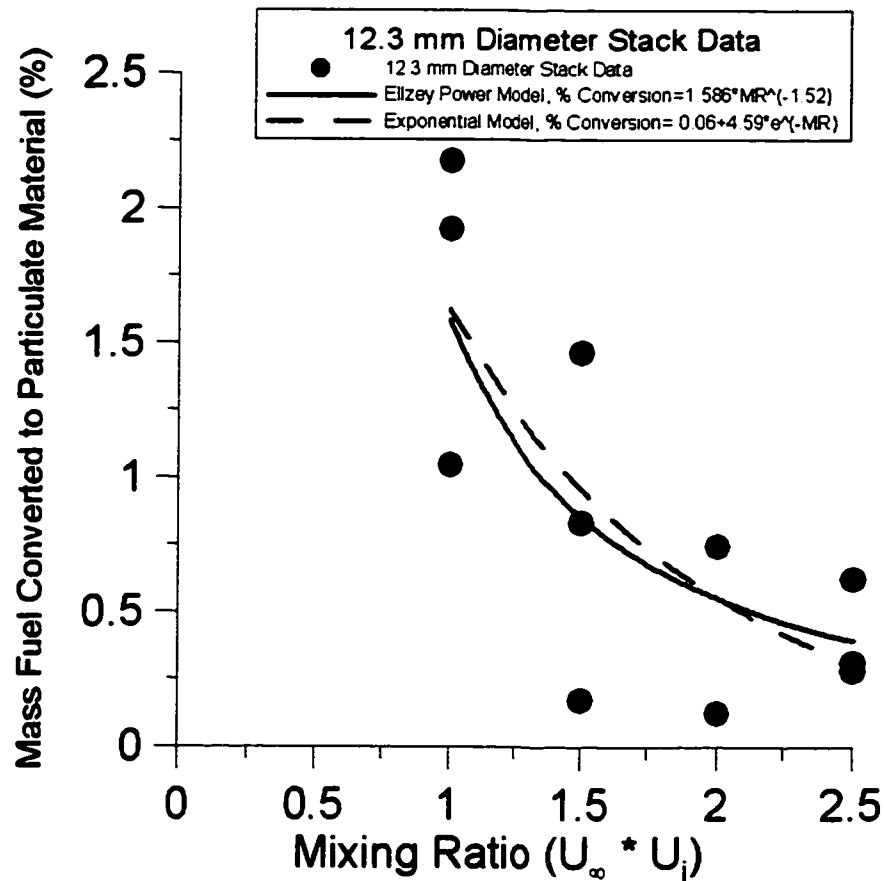


Figure 4.21: The resulting data set for the 12.3 mm diameter model flare stack.

The possible reason for this behavior could be related to the flow profile within the stacks. The 24.7 mm and the 29.9 mm model flare stacks both had turbulent flow profiles. A turbulence generator ensured that the flow was ‘tripped’ into turbulence before it left the stack. However, the small diameter and low flow rate of fuel through the 12.3 mm diameter stack kept the Reynolds Number of the jet flow very low (slightly

over 2800). With the preheating from the recirculating wake vortex, the Reynolds Number would be reduced, so even with the turbulence generator, the flow was likely to relaminarize after the turbulence generator.

To check this hypothesis, the particulate material production rates for the 12.3 mm stack were compared to the results produced by Ellzey for a 2.16 mm diameter stack with a laminar flow profile (all Reynolds Numbers were below 2800). The results for all diameters tested are shown in Figure 4.22. If the data from the 12.3 mm diameter stack is presented using Ellzey's power model, the results published by Ellzey for the 2.16 mm diameter stack agree closely with the results for the 12.3 mm diameter model flare stack. This would indicate that the stack flow profile plays a very significant roll in the particulate material production rate (for very small model scale flares), likely due to the effect it would have on mixing at the stack exit. Turbulent flow profiles produce a significant amount of mixing and as a result, particulate material production would be more susceptible to reduction with an increased mixing ratio. It should be noted that industrial flare stacks generally have a diameter of 100 mm or greater, resulting in a turbulent flow profile.

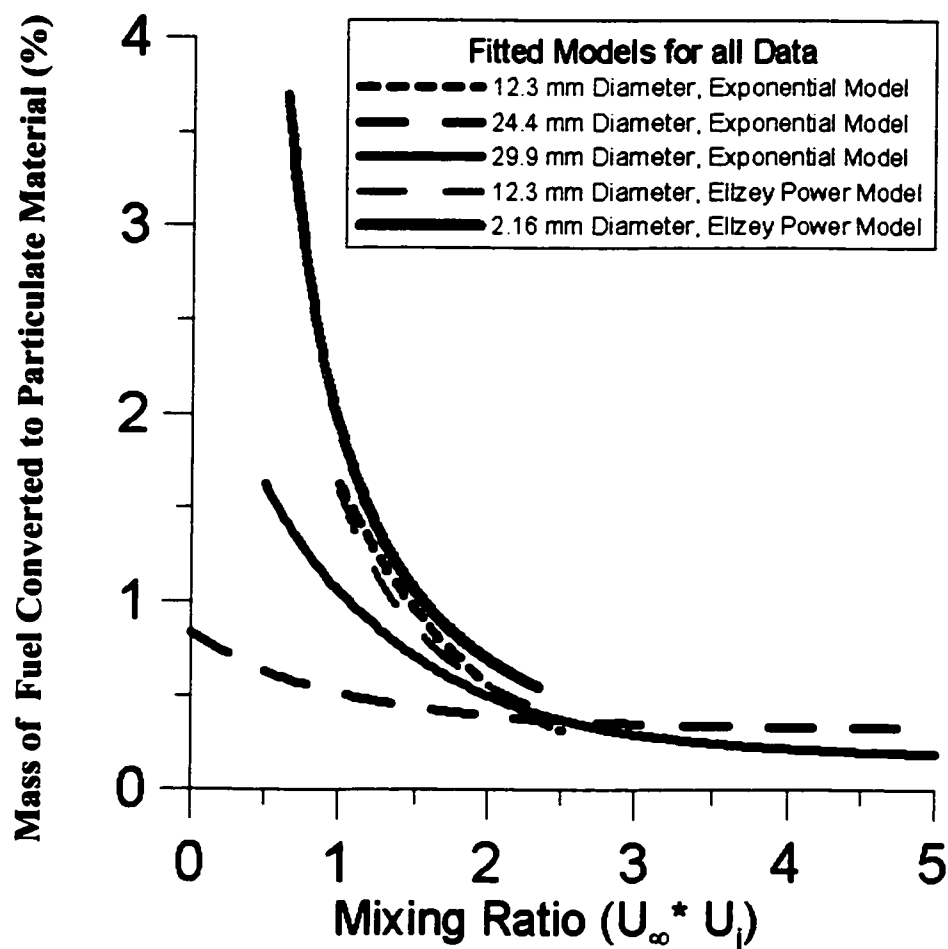


Figure 4.22: Particulate Material yield curves for all the stack diameters tested and published model for 2.16 mm diameter stacks [Ellzey, 1990].

4.6: Particulate Material Emission Models

Based on the data collected from various model scale flare stacks, it has been determined that the particulate material conversion rate for propane fuel decreases with an increase in the mixing ratio. The model scale flare stacks that had a diameter of 24.7 mm or more converted ~0.2 to 0.3 of the propane fuel mass into emitted particulate material for

mixing ratios >3 . As the mixing ratio was decreased below 3, the conversion rate of propane fuel mass into particulate material mass was significantly increased.

The mass conversion data collected for the 12.3 mm diameter flare stack, when fitted to Ellzey's power model, was very similar to the model that Ellzey fit to data collected from a 2.16 mm diameter flare stack. As a cold jet, the velocity profile in the 12.3 mm diameter flare stack would be turbulent (slightly over a Reynolds Number of 2800), but if the flow was preheated as a result of the recirculating wake vortex, it would become laminar. The data presented by Ellzey that was fit to the power model was for laminar jet velocity profiles. It could be theorized that the 12.3 mm diameter flare stack data and the 2.16 mm diameter flare stack data were similar because of the laminar jet velocity profile. The larger diameter flare stacks (24.7 mm and 29.9 mm diameter) both had turbulent jet velocity profiles, even with significant preheating.

4.7: Conclusion:

In this chapter it was determined that increasing the mixing ratio would result in a decrease in the emission of particulate material. The reduction in particulate material emission was exponential with the increase in the mixing ratio. Both the 24.7 mm and the 29.9 mm diameter model flare stacks (which had turbulent jet exit velocity profiles) emitted ~ 0.2 to 0.3 % of the fuel mass as soot in mixing ratio above 3. The 12.3 mm diameter flare stack emitted significantly more particulate material than the larger diameter flare stacks. When the data set for the 12.3 mm diameter flare stack was

compared to a data set taken by Ellzey for a 2.16 mm diameter flare stack with a laminar jet exit velocity profile, the data sets were very similar. It was theorized that both stacks had a laminar jet exit velocity profile and that this significantly increased the amount of particulate material emitted from the flame.

Chapter 5: Particle Imaging and Chemical Composition

Two factors are often used to determine the toxicity of a particle - the size and the chemical composition. The size is important to toxicity because it determines how deeply a particle is likely to penetrate into the respiratory system. In this chapter, SEM (Scanning Electron Microscopy) images were used to identify the size of the particles, and chemical analysis was used to determine the composition. The chemical composition of the particles represents what material is being transported within the respiratory system.

The nasal cavity and the upper respiratory system are effective at filtering particles larger than 3 μm before they can enter the lungs. The Cilia, the hair like fibrous cellular material that lines the lungs, can capture particles about 1 μm in size, expelling them with mucus flow. While particles that are between 0.05 μm and 0.25 μm can be transported out of the lung by airflow before they can be deposited within the tissue, very small particles (<50 nm) have a more rapid and erratic motion, allowing for a greater tendency to impact a respiratory surface. This means that particles with a mean diameter of the order of 0.5 μm (or less than 50 nm) will have the greatest tendency to be retained within the lungs if inhaled [Williamson Samuel J., 1973].

To ensure that all sizes of the particulate material were collected on the filter it was assumed that the worst case would be a single spherule. A spherule is 20-50 nm in diameter and can be described to appear as a solid sphere of carbon [Glassman, 1988].

Larger combustion generated particles are actually aggregations of these spherules and under extreme magnification, the individual spherules are identifiable.

To determine the composition of particulate produced by the model scale flares, samples of particulate material were collected and analyzed by an independent chemical laboratory. A mass spectrometer / gas chromatograph technique was used to determine the mass fraction of detectable PAH compounds within the particulate material. By knowing the mass production rate and the chemical composition (or mass fraction of individual components) of particulate material produced by a model scale flare, it is possible to estimate the rate of chemical release by the model scale flare. With accompanying particle size information, the dispersion of the material can be modeled.

5.1: Particle Imaging

The filters were selected based on the smallest possible particulate material being a single spherule. A spherule has a diameter of up to 50 nm but not less than 20 nm [Glassman, 1988]. The filter selected was an alumina membrane filter with a 20 nm pore size, which was quoted by the manufacturer. To confirm that the pore size was 20 nm and to determine that actual size of the particles, selected filters were imaged with a scanning electron microscope. SEM is a non-destructive magnification technique that involves applying an electric charge to a surface, and detecting the presence of the electrons. A technician trained in the operation of the microscope conducted the imaging of the filters. Images with a magnification of 150,000 times were taken, but it was experimentally

determined that a magnification of over 100,000 times generated an image that did not have an acceptable resolution making the image appear blurry.

5.1.1: Clean Filter Images

The filters were made on an alumina membrane with a 20 nm pore diameter manufactured by Whatman Inc. The filter was directionally dependant; that is it was designed to collect material on the surface of one side. Figures 5.1, 5.2, and 5.3 show the structure of a clean filter.

Figure 5.1 shows the surface of the filtration face of the filter. The individual pores can be identified and they are approximately 20 nm in diameter. There appear to be a small number of particles on the surface of the filter, but these are assumed to be small pieces of alumina left by the production of the filter (Using an X-ray spectrometer that was installed on the SEM determined that only filter material was present). For comparison the backside of the filter was also imaged to illustrate the difference in the two surfaces.

Figure 5.2 shows the reverse side of the filter. The pore size of the reverse side is 200 nm and is consistent with 200 nm filter size produced by the same manufacturer. A side image of the filter is shown in Figure 5.3. This image shows that the layer making up the 20 nm pores is only about 100 nm thick. Below this layer, the filter is a collection of 200 nm diameter tubes. The filter body can be described as a layer of tubes, each

approximately 200 nm in diameter and 60 μm long. This layer of tubes is coated with a layer of alumina to produce a layer of 20 nm holes that is approximately 100 nm thick.

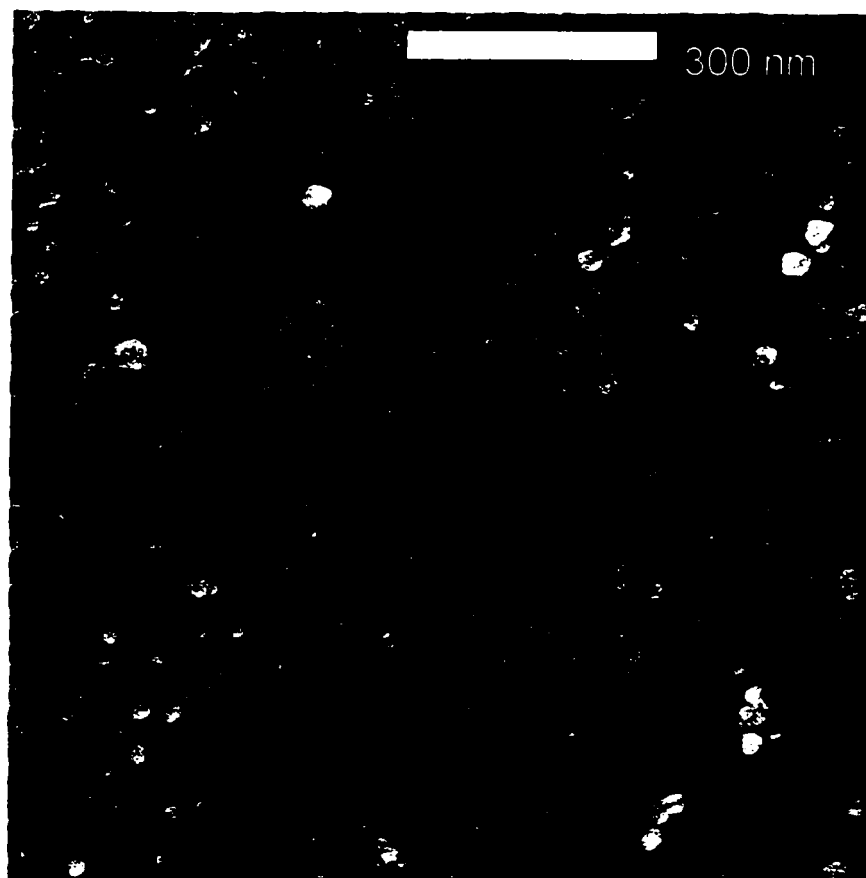


Figure 5.1: Magnification of the collection surface of the 20 nm alumina filter. Individual pores are about 20 nm in diameter as specified by the manufacturer.

5.1.2: Particle Images

Particulate material is formed by carbon based compounds condensing into small spheres called spherules, which then aggregate into larger particles. Individual spherules are normally 20 to 50 nm in diameter, although it is rare for spherules to exist independently for most processes which produce particulate material emissions [Kittelson, 1979].

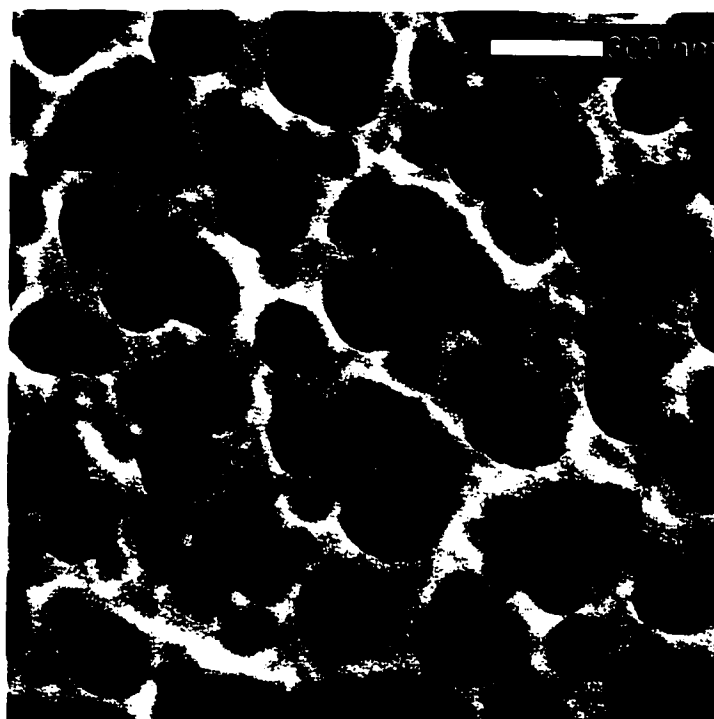


Figure 5.2: Image of the reverse side of the 20 nm alumina filter.

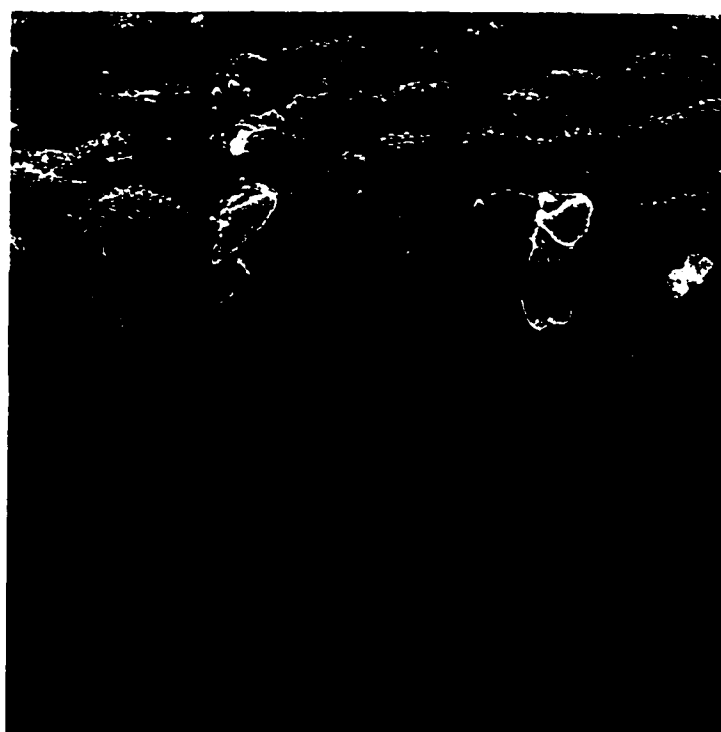


Figure 5.3: A side image of the filtration surface. The magnification is the same as Figure 5.1 and Figure 5.2. The filtering surface is less than 100 nm thick, and is supported on a filter body of 200 nm tubes.

A sample of particulate material emitted by a 24.7 mm diameter quartz flare stack burning a 20 SLPM propane flare with in a 2.0 m/s crossflow was collected on a 20 nm filter. Figure 5.4 shows a SEM image of the particles collected on the filter. Large collections of aggregates are seen across the filter, but observations of many parts of the filter show that aggregates are typically 100 to 300 nm in size. Figure 5.5 shows the particles under greater magnification so that the individual spherules are visible.

At very high magnification there were difficulties associated with focusing the image. The filter pores and the spherules have a very low surface roughness and did not provide any sharp edges to focus on. By collecting the particulate matter with a 200 nm alumina filter, a sharper image was produced. Figure 5.6 shows the material on a 200 nm filter. Most of the sub 200 nm aggregates were able to escape, but the larger aggregates were still retained, and the sharper focusing allowed for better definition of the spherules. The spherules appear to be a uniform 30 nm in diameter, so the 20 nm filters (which are rated to collect 100 % of material larger than 20 nm) ensured complete collection of all sizes of material.

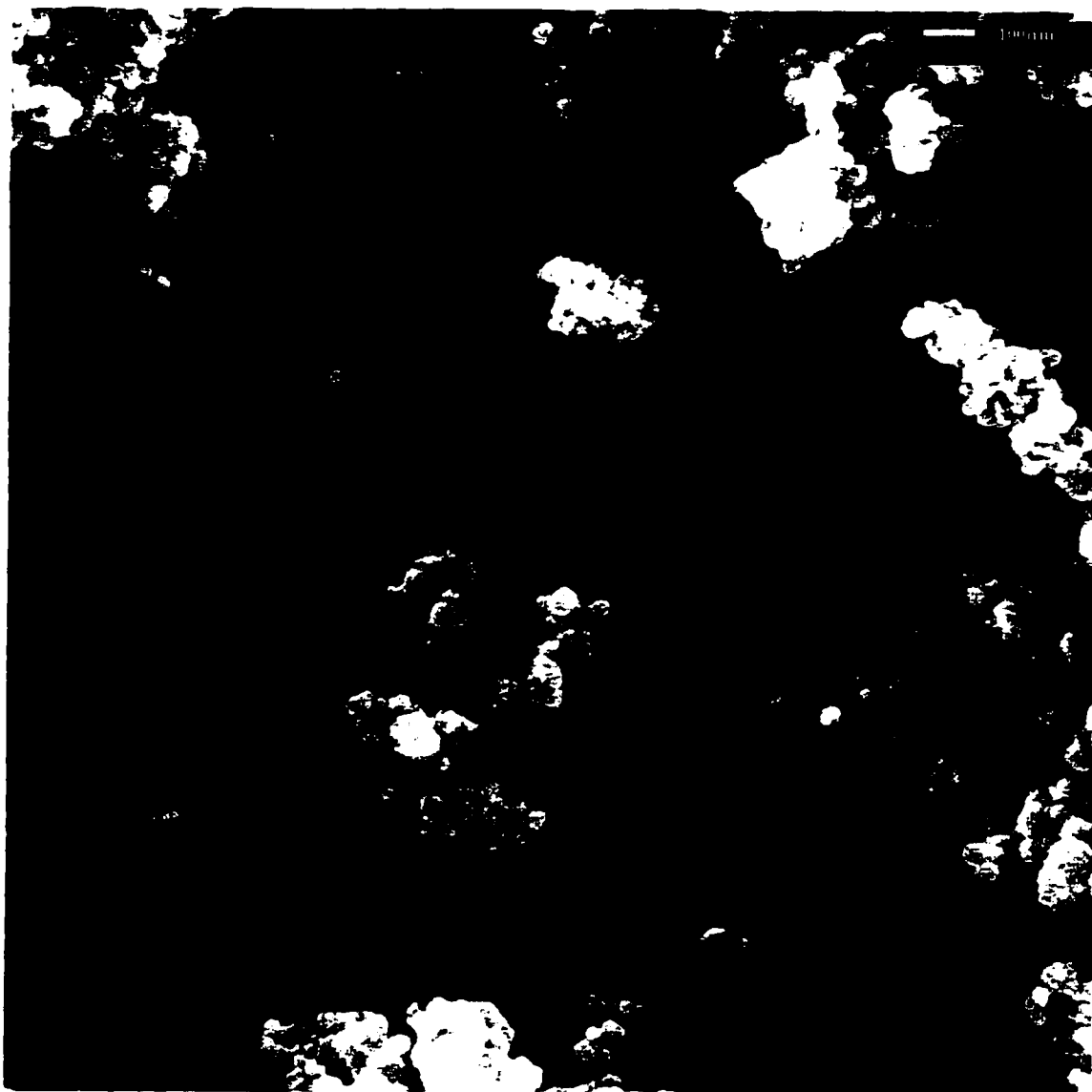


Figure 5.4: A number of aggregates on a 20 nm filter. The large particles are aggregates that have collected together on the filter. Most individual particles are 100 – 300 nm in size.

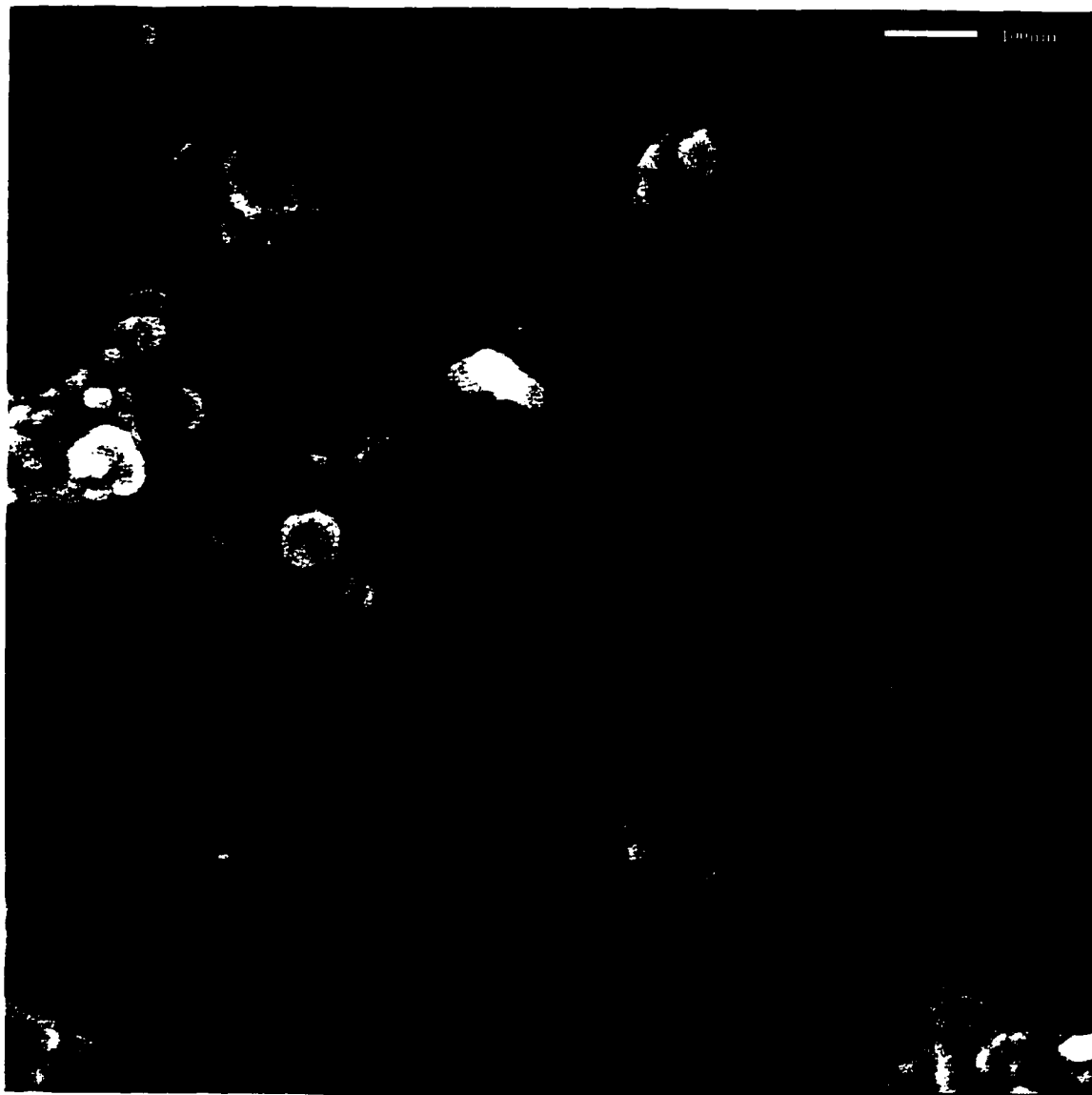


Figure 5.5: Individual spherules are identified in the structure of the aggregates



Figure 5.6: Particulate material collected on a 200 nm filter. The larger pores provide a better background for higher quality images.

Close observation shows that the individual spherules are not perfectly spherical in shape. Particulate material produced by the combustion of heavy hydrocarbons (such as plastics, rubber, and paraffin oils) has smooth, evenly shaped spherules, such as shown in Figure 5.7. The spherules produced by the model scale propane flare have a rough,

uneven surface as seen in Figure 5.8. Further exploration of this difference might provide insight into the formation of these particular particles.



Figure 5.7: An example of particulate material produced by the combustion of a synthetic rubber. Individual spherules are even in size with a smooth surface [Mercer, 1976].

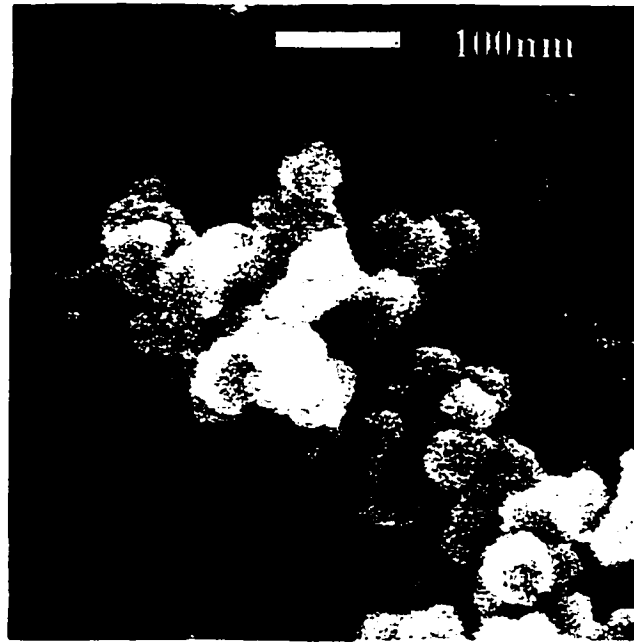


Figure 5.8: A close up image of a single particle. The uneven surface is more readily defined at this magnification.

5.1.3: Particulate Material Formation

While there are many different models for the formation of particulate material, one of the simplest is the acetylene model. The acetylene model is based on the formation of acetylene from the pyrolyzation of the fuel. Figure 5.9 gives a brief illustration of how the acetylene forms into benzene rings and PAH compounds, which can develop into particulate material [Glassman, 1988]. Figure 5.10 shows that as the PAH compounds form, they collect together to form platelets, which condense into spherules [Broome, 1971]. Large spherules will have a smoother surface since the flat platelets will be able to bind to the surface more evenly. In addition, some compounds (such as sulfur) can

form acidic or corrosive substances that can dissolve the rough surface of a spherule, smoothing the surface or even creating a more adhesive layer to promote particle growth.

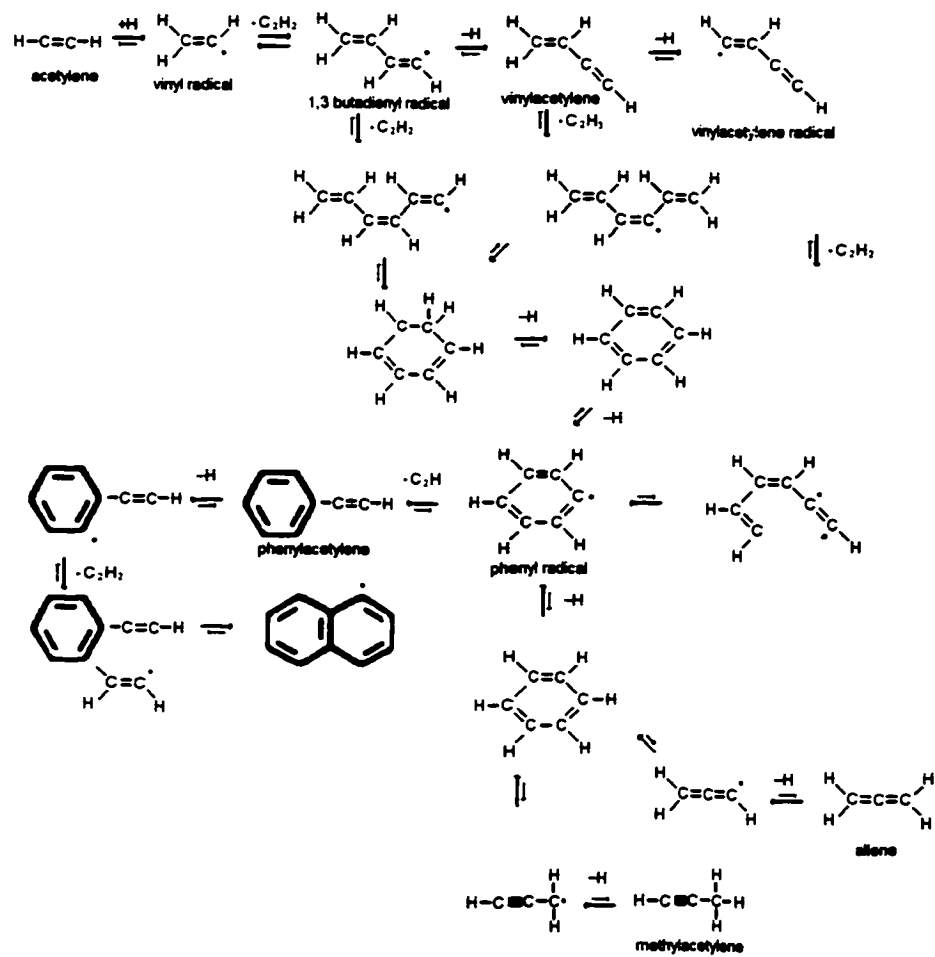


Figure 5.9: The acetylene model for particulate material formation. Acetylene is formed from the pyrolysis of fuel and as free hydrogen radicals attack it, it grows into polyaromatic compounds [Glassman, 1988].

The uneven surface of the spherules produced by the model scale flares certain factors and processes may be important.

1. The fuel is low in sulfur (or other acid forming substance). This would keep the aggregate size small since there will be less adhesion between the spherules. The propane fuel used was very low in sulfur (fuel analysis showed that none was present).
2. The surface of the spherules contain a large concentration of plate-like chemical compounds. This could create the sharp edges that are seen on the images. Large plate like structures (which would only need to be a few nanometers in length) would not sit evenly on a small round surface and would create uneven areas near the edges of the platelets.
3. Partial oxidation of the spherules will create a more uneven surface. Figure 5.11 shows the layered interior of a particulate material spherule [Donnet, 1976]. By exposing the particulate material to nitric acid the spherules swell causing the layers to separate, allowing better imaging of the interior structure. Towards the center of a spherule, the platelets are less organized and the internal structure of the spherule is less dense than the more crystalline exterior. As a result, oxygen radicals that penetrate into the particulate material spherule between the platelets will oxidize the interior more rapidly than the exterior. The edges of the platelets will also be oxidized, although more slowly than the interior. Thus oxidation would create cracks that allow more oxygen into the spherule and result in an uneven surface.

Any of these factors (and very possibly all) could result in the unevenly shaped spherules that appeared in the magnified images.

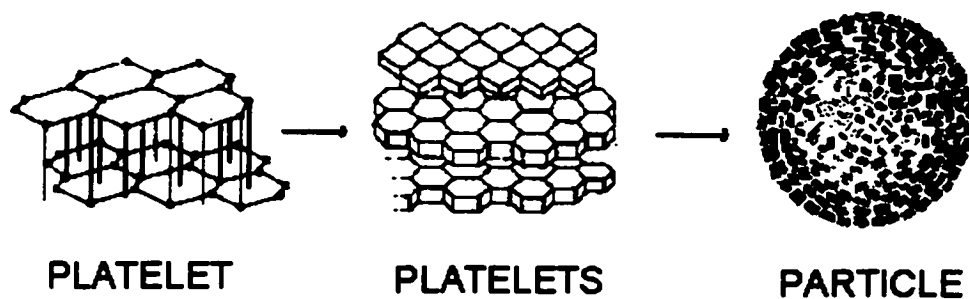


Figure 5.10: The formation of PAH compounds promotes that formation of platelets, which condense into spherules [Broome, 1971].



Figure 5.11: Particulate material spherules expanded using nitric acid. The layered shape is highlighted. Towards the center the platelets are less organized and less dense [Donnet, 1976].

5.2: Chemical Composition

The process by which particulate material forms involves the formation and condensation of carbon compounds including many complex PAH compounds. During the preliminary investigations, a particulate material sample was collected and analyzed for the presence of toxic compounds in an attempt to locate possible sources of toxic releases from the model flares. The preliminary particulate material sample (Chapter 2) indicated detectable quantities of PAH compounds were present within the particulate material, but the concentration could not be quantified. If the concentration of PAH compounds within a measured sample of particulate material was known, then the mass production rate of PAH compounds by the model scale propane flares could be determined.

A sample of particulate material was collected from a model scale propane flame with the intent of determining its chemical composition. The 24.7 mm diameter flare stack was used with a 1 m/s exit velocity (20 liters/min propane). Because more particulate material is generated at a low mixing ratio, and the goal was to collect a large sample, the cross wind velocity was set to 2 m/s. The test was conducted until there was a significant collection of particulate material on the filter (about 60 minutes using the same setup as described in Chapter 4). A total of 1.18 mg of particulate material was collected on the filter. The handling of the filter was conducted in accordance with NMAM 5515, except that a filter was used instead of an absorbent tube, which has stricter standards for handling than a filter. The results of the chemical analysis are listed in Table 5.1. The

analysis searched for 21 different PAH compounds, which were standard compounds included for the type of analysis that was conducted.

The mass fraction of the measurable PAH compounds within the particulate material sample totaled to 0.1 % of the sample mass. This can be used to estimate the quantity of PAH compounds emitted by the flame based on the correlation from Chapter 4 for a 24.7 mm diameter flare stack with a turbulent velocity profile. Using the models developed in Chapter 4, a 1 m/s jet in a 2 m/s crossflow converted approximately 0.4 % of the fuel into particulate material. If the flame had burnt for 1 hour, it would have burned 2360 g of propane (20 SLPM at 1.967 g/liter) and emitted 9.4 g of particulate material. This particulate material would have contained 0.0094 g (9.4 mg) of the 6 detected PAH compounds. The amount of individual PAH compounds emitted varies considerably. For example, Naphthalene (representing 16.5 % of the PAH mass found in the test sample, or 0.66 μg Naphthalene/g propane) has an oral LD50 (Lethal Dose in 50 % of subjects) of 490 mg/kg in rats [NTP #91-20-3]. Pyrene, representing 17.3 % of the PAH mass found in the test sample, or 0.68 μg /g propane, has an LD50 of 700 mg/kg in mice. It will begin causing cellular mutations in mammalian embryos at levels as low as 10 mg/liter of material [NTP #129-00-0]. The presence of the material within the particulate material particles provides a means of transportation for the material, allowing it to be deposited within the environment or even inhaled or ingested by living creatures.

Table 5.1: The quantity of PAH compounds found in particulate material sample.

Chemical Compound	Quantity in Sample ($\mu\text{g}/\text{mass fraction}$)	Detectable Limit (μg)
Naphthalene	0.2/0.00017	0.1
Acenaphthylene	0.3/0.00025	0.1
Acenaphthene	<DL	0.1
Fluorene	0.07/0.00006	0.05
Phenanthrene	0.27/0.00023	0.05
Anthracene	<DL	0.05
Fluoranthene	0.16/0.000136	0.05
Pyrene	0.21/0.00018	0.05
Beno(c)phenanthrene	<DL	0.05
Benzo(a)anthracene	<DL	0.1
Chrysene	<DL	0.05
7,12-dimethylbenz(a)anthracene	<DL	0.5
Benzo(b&j)fluoranthene	<DL	0.1
Benzo(k)fluoranthene	<DL	0.1
3-Methylcholanthrene	<DL	0.05
Indeno(1,2,3-cd)pyrene	<DL	0.1
Benzo(a)pyrene	<DL	0.05
Dibenz(a,h)anthracene	<DL	0.05
Benzo(g,h,i)perylene	<DL	0.05
Dibenzo(a,h)pyrene	<DL	0.1
Dibenzo(a,i)pyrene	<DL	0.1
Total	1.21/0.001	

5.3: Conclusions

Particles emitted by the flares were assumed to have a minimum diameter of 20 to 50 nm.

Particulate material produced by a flame is made up of small particles called spherules, which acquire their name from their spherical shape and have a diameter of 20 to 50 nm.

Larger particles are agglomerations of spherules, which adhere together into an irregularly shaped particle. Scanning Electron Imaging was used to study particulate matter generated by scale model flares. Spherule diameters were shown to be about

30 nm and the mean size of the agglomerated particles produced by the model scale flames was approximately 100 to 300 nm. A significant number of smaller particles existed, even as individual spherules, but from the images it was estimated that most of the mass existed as particles with a mean size of 100 to 300 nm.

The quantity of PAH compounds present within the particulate material was measured by chemical analysis of sample of particulate material of a known mass. The chemical analysis was conducted in accordance with NMAM 5515, and measured the quantity of 21 different PAH compounds within the sample. The chemical analysis determined that 0.1 % of the mass of particulate material emitted from the propane flame was in the form of detectable PAH compounds. The mass of 6 individual PAH compounds exceeded detectable limits: Acenaphthylene, Phenanthrene, Pyrene, Naphthalene, Fluoranthene, and Fluorene. Each of the PAH compounds has known toxic properties. Although the mass of PAH compounds emitted from the flame was not large (approximately 4 μ g of PAH compounds per gram of propane), if emitted over an extended period of time, the quantity of each PAH could accumulate to toxic levels.

Chapter 6: Conclusions

The Flare Research Project studied the efficiency of conversion of pure hydrocarbons into carbon dioxide by simulating flares with model scale flare stacks in a wind tunnel. A desire to explore the emission of toxic compounds by incomplete combustion of hydrocarbon fuels under similar conditions led to this work.

6.1: Preliminary Investigation

When this project was initiated, the emissions that were released from flares were not well understood. Possibilities for the form of toxic emissions included: fuel that manages to escape from the flame without burning, gaseous toxic compounds that are formed by pyrolysis of the fuel, non-gaseous compounds that form and condense into the particulate material emitted by the flame.

The preliminary investigation included taking samples of air and combustion products from the wind tunnel. These samples were analyzed directly or concentrated through absorbent tubes to concentrate specific compounds. All were sent for analysis by an independent lab. The particulate matter was also collected on a large filter and the sample was sent for analysis by an independent lab.

The results of the preliminary investigation determined that the hydrocarbons appearing within the wind tunnel during the tests were fuel that escaped from the flame without

being affected. For this scale of natural gas and propane flames and the standard analytical techniques used, the emission of toxic gaseous compounds (aldehydes, PAH compounds, VOC's, and BTEX) was at or below the detectable limit. The particulate matter was analyzed for the presence of PAHs and it was determined that a measurable quantity was present within the particulate material. From these results it was determined that further investigation would focus on the particulate emitted by the flame.

6.2: Plume Location

The first step to investigating the particulate plume was to locate the plume so that it could be collected and measured. To locate the plume a dual channel FFID was converted into a real time particulate counter and was used to survey the number concentration of particles within the plume.

The detector determined that the particle plume was confined within the boundaries of the thermal plume, so any collection device that could collect the thermal plume would collect the particle plume as well. In addition, the highest concentration of particles was located directly behind the tail of the flame. If the outer portion of the particle plume managed to escape the collection device for any reason, the quantity of lost mass would be very small when compared to the amount of mass collected. This ensured that as long as the core of the plume (the region directly behind the tail of the flame) was collected, any collection errors would be small.

Another discovery of the plume mapping was that as the crossflow was increased, the particle concentrations were reduced. This suggested that increasing the crossflow would decrease the mass production rate of particulate matter. This would need to be confirmed with direct mass measurements, but it did provide a hypothesis for future results.

6.3: Particulate Mass Measurement

To measure the mass of particulate matter emitted by the flame, the entire plume was collected and blended into a homogenous mixture, from which a small portion was filtered. The collection aspect was accomplished by placing a large collection duct within the wind tunnel down wind of the flame. The location of the particle plume was known so the duct was placed to collect the entire plume. Mixing was accomplished by a 9.14 m mixing duct, which used turbulent mixing to blend the gas flow to a homogenous concentration profile. A small sample was isokinetically extracted and passed through a membrane filter with a 20 nm pore size. The mass of material collected on the filter was measured and recorded. Using information on all the flows involved, the mass conversion rate of fuel into particulate material was determined.

6.4: Particulate Production Rates

Experiments conducted using the 24.7 mm diameter model flare stack indicated that as the mixing ratio was increased, the amount of fuel converted into particulate material was

decreased. This is likely to be a result of increased mixing between the jet and the cross flow. The rate of decrease was exponential, decreasing rapidly when the mixing ratio was low, but becoming stable for mixing ratios above 3. The stable rate of particulate material production for sales grade propane was about 0.3 %, or about 3 mg of particulate material per gram of fuel.

When the diameter of the stack was increased to 29.9 mm, the final stable level of particulate material production was about the same as it was for the 24.7 mm diameter stack at about 0.3 %. However, the rate at which particulate material production decreased with increasing the mixing ratio was more gradual for the low mixing ratios. This would suggest that increasing the jet diameter will generate a flame that is more resistant to mixing, and as a result will generate more particulate material.

When the diameter of the stack was reduced to the 12.3 mm diameter stack, the Reynolds number in the stack was reduced enough that the heating from the recirculation would cause the gas flow within the flare stack to be laminar. The resulting production rates of particulate material were much higher than the production rates for the larger diameter stacks. In addition, the production rates for the 12.3 mm diameter stack were almost identical to the production rates produced by Ellzey for a 2.6 mm diameter stack with a laminar velocity profile. It could be concluded that a laminar velocity profile causes less mixing than a turbulent velocity profile leading to emission of more particulate material. It should be noted that most industrial flares are 100 mm or larger in diameter, so they would be unlikely to have a laminar velocity profile.

6.5: Particle Imaging

When the filters were originally selected, the pore size was determined by assuming that the particles would have a minimal size of a single spherule, which is circular and has a diameter of 20 to 50 nm. Based on this assumption, a filter with a pore size of 20 nm was selected. To confirm the actual size of the particles, some of the samples were imaged using a Scanning Electron Microscope (SEM) capable of taking detailed images of nanometer sized particles.

Based on the images produced by the SEM, it was determined that a majority of the particles were 100 to 300 nm in size along their longest axis, although some individual spherules were found. The diameters of the spherules were approximately 20 nm, but it was noticed that when the images were magnified, the spherules had a very uneven surface. This could be a result of partial combustion of the spherules, or even the chemical composition of the particles. Regardless of the cause of the surface irregularities on the spherules, they had developed an appearance that was very different from engine particulate material, or particulate material produced by the combustion of complex carbon based material, such as rubber.

6.6: Chemical Composition

A sample containing 1.18 mg of particulate material was collected with the intent of conducting a chemical analysis. This particulate material was collected and analyzed by MS/GC in accordance with NMAM 5515 for levels of 21 selected PAH compounds. It was found that the sample contained 0.1 % by mass of 6 detected PAH compounds. Most of the mass of PAH compounds was in the form of Naphthalene ($C_{10}H_8$) and Acenaphthylene ($C_{12}H_8$), but 17.3 % of the PAH mass was Pyrene ($C_{16}H_{10}$), a very toxic compound. These compounds contribute to the toxicity of the particulate material they are contained within. The particulate also provides a means of transportation for the compounds.

6.7: Future Work

There are many different projects that could be developed to continue the research that was presented in this thesis. The immediate work could involve using different diameter stacks to produce more curves to determine how the flare scale (stack diameter) would affect the production of particulate material. Experiments with flare stacks with diameters of 100 mm and larger will require a larger wind tunnel or alternate arrangements to produce the required crossflow. This could produce results for turbulent jets of the size of solution gas flare stacks.

Different fuels could be used to generate the turbulent jet. Methane is a weak generator of particulate material, but ethane, ethylene, and propylene have greater particulate emission rates. In addition mixed phase fuels could be tested. Equipment is available to attempt particulate material emission experiments on methane flows seeded with liquid fuels. Such an experiment would simulate industrial flares with substantial amounts of heavy, non-gaseous hydrocarbons entrained within the fuel stream.

Additional exploration of the composition of the particulate material could be conducted. The sample that was analyzed indicated that 0.1 % of the particulate mass was in the form of PAH compounds. Additional samples would test the repeatability of this measurement. The preliminary investigation indicated that aldehydes, BTEX, or PAH compounds could not be detected at significant levels within the air within the tunnel, but there were PAH compounds within the particulate. It is possible that Aldehydes, Benzene and other toxic compounds are present within the particulate material, and additional samples could be collected to explore this possibility.

References

1. ASHRAE Standard 51-75 (1997), *Measuring Flow in Ducts*, ASHRAE Fundamentals, 14.16-17, Atlanta
2. Bourguignon E., Johnson M. R. and Kostiuk L. W. (1999). *The Use of a Closed-Loop Wind Tunnel for Measuring the Combustion Efficiency of Flames in a Cross flow*, Combustion and Flame, 119:319 – 334, Pittsburgh.
3. Brockmann J. E., *Sampling and Transportation of Aerosols*, United States Department of Energy, Contract # DE-AC04-76DP00789.
4. Broome D. and Khan I. (1971). *The Mechanism of Soot Release from Combustion of Hydrocarbon Fuels*, Air Pollution Control in Transport Engine, p.185
5. Brzustowski T. A., Gollahalli S. R. and Sullivan H. F. (1975). *The Turbulent Hydrogen Diffusion Flame in a Cross-Wind*, Combustion Science and Technology, 11:29 – 33
6. Cambustion Ltd. HFR400 Fast FID User Manual V2.1.
7. Cadle R. D. (1975). *The Measurement of Airborne Particulate*, Wiley -Interscience Publications
8. Calcote H. F. (1981). *Mechanisms of Soot Nucleation in Flames-A Critical Review*, Combustion and Flame, 42:215 – 242, Pittsburgh.
9. Donnet J. B. and Coet A. (1976). *Carbon Black - Physics, Chemistry and Elastomer Reinforcement*, Marcel Dekker Inc.
10. Ellzey J. L., Berbee J. G., Tay Z. F. and Foster D. E. (1990). *Total Soot Yield from a Propane Diffusion Flame in Cross flow*, Combustion Science and Technology, 71:42-52

11. "Flame Out", Feb. 10, 2000, Globe and Mail
12. Fukushima H., Asano I., Nakamura S., Ishida K. and Gregory D. (2000). *Signal Procession and Practical Performance of a Real-Time PM Analyzer Using Fast Fids*, SAE (2000-01-1135)
13. Glassman I. (1988). *Soot Formation in Combustion Processes*, Twenty-Second Symposium (International) on Combustion, p. 295-311
14. Gollahalli S. R., Brzustowski T. A. and Sullivan H.F. (1975). *Characteristics of a Turbulent Propane Diffusion Flame in a Cross-Wind*, Transactions of the CSME, Vol. 3, No. 4:205 – 214
15. Gollahalli S. R. and Nanjundappa B. (1995). *Burner Wake Stabilized Gas Jet Flames in Cross-Flow*, Combustion Science and Technology, 109:327 – 346,
16. Howard Hughes Medical Institute Laboratory Chemical Safety Summaries " *Sulfur Dioxide*", Howard Hughes Medical Institute.
17. Hottel H. C. and Hawthorne W. R.(1949) *Diffusion in Laminar Flame Jets*, Third Symposium on Combustion and Flame and Explosion Phenomena, p.254 – 266
18. Hasselbrink E. F. and Mungal M. G. (1998). *Characteristics of the Velocity Field Near the Instantaneous Bas of Lifted Non-Premixed Turbulent Jet Flames*, Twenty-Seventh Symposium (International) on Combustion
19. Hasselbrink E. F. and Mungal M. G. (1998). *Observations on the Stabilization Region of Lifted Non-Premixed Methane Transverse Jet Flames*, Twenty-Seventh Symposium (International) on Combustion

20. Howes J. E., Hills T. E., Smith R. N., Ward G. R. and Herget W. F. (1981).
Development of Flare Emission Measurement Methodology, EPA Contract No. 62-02-2682, Task Directive 118, U.S. Environmental Protection Agency
21. Huang R. F. and Wang S. M. (1999). *Characteristic Flow Modes of Wake-Stabilized Jet Flames in a Transverse Air Stream*, Combustion and Flame, 117:59 – 77, Pittsburgh.
22. Huang R. F. and Yang M. J. (1996). *Thermal and Concentration Fields of Burner-Attached Jet Flames in Cross Flow*, Combustion and Flame, 105:211 – 224, Pittsburgh.
23. Huang R. F. and Chang J. M. (1994). *The Stability and Visualized Flame and Flow Structures of a Combusting Jet in Cross Flow*, Combustion and Flame, 98:267 – 278, Pittsburgh.
24. Johnson M.R., Spangelo J.L. and Kostiuk L.W. (2001). *A Characterization of Solution Gas Flaring in Alberta*, Air and Waste Management, Accepted June.
25. Johnson M. R. (2001). *Wake Stabilized Diffusion Flames in Cross flow: Application to the Efficiencies of Gas Flares*, Ph.D. Thesis, University of Alberta, Canada
26. Johnson M. R. and Kostiuk L. W. (2000). *Efficiencies of Low Momentum Jet Diffusion Flames in Cross flow*, Combustion and Flame, 123:189 – 200, Pittsburgh.
27. Kalghatgi G. T. (1983). *The Visible Shape and Size of a Turbulent Hydrocarbon Jet Diffusion Flame in a Cross-wind*, Combustion and Flame, 52:91 – 106, Pittsburgh.
28. Kaplan H. L., Grand A. F. and Hartzell G. E.(1983) *Combustion Toxicology, Principles and Test Methods* Technomic Publishing

29. Kittelson D. B., Dolan D. F., Diver R.B. and Aufderheide E. (1979). *Diesel Exhaust Particle Size Distributions-Fuel and Additive Effects*, Univ. of Minnesota
30. Lee K. C. and Whipple G. M. (1981). *Waste Gas Hydrocarbon Combustion in a Flare*, Union Carbide Corporation, South Charleston, WV.
31. Margason R. J. (1993). *Fifty Years of Jet in Cross Flow Research*
32. Muniz L. and Mungal M. G. (1997). *Instantaneous Flame-Stabilization Velocities in Lifted-Jet Diffusion Flames*, Combustion and Flame, 111:16-31, Pittsburgh.
33. Majeski A. J., Wilson D. J. and Kostiuk L.W. (2000). *Measuring and Predicting the Length of a Propane Jet Diffusion Flame*, presented at the Combustion Institute, Canadian Section, 2000 Spring Technical Meeting, Ottawa, Ontario, May 15-17, 2000, Paper #7, 6 pages.
34. Mullholland G. W., Johnsson E. L., Fernandez M. G., and Shear D.A (2000). *Design and Testing of a New Smoke Concentration Meter* (1-24-00)
35. Mercer H. N., Boyer A. H., Brusky P. L. and Deviney M. L. (1976), "Rubber Chemistry and Technology", Vol. 49:1068
36. Mantell C. L. (1968). *Carbon and Graphite Handbook*, Interscience Publishers, P. 74.
37. "National Toxicity Program Chemical Repository – Hydrogen Sulfide" #7783-06-4, National Toxicology Program.
38. *National Toxicity Program Chemical Repository – Methane*, #74-82-8, National Toxicology Program.
39. "National Toxicity Program Chemical Repository –Naphthalene" #91-20-3, National Toxicology Program, National Institute of Environmental Health Sciences, Research Triangle Park, NC.

40. "National Toxicity Program Chemical Repository –Pyrene" #129-00-0, National Toxicology Program, National Institute of Environmental Health Sciences, Research Triangle Park, NC.
41. Palmer P. A. (1972). *A Tracer Technique for Determining Efficiency of an Elevated Flare*, E. I. Dupont de Nemours and Co., Wilmington, DE.
42. Petroleum Communication Foundation, *Flaring: Questions + Answers*, February 2000, (Calgary, Alberta).
43. Pitts W. M. (1988). *Assessment of Theories for the Behavior and Blowout of Lifted Turbulent Jet Diffusion Flames*, Twenty-Second Symposium (International) on Combustion, p. 809-816
44. Pohl J. H., Lee J., Payne R. and Tichenor B. A. (1986). *Combustion Efficiency of Flares*, Combustion Science and Technology, 50:217-231
45. Poudenx P. (2000). *Plume Sampling of a Flare in Crosswind: Structure and Combustion Efficiency*, M.Sc. Thesis, University of Alberta, Canada
46. Roper F. G. (1977). *The Prediction of Laminar Jet Diffusion Flame Sizes: Part I, Theoretical Model*, Combustion and Flame, 29:219-226, Pittsburgh
47. Scheaffer R. L. and McClave J. T. (1995). *Probability and Statistics for Engineers, Fourth Edition*, Duxbury Press, p.304 – 305.
48. Siegel K. D. (1980). *Degree of Conversion of Flare Gas in Refinery High Flares*, Ph.D. Dissertation, University of Karlsruhe, Germany
49. Smith S. H. and Mungal M. G. (1998). *Mixing, Structure, and Scaling of the Jet in Cross flow*, Journal of Fluid Mechanics, 357:83-122

50. Spector D. M. (1998). *A Review of The Scientific Literature As It Pertains to Gulf War Illnesses*, RAND MR1018/6-OSD
51. Strosher M. (1996). *Investigation of Flare Gas Emissions in Alberta*, Alberta Research Council Report to Environment Canada, Alberta Energy and Utilities Board, and Canadian Association of Petroleum Producers, 145 pages
52. Sun J.H. and Chan S.H. (1996). *A Time-Resolved Measurement Technique for Particulate Number Density in Diesel Exhaust Using a Fast-Response Flame Ionization Detector*, Measurement Science and Technology, 8:279-286
53. Williamson Samuel J. (1973). *Fundamentals of Air Pollution*, Addison-Wesley Publishing.

Appendix 1: Facility Details:

This study was conducted using facilities provided by the University of Alberta Combustion and Environment Group. This research group is responsible for the maintenance and operation of the combustion wind tunnel in the Department of Mechanical Engineering.

A1.1: Combustion Wind Tunnel:

The combustion wind tunnel has an internal volume of 350 m³ and is depicted in Figure A1.1. The combustion wind tunnel occupies two floors, with the test section and equipment on the first floor and the motor, mixing sections, and exhaust dampers located on the second floor. The main drive is a 150 kW DC motor with the option of manual or computer control. The wind within the test section can have a velocity of up to 35 m/s (126 kph) and has a low turbulence (~0.4%) due to the contraction section before the test section.

The test section is 2.4 m wide and 1.2 m tall. Within the test section the model scale flare stacks are mounted and the flares are burned. After the test section is the first of two mixing sections. Within the first mixing section, two 0.60 m diameter mixing fans are mounted to begin mixing the plume from the flame with the remaining air in the tunnel. Prior to the main drive, a third mixing fan is mounted. The second mixing section has

three mixing fans angled too create an opposing wind. When all six mixing fans are operational, they insure that the air within the wind tunnel is well mixed and uniform.

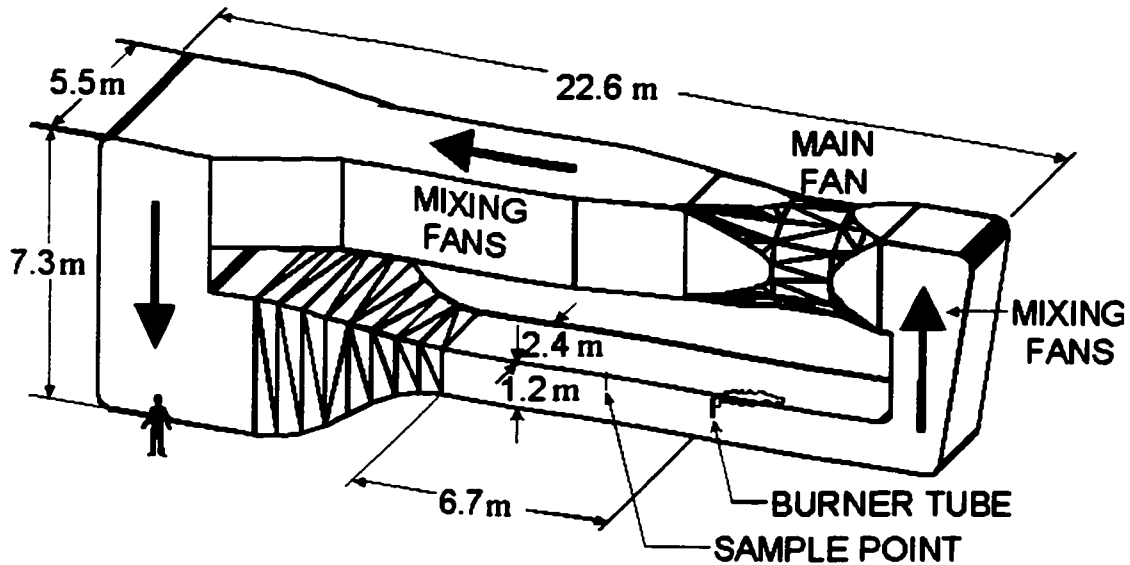


Figure A1.1: The combustion wind tunnel.

For experiments that include an analysis of the air within the wind tunnel, a sample point is located a short distance upstream of the flare stack. For continuous monitoring, a 6 mm diameter sample tube extracts a sample for analysis. If a stored sample is going to be collected, a 5 cm diameter sample port is located on the wall of the wind tunnel at a similar location to the 6 mm diameter sample line. The wind tunnel is not completely air tight, so experiments that require a sealed for an extended period of time use the 5 cm sample port to extract a large sample for analysis. The wind tunnel is sealed well enough to run short experiments.

A1.2: Fuel Supply:

The fuels used in the experiments include both natural gas and propane. Each of these fuel supply systems is detailed in Figures A1.2 and A1.3. Natural gas is supplied from a pressurized tank. The pressure is reduced using a series of regulators to a pressure that is usable by the mass flow controllers. The temperature is maintained by a heating bath at 23 °C. The mass flow controller is controlled by a computer interface that is used to set the supply of fuel to the model flare stack.

The propane feed system is almost identical to the natural gas feed system. The same heating bath and mass flow controller was used to control both fuels. The main difference is that the propane is supplied in a liquid form. The liquid propane needed to be vaporized prior to being supplied to the mass flow controller. This was accomplished by passing the liquid propane through a separate heating bath. Unlike the natural gas supply system, propane was not supplied under high pressure and only a single regulator was required to bring the propane vapor to a usable pressure.

Both systems were equipped with solenoid shut off valves prior to the mass flow controller. The propane system had a second valve mounted after the tank to control the flow. A thermocouple was used to monitor the temperature of the gas being supplied to the mass flow controller to insure that it was constant during the experiments. The mass flow controller can be affected by large changes in temperature, so the heating bath insures consistency of fuel flow.

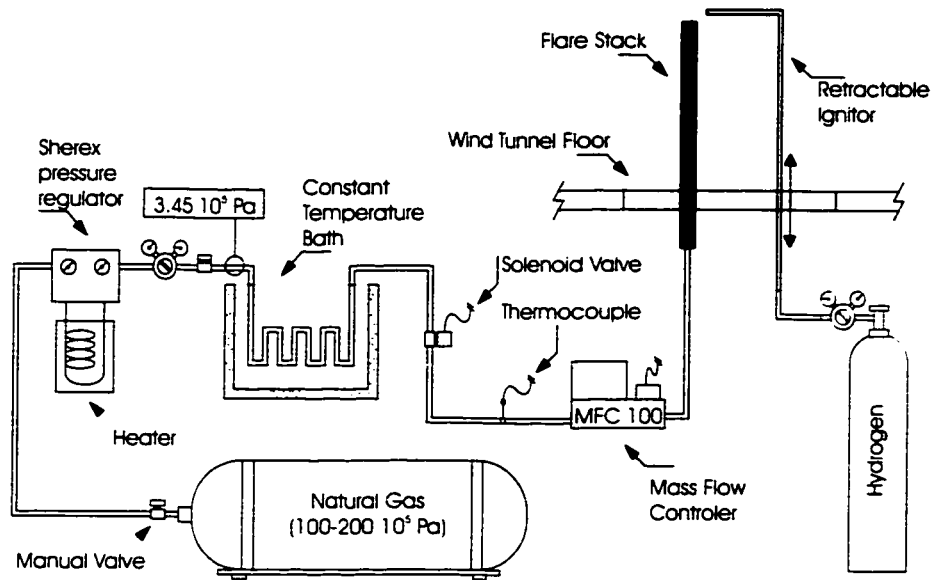


Figure A1.2: The natural gas supply system

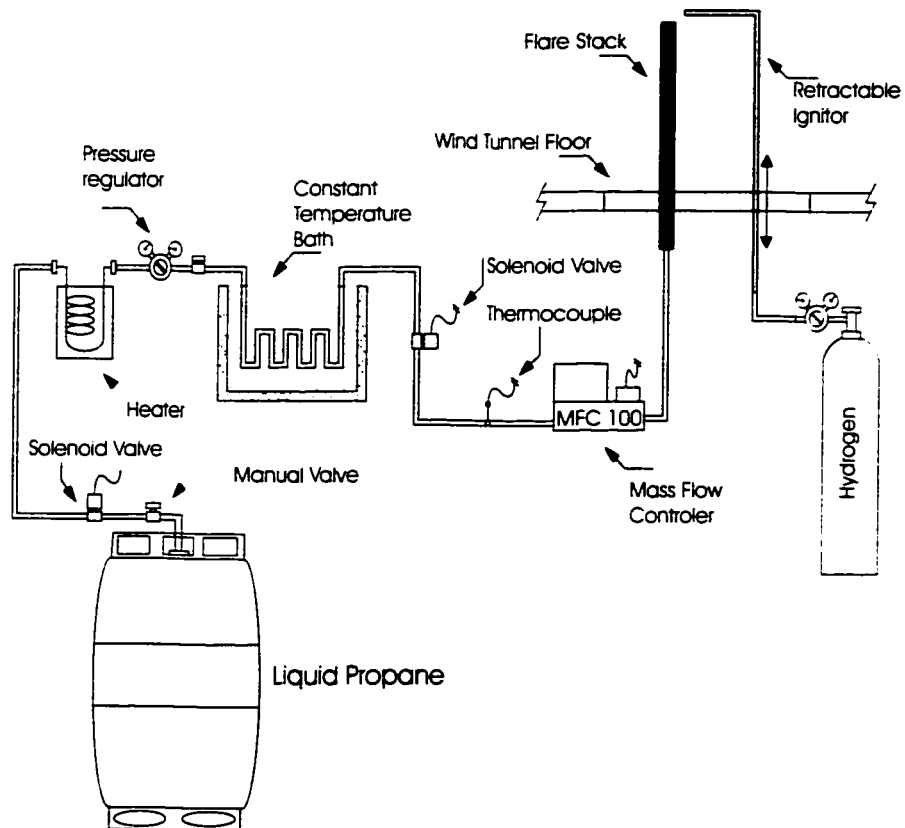


Figure A1.3: The propane supply system.

To prevent the wind tunnel from being contaminated by hydrocarbons during ignition, a hydrogen igniter is used to light the fuel as it is supplied to the stack. The hydrogen flame is burnt at the tip of the stack, and as the fuel begins to flow it is lit without escaping into the wind tunnel.

A1.3: Model Flare Stacks:

The model flare stacks used in the experiments were based on 4 " diameter schedule 40 steel pipe, which is commonly used to build industrial flare stacks. Fused quartz tubes were selected to have a similar inner to outer diameter ratio to the schedule 40 pipe. Table A1.1 lists the different stacks used in the experiments and the diameter measurements associated with each.

Table A1.1: The dimensions of the quartz flare stacks used in these experiments.

Stack Name	Inner Diameter (mm) (d_s)	Outer Diameter (mm) (d_o)	Depth (mm)	Length (mm)
12.3 mm	10.8	12.3	88	990
24.7 mm	22.1	24.7	180	988
29.9 mm	26.8	29.9	210	990

To simulate the turbulent interior flow profile that is expected with the industrial sized flare stack, orifice style turbulence generators were inserted into the flare stacks. Figure A1.4 shows the placement of the turbulence generator. The dimensions are listed in Table A1.1.

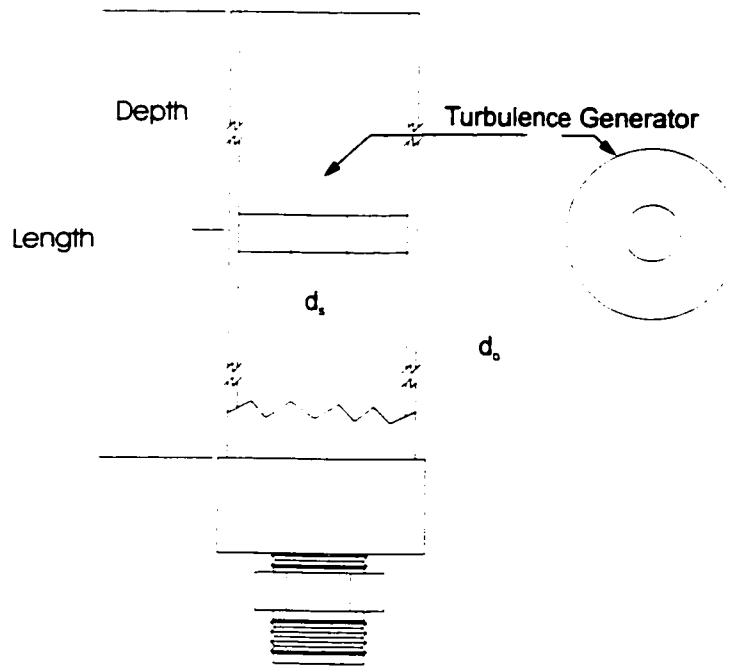


Figure A1.4: The orifice placement for the model flare stacks.

A1.4: Traversing Mechanism:

Some of the experiments conducted in the wind tunnel require the manipulation of probes around the test section. To accomplish this, a 2-D traversing mechanism was installed. Depicted in Figure A1.5, the traversing mechanism uses a pair of stepper motors and worm gears to manipulate the mounting plate around the interior of the tunnel. The traverse is only mechanically actuated in two dimensions, to move along the length of the tunnel, the traverse must be manually moved along the rails and bolted into place.

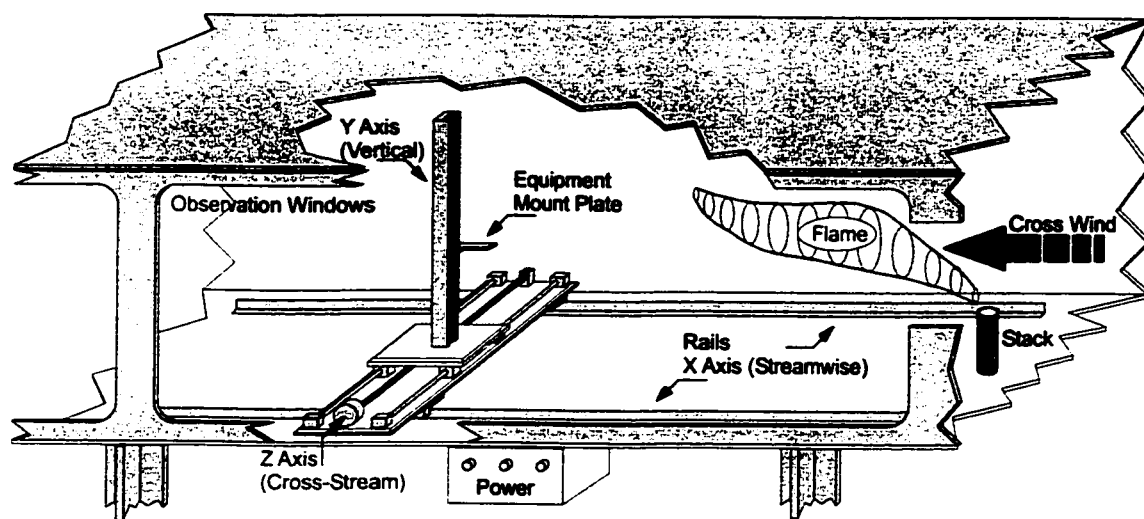


Figure A1.5: The traverse mechanism used in the test section of the combustion wind tunnel.

Appendix 2: Deposition of Soot in the Mixing Tunnel:

When sampling particles, there is a possibility that some of the particles will adhere to surfaces around the sampling system and be removed from the flow prior to the filter. This is referred to as deposition, or the laying down of matter by a natural process. Particles can come into contact with the ways of the wind tunnel, the mixing tunnel or the sampling system and possible adhere to these surfaces.

A2.1: Required Terms:

A number of terms need to be introduced to calculate the deposition of particles in a circular duct [Brockmann].

C_c - The Slip Correction Factor

$$C_c = 1 + \frac{1}{Pd_p} [15.39 + 7.518 \exp(-0.0741Pd_p)]$$

P - Pressure in kPa

d_p - Particle diameter in μm .

τ - The particle relaxation time, defined as:

$$\tau = \frac{\rho_p d_p^2 C_c}{18\eta}$$

ρ_p - the particle density (kg/m^3)

η - The viscosity of the carrier gas in μP

Stk - Stokes Number, defined as:

$$Stk = \tau U_o / d$$

U_o - The average velocity of transport.

d - Characteristic system dimension (m)

Re_f - The flow Reynolds Number, defined as:

$$Re_f = \rho_g U d / \eta$$

A2.2: Sample Efficiency:

The sampling efficiency is defined by the function:

$$\eta_{\text{sample}} = \eta_{\text{inlet}} * \eta_{\text{transport}}$$

η_{sample} - Efficiency of the measurement of the sample.

η_{inlet} - Portion of the particles that are collected.

$\eta_{\text{transport}}$ - Portion of the avoid deposition during transport.

The particle collection system can be characterized as two separate systems, the mixing tunnel and the particle sampling system. Both systems use isoaxial sampling, where the sampling axis is along the same axis as the flow the sample is being drawn from. The

mixing tunnel collects the entire plume, not just a sample, so the inlet efficiency can be defined to be 100%. The sampling system does have a sample inlet so the inlet efficiency needed to be determined.

A2.3: Inlet Efficiency:

For Isoaxial sampling η_{inlet} is defined as:

$$\eta_{\text{inlet}} = \eta_{\text{asp}} * \eta_{\text{transmission}}$$

η_{asp} - The aspiration efficiency.

$\eta_{\text{transmission}}$ - The transmission efficiency.

The aspiration efficiency has been correlated to be:

$$\eta_{\text{asp}} = 1 + (U_o / U - 1)[1 - (1 + \{2 + 0.617(U_o / U)^{-1}\} * Stk)^{-1}]$$

While there are other models for determining η_{asp} , they all use the U_o/U ratio (the ratio of average velocity to actual velocity). Since isokinetic sampling was used, $U_o/U = 1$, so η_{asp} is 100%.

The transmission efficiency of a system that uses isokinetic sampling or super-isokinetic sampling is 100%. Since isokinetic sampling was used, $\eta_{\text{transmission}}=100\%$ for the sampling system. This gives η_{inlet} to be 100%.

A2.4: Transport Efficiency:

The air flow within the mixing duct is turbulent. As a result, any deposition will not result from particle diffusion or from gravimetric settling, but from turbulent inertial effects. The turbulent transport efficiency in a tube is:

$$\eta_{\text{trans:turbulent}} = \exp(-\pi d L V_t / Q)$$

- d - Diameter (m) of the duct
- L - Length (m) of the duct
- Q - Flow Rate (m³/s)
- V_t - Turbulent Deposition Velocity

V_t is defined as:

$$5.03(V_t / U) \text{Re}_f^{1/8} = 0.0006 \tau_+^2$$

where τ_+ is the dimensionless particle relaxation time, defined as:

$$\tau_+ = 0.0395 \text{Stk Re}_f^{3/4}$$

In addition to the length of the tube, both the mixing tunnel and the sampling system has bends in them. The transport efficiency through a bend is defined as:

$$\eta_{\text{bend}} = 1 - \text{Stk}\phi$$

ϕ - The angle of the bend in radians.

With all this information it is possible to calculate the deposition of the entire system.

A2.5: Calculated Deposition:

The calculations that follow are for the following conditions:

1. 100nm diameter particles. From the particle images, this is a reasonable order of magnitude to select.
2. The mixing tunnel is 7.3 m long, 0.6 m diameter, and has a single 180° bend in it.
3. A wind speed of 2 m/s.
4. The sampling system has a diameter of 3 mm, and a length of 400 mm. The bends are very gradual and will not be considered.
5. The density of soot could be considered to be the same density of light grade lamp black. Lamp black is combustion soot that was used as a black dye and has a density of 1.7 g/cc [Mantell, 1968].

Based on these conditions the following efficiencies were calculated.

Inlet efficiency is 100%. As mentioned before, the mixing tunnel collects the entire plume, not just a sample so complete collection is used. The sampling system uses isokinetic sampling, so the inlet efficiency is 100%.

The transport efficiency for the mixing tunnel calculates out to be 99.99% transmittance through the tunnel. The 180° bend in the beginning of the tunnel is less efficient and had 99.49 % transmittance.

The sampling system has a calculated transmittance of 99.99%.

When all these transport efficiencies are combined, a final transport efficiency of 99.47% is calculated. Which suggests that 0.5% of the particle matter becomes deposited within the system during testing.

Appendix 3: Error Analysis:

There are a number of measurement errors that are present throughout the process that can produce an error in results.

A3.1: Facility Errors:

There are a number of small errors associated with the operation of the wind tunnel:

1. A pitot tube and a series of Ashcroft pressure transducers measure the velocity within the wind tunnel. As the pressure becomes reduced, which transducer is recording the pressure is changed to maintain less than 1% error through out the process. The pressure reading was compensated for atmospheric fluctuation by another pressure transducer.
2. The fuel flow rate is monitored by a set of electronic mass flow controllers. To reduce the error the temperature of the fuel entering the flow meter was maintained at 23 °C. This kept the accuracy of the flow meter to 1% with a 0.2% repeatability.

A3.2: Mixing Tunnel Errors:

The mixing tunnel had several locations that could generate an error in the readings:

1. The temperature was measured both at the plane of entry and the point of sampling, the measurements were made by a number of type K thermocouples and the electronics were rated to 1% accuracy.
2. An area sampling pitot tube assembly monitored the wind speed within the mixing tunnel. The pitot tube was calibrated against a mass flow of methane using the mass flow controllers that monitor the fuel flow (1% accuracy). The pressure from the area sampling pitot tube was monitored by a series of Ashcroft pressure transducers similar to the system used to monitor the airflow within the combustion wind tunnel. The accuracy of the pressure transducers was always less than 1%.
3. The mixing profiles within the mixing tunnel were monitored and the variance across the mixing tunnel was <1%. The velocity profiles were measured by a pitot tube and the same pressure transducers as the area averaging pitot tube, and also had a variance <1%.

The dimensions of the mixing tunnel were well known through repeated measurements so no error was included.

A3.3: Sampling System:

The sampling system collected the sample that was passed through the system. The dimensions of the sample probe were measured repeatedly and were well known. The filter flow calibration was conducted over a long period of time so the error involved was very low. The main error occurred with the pressure that generated the flow. The pressure was monitored by the vacuum controller and was determined by a series of calculations conducted by the computer. Once the vacuum controller was set, the error was rated at 1%. The limitations on the system were more associated with the vacuum that could be generated by the pump, not the controller so the error could be much less than 1%.

A3.4: Filter Measurement:

The masses collected on the filters were very small and it was determined that the measurement of the filter masses was the most likely source of error. The scale used to measure the mass of the filters had a resolution of 10 μg while most of the filters collected 100 to 200 μg in material. In addition, the filters needed to be weighed twice, once before the collection of material, and once afterwards. Temperature and humidity errors are considered to be non-existent since the filters and the scale were stored in the environmental chamber at all times.

A3.5: Mass Conversion:

As shown in chapter 4, the conversion of fuel into soot is determined by:

$$Y_{soot} = \frac{\dot{M}_{soot}}{\dot{M}_{fuel}} = \left[\frac{\Delta m_{filter} / \Delta t}{\dot{M}_{fuel}} \cdot \frac{Q_{duct}}{Q_{filter}} \right]$$

- Y_{soot} - The total soot yield or conversion rate
- $\dot{M}_{soot}, \dot{M}_{fuel}$ - The mass flow of soot and fuel
- Δm_{filter} - The change in filter mass
- Δt - The test time
- Q_{duct}, Q_{filter} - The flow through the duct and the flow through the filter

Δm_{filter} is determined by measuring the mass of the filters before and after the tests were conducted. So:

$$\Delta m_{filter} = m_{after} - m_{before}$$

where:

- m_{before}, m_{after} - The mass of the filter before and after the test.

Now Q_{filter} is determined from the filter calibration, and in chapter 4 this was presented as:

$$Q_{filter} = 0.013 + 0.104 * (PD) - 0.0002 * (PD)^2$$

Where:

PD - Pressure Drop across the filter (kPa)

Q_{duct} was programmed into the computer and was calculated automatically based on the differential pressure. The pressure drop is dependent on density and is affected by changes in temperature. With a regular Pitot tube, the velocity is determined by:

$$\frac{p - p_1}{\frac{1}{2} \rho V_1^2} = C_p$$

and:

$$\rho = \frac{p}{RT}$$

So if the atmospheric pressure is the same, and the fluid is the same, then the density will change based on temperature as:

$$\rho = \rho_o \left[\frac{T_o}{T} \right]$$

Where

ρ_o, T_o - The basic density and temperature.

ρ, T - The experimental density and temperature.

So, for the 1.78 mm water Ashcroft, the correlation was:

$$\text{Velocity} = 1.625858069 + 0.8490405813 * \text{PD} - 0.04654044383 * \text{PD}^2$$

And the pressure drop is:

$$\Delta p = C_p \frac{1}{2} \rho V_1^2$$

or:

$$\Delta p = C_p \frac{1}{2} \rho_o \left[\frac{T_o}{T} \right] V_1^2$$

So the flow through the duct could be described as:

$$\text{Volume flow} = \left\{ 1.625 + 0.849 * \left[PD \frac{T}{T_o} \right] - 0.046 * \left[PD \frac{T}{T_o} \right]^2 \right\} * \left\{ \left[\frac{0.61}{4} \right]^2 \pi \right\}$$

A3.6: The Error Equation:

$$\varepsilon_M^2 = \sum_{i=1}^N \left(\frac{\partial M}{\partial x_i} \right)^2 \varepsilon_{x_i}^2$$

Where:

- M - Mass Conversion
- N - Number of Variables
- ε - Error

The final equation for the determination of mass conversion of fuel into soot is:

$$Y_{soot} = \frac{\dot{M}_{soot}}{\dot{M}_{fuel}} = \left[\frac{\left[\frac{m_{after} - m_{before}}{\Delta t} \right] \cdot \left[\left\{ 1.625 + 0.849 * \left[PD_{ashcroft} \frac{T}{T_o} \right] - 0.046 * \left[PD_{ashcroft} \frac{T}{T_o} \right]^2 \right\} * \left\{ \frac{0.61}{2} \right\}^2 \pi \right]}{\left[0.013 + 0.104 * PD_{vacuum} - 0.0002 * PD_{vacuum}^2 \right] / 60000} \right]$$

$$\varepsilon_{soot}^2 = \left[\sum_{i=1}^N \left[\frac{\partial Y}{\partial mass_i} \right]^2 \varepsilon_{mass_i}^2 \right] + \left[\sum_{i=1}^N \left[\frac{\partial Y}{\partial PD_i} \right]^2 \varepsilon_{PD_i}^2 \right] + \left[\left[\frac{\partial Y}{\partial T} \right]^2 \varepsilon_T^2 \right]$$

In the following equations

$$A = \frac{\left[\frac{m_{after} - m_{before}}{\Delta t} \right]}{\dot{M}_{Fuel}}$$

$$B = \left[\left\{ 1.625 + 0.849 * \left[PD_{ashcroft} \frac{T}{T_o} \right] - 0.046 * \left[PD_{ashcroft} \frac{T}{T_o} \right]^2 \right\} * \left\{ \frac{0.61}{2} \right\}^2 \pi \right]$$

$$C = \left[0.013 + 0.104 * PD_{vacuum} - 0.0002 * PD_{vacuum}^2 \right] / 60000$$

The total error has three different sections, mass error, pressure error, and temperature error.

The mass error is

$$\varepsilon^2_{mass} = \sum_{i=1}^N \left[\frac{\partial Y}{\partial mass_i} \right]^2 \varepsilon^2_{mass_i}$$

There are three mass variables, the mass of the filters before the test, the mass of the filters after the test and the mass of the fuel that is combusted. When the three are put together, the result is:

$$\varepsilon^2_{mass} = \left[\frac{B}{C * \dot{M}_{fuel} * \Delta t} \right]^2 \varepsilon^2_{m_{after}} + \left[\frac{-B}{C * \dot{M}_{fuel} * \Delta t} \right]^2 \varepsilon^2_{m_{before}} + \left[-\frac{(m_{after} - m_{before})B}{\dot{M}_{fuel}^2 * \Delta t * C} \right]^2 \varepsilon^2_{\dot{M}_{fuel}}$$

The pressure error is

$$\varepsilon^2_{PD} = \sum_{i=1}^N \left[\frac{\partial Y}{\partial PD_i} \right]^2 \varepsilon^2_{PD_i}$$

There are two pressure variables, the voltage from the Ashcrofts measuring the velocity within the mixing tunnel and the pressure from the vacuum controller. The resulting error from the pressure is:

$$\varepsilon_{PD}^2 = \left[\frac{A * \left\{ \frac{0.61}{2} \right\}^2 * \pi}{C} * \left(0.849 \frac{T}{T_o} - 0.092 \frac{T}{T_o} \left\{ PD_{ashcroft} \frac{T}{T_o} \right\} \right) \right]^2 \varepsilon_{PD_{ashcroft}}^2 + \left[\left\{ \frac{-A * B}{C^2 * 60000} \right\} \{ 0.104 - 0.0004 PD_{vacuum} \} \right]^2 \varepsilon_{PD_{vacuum}}^2$$

The temperature error is

$$\varepsilon_{Temp}^2 = \sum_{i=1}^N \left[\frac{\partial Y}{\partial T_i} \right]^2 \varepsilon_{T_i}^2$$

There is only one temperature variable, which is the measured temperature within the mixing tunnel at the sampling point. The temperature error is:

$$\varepsilon_{Temp}^2 = \left[\frac{A * \left\{ \frac{0.61}{2} \right\}^2 * \pi}{C} * \left(\frac{0.849 PD_{ashcroft}}{T_o} - \frac{0.092 PD_{ashcroft}}{T_o} \left\{ PD_{ashcroft} \frac{T}{T_o} \right\} \right) \right]^2 \varepsilon_T^2$$

A3.7: Sample Error:

An error analysis for an average 500 µg soot sample when all of the soot emitted was collected would have the following error analysis:

- 10 µg pre-test mass resolution.
- 10 µg post-test mass resolution.
- 10 mbar for the vacuum controller (0.145 psi).
- 1% for the concentration profile within the mixing tunnel.
- 0.05 m/s for the area sampling pitot tube, or 0.05 V on the Ashcroft.
- 1 % for the fuel's mass flow rate (48.5 SLPM max, so 0.485 SLPM error or 0.95 g/min error).
- 0.1 °C for the thermocouple.

The fuel flow was propane that was injected at 20 SLPM (39.34 g/min), the temperature was 30 °C above standard. The vacuum controller was set to 500 mbar (7.25 psi) of vacuum, and the Ashcroft was ~ 0.07 “ Water (5 V output). The test was run for 30 min.

From the calculations:

$$A = 4.24 * 10^{-7}$$

$$B = 1.4365$$

$$C = 7.89 * 10^{-5}$$

So the error calculates to:

$$\varepsilon_{mass}^2 = (237.98)(0.00001)^2 + (237.98)(0.00001)^2 + (3.8 * 10^{-8})(0.95)^2$$

$$\varepsilon_{PD}^2 = (3.48 * 10^{-7})(0.05)^2 + (1.376 * 10^{-6})(0.145)^2$$

$$\varepsilon_{temp}^2 = (3.7 * 10^{-11})(0.1)^2$$

$$\varepsilon_{soot}^2 = 1.12 * 10^{-7}$$

$$\varepsilon_{soot} = 0.000334$$

For this example $\varepsilon_{soot} = 0.7719$ % conversion, and would have an error of +/- 0.0334 %.

So the final range would be $0.8053 \% < \varepsilon_{soot} < 0.7385 \%$, or +/- 4.3% error.

Appendix 4: Settling Time of Particles in a Flow

It needed to be determined how particles would settle out of the flow and if this was a concern with regard to the collection of the plume. If the particles settled quickly, then there was a risk that the particle plume and the thermal plume would not coincide. In addition, rapidly settling particles would result in increased depositions within the mixing tunnel assembly.

A4.1: Force Balancing

There are two significant forces on the particles, the force due to gravity and the drag force as a result of movement. The force due to gravity was derived from:

$$F_g = \frac{1}{6} \pi d^3 * \rho_p * g$$

Where:

- | | | |
|----------|---|---|
| F_g | - | Force from gravity |
| d | - | Diameter of the particle |
| ρ_p | - | Density of the particle |
| g | - | Gravitational constant (9.81 m/s ²) |

When the particle was in motion, there was a drag force on the particle that would try to counteract the motion. The drag force could be determined by:

$$F_d = C_D * \frac{1}{2} \rho_a V^2 * \frac{\pi d^2}{4}$$

Where:

- F_d - Drag force
- C_D - The Drag Coefficient
- ρ_a - The density of the fluid
- V - The velocity of the particle

The coefficient of drag is defined as:

$$C_D = \frac{24}{(\rho_a V d / \mu)}$$

Where:

- μ - The viscosity of the fluid

If the particle is at a stable velocity, the forces would be equal to prevent any acceleration of the particle. So if the forces are set to be equal, the velocity can be determined by:

$$V = \frac{d^2 \rho_p g}{18\mu}$$

1. The mean diameter of the particles is about 200 nm (radius of 100 nm).
2. Lamp black is combustion soot that was used as a black dye and has a density of 1.7 g/cc [Mantell, 1968].
3. The viscosity of air at 50 °C is 0.0000195 N*s/m²

From these values, it can be determined that the stable velocity of a particle in the listed conditions will be 1.9×10^{-9} m/s. This value is small enough to state that there is little risk of the particle plume separating from the thermal plume due to gravitational force within the confines of the experiments.